FLAME-RETARDANT POLYMERIC MATERIALS AND POLYMER COMPOSITES

EDITED BY: Yongqian Shi, Bin Yu, Xin Wang and Anthony Chun Yin Yuen

PUBLISHED IN: Frontiers in Materials and Frontiers in Chemistry

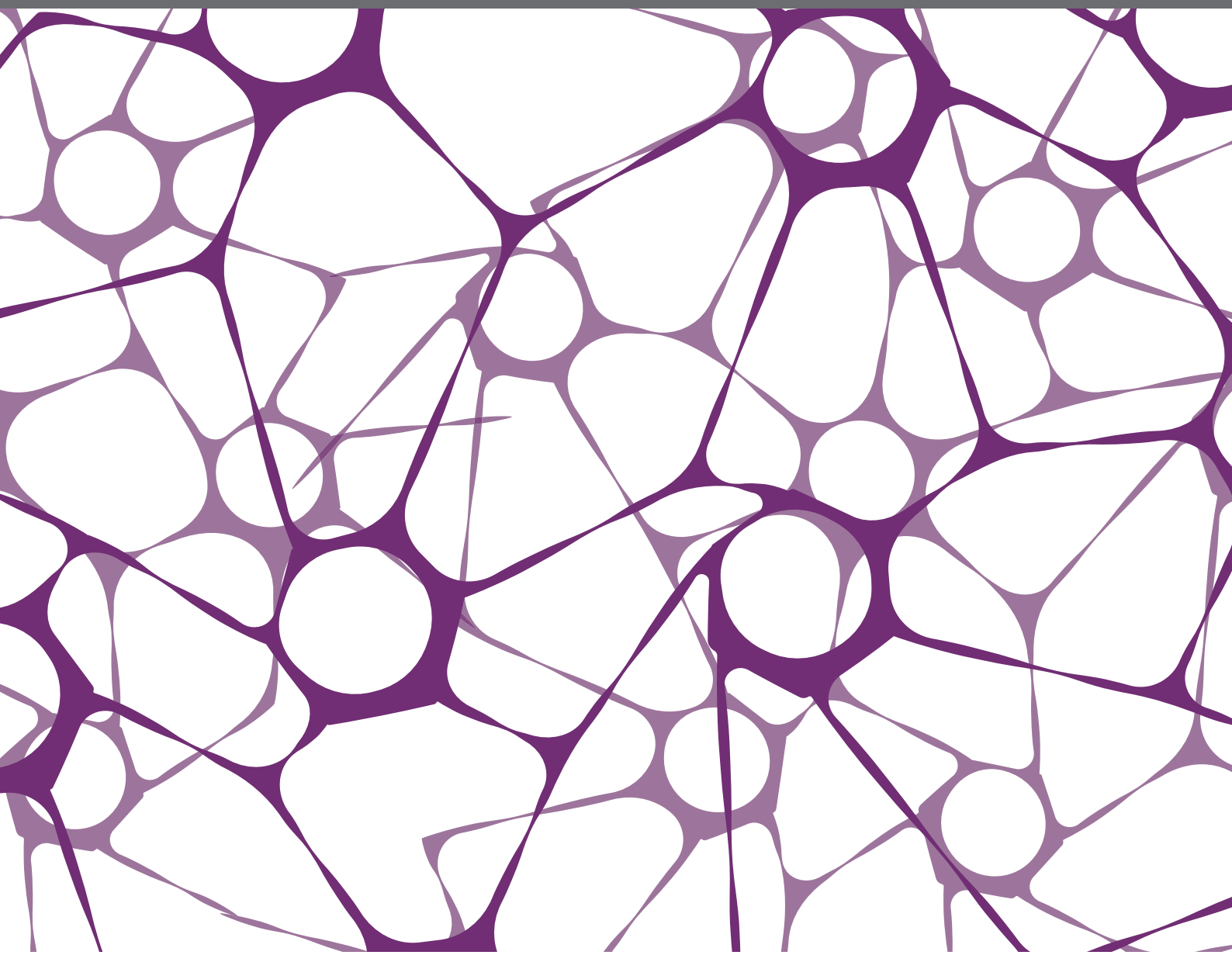

frontiers Research Topics

frontiers

ISSN 1664-8714
ISBN 978-2-88971-129-1
DOI 10.3389/978-2-88971-129-1

About Frontiers

Frontiers is more than just an open-access publisher of scholarly articles: it is a pioneering approach to the world of academia, radically improving the way scholarly research is managed. The grand vision of Frontiers is a world where all people have an equal opportunity to seek, share and generate knowledge. Frontiers provides immediate and permanent online open access to all its publications, but this alone is not enough to realize our grand goals.

Frontiers Journal Series

The Frontiers Journal Series is a multi-tier and interdisciplinary set of open-access, online journals, promising a paradigm shift from the current review, selection and dissemination processes in academic publishing. All Frontiers journals are driven by researchers for researchers; therefore, they constitute a service to the scholarly community. At the same time, the Frontiers Journal Series operates on a revolutionary invention, the tiered publishing system, initially addressing specific communities of scholars, and gradually climbing up to broader public understanding, thus serving the interests of the lay society, too.

Dedication to Quality

Each Frontiers article is a landmark of the highest quality, thanks to genuinely collaborative interactions between authors and review editors, who include some of the world's best academicians. Research must be certified by peers before entering a stream of knowledge that may eventually reach the public - and shape society; therefore, Frontiers only applies the most rigorous and unbiased reviews.
Frontiers revolutionizes research publishing by freely delivering the most outstanding research, evaluated with no bias from both the academic and social point of view. By applying the most advanced information technologies, Frontiers is catapulting scholarly publishing into a new generation.

What are Frontiers Research Topics?

Frontiers Research Topics are very popular trademarks of the Frontiers Journals Series: they are collections of at least ten articles, all centered on a particular subject. With their unique mix of varied contributions from Original Research to Review Articles, Frontiers Research Topics unify the most influential researchers, the latest key findings and historical advances in a hot research area! Find out more on how to host your own Frontiers Research Topic or contribute to one as an author by contacting the Frontiers Editorial Office:frontiersin.org/about/contact

FLAME-RETARDANT POLYMERIC MATERIALS AND POLYMER COMPOSITES

Topic Editors:
Yongqian Shi, Fuzhou University, China
Bin Yu, University of Southern Queensland, Australia
Xin Wang, University of Science and Technology of China, China
Anthony Chun Yin Yuen, University of New South Wales, Australia

Citation: Shi, Y., Yu, B., Wang, X., Yuen, A. C. Y., eds. (2021). Flame-Retardant Polymeric Materials and Polymer Composites. Lausanne: Frontiers Media SA. doi: 10.3389/978-2-88971-129-1

Table of Contents

frontiers in Materials

EDITORIAL
published: 07 June 2021
doi: 10.3389/fmats.2021.703123

Editorial: Flame-Retardant Polymeric Materials and Polymer Composites

Yongqian Shi[1], Bin Yu[2], Xin Wang[3] and Anthony Chun Yin Yuen[4]*

[1]College of Environment and Resources, Fuzhou University, Fuzhou, China, [2]Centre for Future Materials, University of Southern Queensland Toowoomba, Toowoomba, QLD, Australia, [3]State Key Laboratory of Fire Science, University of Science and Technology of China, Hefei, China, [4]School of Mechanical and Manufacturing Engineering, University of New South Wales, Kensington, NSW, Australia

Keywords: polymer composites, flame retardancy, smoke toxicity, fire simulation, sustainability

Editorial on the Research Topic

Flame-Retardant Polymeric Materials and Polymer Composites

INTRODUCTION

Lightweight polymeric materials have been widely applied in modern society. However, many of these polymeric materials are highly flammable, causing great fire risks to people's lives and belongings. The fire hazards associated with these flammable polymeric materials have been regarded as a major issue to be addressed. These flammable polymeric materials have been identified as the root cause of many severe fire incidents, which have given rise to over 40,000 deaths worldwide and total fire losses accounting for around 1% of the gross domestic product (GDP) of the country. Therefore, the minimization of the fire risk of these flammable polymeric materials has become a compulsory requirement for their practical application in industry. The development of environmentally benign flame-retardant polymers/composites represents one effective strategy to address the fire issues associated with these flammable polymers.

This research topic, Flame-Retardant Polymeric Materials and Flame-Retardant Polymer Composites (FRPMs and FRPCs), aims to feature the latest technological and scientific advances and future opportunities and challenges on flame-retardant materials. We also aim to broaden and deepen the scientific and technological knowledge with the most recent advances in the preparation, performance, and application of FRPMs and FRPCs with respect to the concept of long-term environmental, economic, and social sustainability. This research topic will be of great value to engineers, scientists, and decision-makers who are working in academia, industry, and government sectors. Also, it will greatly contribute to catalyzing the discovery and development of FRPMs and FRPCs while highlighting their associated challenges in sustainable development. As depicted in **Figure 1**, the cutting-edge flame retardant technologies utilized for polymer composites can be sub-divided into three main categories: 1) char-enhancing, 2) self-extinguishing and 3) bio-inspiring.

This series includes eight research articles that cover a wide range of flame retardant polymer materials, including epoxy resin (Kong et al., 2020; Yi et al., 2020), polypropylene (Liu et al., 2020), polystyrene (Shi et al., 2020), polyurethane (Hu et al., 2021), polyvinyl alcohol (Wang et al., 2020) and flame retardants based fire-fighting foams (Li et al., 2021a; Li et al., 2021b).

OPEN ACCESS

Edited and reviewed by:
Mazeyar Parvinzadeh Gashti, PRE Labs Inc., Canada

****Correspondence:***
Yongqian Shi
shiyq1986@fzu.edu.cn

Specialty section:
This article was submitted to Polymeric and Composite Materials, a section of the journal Frontiers in Materials

Received: *30 April 2021*
Accepted: *17 May 2021*
Published: *07 June 2021*

Citation:
Shi Y, Yu B, Wang X and Yuen ACY (2021) Editorial: Flame-Retardant Polymeric Materials and Polymer Composites. Front. Mater. 8:703123. doi: 10.3389/fmats.2021.703123

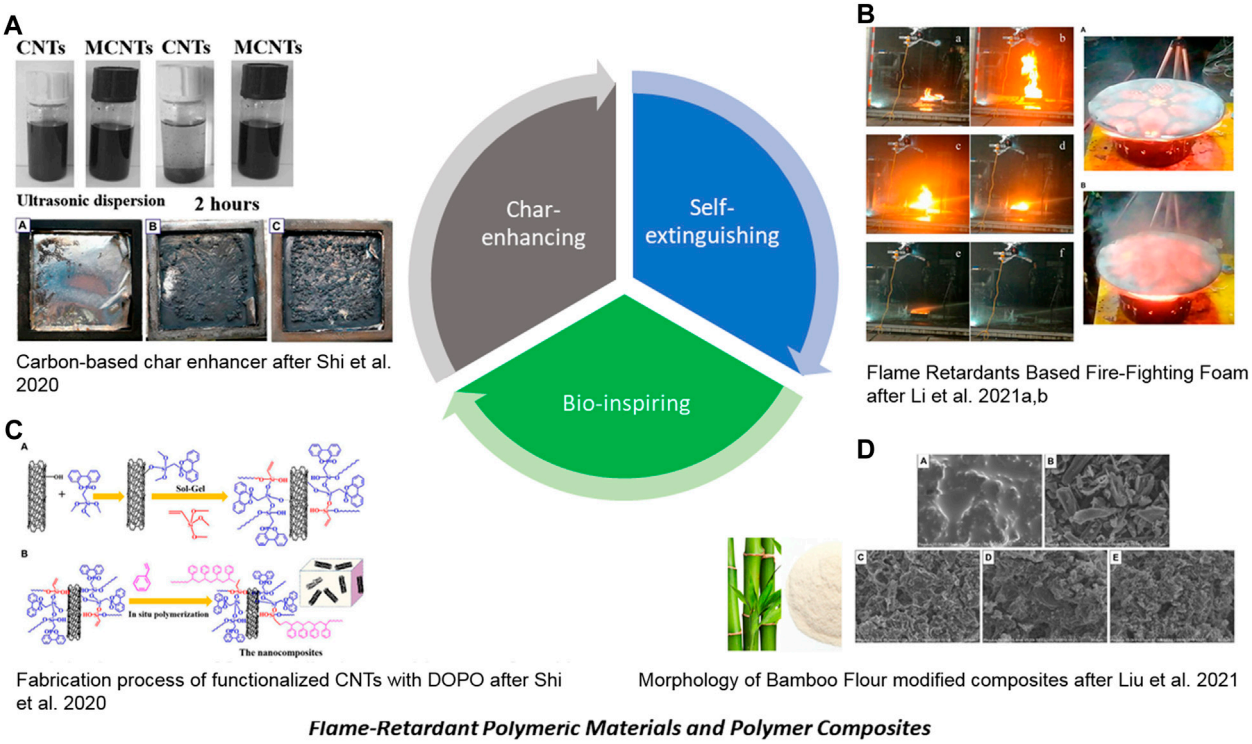

FIGURE 1 | Advancement and driving mechanisms of flame-retardant technologies for polymer composites. Images in **(A)**, **(B)**, **(C)** and **(D)** are adapted from Shi et al. (2020), Li et al. (2021a), Li et al. (2021b), and Liu et al. (2021) respectively, published under the terms of Creative Commons Attribution 4.0 (CC BY 4.0).

Yi et al. (2020) presented a Spiro-phosphorus (P)-based reactive flame-retardant epoxy resin curing agent. The synthesized epoxy thermosets exhibit higher carbon residue yield with significant improvements to flame retardancy and mechanical properties.

Kong et al. (2020) studied the effects of graphene oxide-cobalt-nickel phosphate (GO-$NiCoPO_3$) on the flame retardancy of epoxy resin. The results showed GO-$NiCoPO_3$ significantly enhanced char formation to reduce heat transfer, inhibit combustion, and improve the thermal stability of composites.

Liu et al. (2020) presented a flame retardant polypropylene composite via melt blending, incorporating ammonium polyphosphate (APP) and bamboo flour (BF). The effects of BF mechanical properties, crystallization behavior, thermal degradation, flame retardancy, and especially the smoke suppression effect of PP/APP composite materials were studied.

Shi et al. (2020) synthesized DOPO, and silicon-containing agents modified multiwalled carbon nanotubes (MCNTs) and investigated the application as a reinforcer for thermal and flame retardant properties of polystyrene nanocomposites.

Hu et al. (2021) presented flame retarded rigid polyurethane foams composites incorporating aluminium diethylphosphinate (ADP) combined with expanded graphite (EG) to form a synergistic flame retarded system. The effects of ADP and EG on the structure, thermal conductivity, thermal stability, and flame retardant performance of RPUF was investigated.

Wang et al. (2020) studied ternary h-BN@PDA@TiO2 hybrid nanoparticle as functional fillers for PVA nanocomposites. The results showed that the hybrid particles could significantly improve the thermal conductivity and flame retardant performance of the PVA composites and effectively inhibit toxic gases emissions such as combustible pyrolysis products and CO.

Li et al. (2021a) presented the preparation and fire suppression performance of mixing nano magnesium hydroxide particles and water-soluble flame retardant 8124 as an aqueous film forming fire extinguishing agent (AFFF). The suppression agent was applied on a 30 cm circular gasoline fire, and performance was investigated by analyzing the CO concentration and gas temperature.

Li et al. (2021b) also studied the addition of Talc into AFFF extinguishing agent. The fire resistance and fire extinguishing properties of the composite foam were studied. The network structure of composite foam was important to the improved stability of the foam, and the Talc powder formed a dense layer covering the oil surface, which effectively isolated the oil from the air.

In combination, these complementary contributions provide a body of knowledge in the field of Flame-Retardant Polymeric Materials and Flame-Retardant Polymer Composites, hence the apt name of this exciting publication.

AUTHOR CONTRIBUTIONS

All authors listed have made a substantial, direct, and intellectual contribution to the work and approved it for publication. YS writes the manuscript; BY, XW, and AY have revised the manuscript.

FUNDING

This work is financially supported by the National Natural Science Foundation of China (Grant No. 51803031) and Australian Research Council Industrial Transformation Training Center (ARC IC170100032).

ACKNOWLEDGMENTS

This issue would not have been possible without the contributions of talented authors, hardworking and professional reviewers, and the dedicated editorial team of Frontiers in Materials. Congratulations to all authors who have contributed to this special issue. In addition, we would like to express our sincere gratitude to all reviewers and the editorial team of Frontiers in Materials.

REFERENCES

Hu, Y., Zhou, Z., Li, S., Yang, D., Zhang, S., and Hou, Y. (2021). Flame Retarded Rigid Polyurethane Foams Composites Modified by Aluminum Diethylphosphinate and Expanded Graphite. *Front. Mater.* 7, 471. doi:10.3389/fmats.2020.629284

Kong, Q., Zhang, C., Zheng, G., Zhang, M., Zhou, T., and Zhang, J. (2020). Effect of Graphene Oxide–Modified Cobalt Nickel Phosphate on Flame Retardancy of Epoxy Resin. *Front. Mater.* 7, 316. doi:10.3389/fmats.2020.588518

Li, X., Guo, R., and Qian, X. (2021a). Preparation and Absorption Carbon Monoxide Properties of a Novel Flame Retardants Based Fire-Fighting Foam. *Front. Mater.* 8, 48. doi:10.3389/fmats.2021.646509

Li, X., Guo, R., and Qian, X. (2021b). Study on Flame Retardancy and Mechanism of Talc Composite Foams. *Front. Mater.* 8, 61. doi:10.3389/fmats.2021.661906

Liu, Y., Li, H., Chen, Q., Luo, F., and Cao, C. (2020). Effect of Bamboo Flour on Flame Retardancy and Smoke Suppression of Polypropylene/Ammonium Polyphosphate Composites. *Front. Mater.* 7, 311. doi:10.3389/fmats.2020.574924

Shi, C., Qian, X., Jing, J., and Che, H. (2020). Functionalized CNTs with DOPO and Silicon Containing Agents: Effective Reinforcer for Thermal and Flame Retardant Properties of Polystyrene Nanocomposites. *Front. Chem.* 8, 627642. doi:10.3389/fchem.2020.627642

Wang, X., Hu, W., and Hu, Y. (2020). Polydopamine-Bridged Synthesis of Ternary h-BN@PDA@TiO2 as Nanoenhancers for Thermal Conductivity and Flame Retardant of Polyvinyl Alcohol. *Front. Chem.* 8, 587474. doi:10.3389/fchem.2020.587474

Yi, L., Huang, Z., Cao, Y., and Peng, Y. (2020). Synthesis of a Novel Spiro Phosphorus–Nitrogen Concerted Reactive Flame-Retardant Curing Agent and its Application in Epoxy Resin. *Front. Mater.* 7, 293. doi:10.3389/fmats.2020.00293

Conflict of Interest: The authors declare that the research was conducted in the absence of any commercial or financial relationships that could be construed as a potential conflict of interest.

frontiers in Materials

ORIGINAL RESEARCH
published: 11 September 2020
doi: 10.3389/fmats.2020.00293

Synthesis of a Novel Spiro Phosphorus–Nitrogen Concerted Reactive Flame-Retardant Curing Agent and Its Application in Epoxy Resin

Liang Yi[1], Zhixiong Huang[1], Yu Cao[2] and Yongli Peng[2]*

[1] Key Laboratory of Advanced Technology for Specially Functional Materials, Ministry of Education, School of Materials Science and Engineering, Wuhan University of Technology, Wuhan, China, [2] School of Materials Science and Engineering, Wuhan Institute of Technology, Wuhan, China

OPEN ACCESS

Edited by:
Yongqian Shi,
Fuzhou University, China

Reviewed by:
Gang Tang,
Anhui University of Technology, China
Bihe Yuan,
Wuhan University of Technology, China
Lei Song,
University of Science and Technology of China, China

****Correspondence:***
Liang Yi
liangyi_whut@163.com

Specialty section:
This article was submitted to Polymeric and Composite Materials, a section of the journal Frontiers in Materials

Received: *01 June 2020*
Accepted: *04 August 2020*
Published: *11 September 2020*

Citation:
Yi L, Huang Z, Cao Y and Peng Y (2020) Synthesis of a Novel Spiro Phosphorus–Nitrogen Concerted Reactive Flame-Retardant Curing Agent and Its Application in Epoxy Resin. Front. Mater. 7:293. doi: 10.3389/fmats.2020.00293

Spiro-phosphorus (P)-based reactive flame retardant (SPDPT), a novel reactive flame-retardant epoxy resin (EP) curing agent, was prepared through the one-pot synthesis of triacetonediamine, pentaerythritol, and P oxychloride. The successful preparation of SPDPT was confirmed through Fourier-transform infrared (FTIR) spectroscopy, ^{1}H NMR spectroscopy, ^{31}P NMR spectroscopy, and elemental analysis. The flame-retardant epoxy thermoset [e.g., EP/4′4-diaminodiphenyl sulfone (DDS)/SPDPT] was prepared by using DDS as the co-curing agent. Differential scanning calorimetry (DSC) results show that SPDPT can cure EP. Thermogravimetric analysis (TGA) results show that improve the carbon residue yield of the epoxy thermoset after burning. When the P content was 1.0 wt%, the limiting oxygen index value of the EP/DDS/SPDPT-4 sample was 26.4%, and UL94 reached the V-0 rating. The tensile property of the epoxy thermoset reached 37.20 MPa, the flexural property reached 63.82 MPa, and the impact property reached 21.57 KJ·m^{-2}.

Keywords: epoxy resin, carbon residue yield, Fourier-transform infrared, curing agent, flame retardant

INTRODUCTION

Epoxy resin (EP) boasts merits, such as excellent adhesion, strong mechanical strength, low shrinkage, good electrical insulation, and outstanding corrosion resistance (Huo et al., 2019; Luo et al., 2019), and has been widely applied in various industries, such as coating, adhesive, aerospace material, and substrate material (Perret et al., 2011a,b; Qiu et al., 2016; Mestry and Mhaske, 2019; Zhang et al., 2019). However, flammability has been one of the major limiting factors of EP applications (Huo et al., 2016; Lin et al., 2016). Therefore, the flame retardancy of EP composites has been investigated widely (Shi et al., 2017; Xu et al., 2019; Chu et al., 2020; Ding et al., 2020). In the past few years, researchers have strove to improve the flame retardancy of EP by introducing DOPO (9,10-dihydro-9-oxa-10-phosphaphenanthrene-10-oxide) -based flame retardants (Luo et al., 2015; Zhang et al., 2017; Deng et al., 2018; Zhao et al., 2018), phenolic resin (Wang P. et al., 2018), PN-containing compound flame retardants (Chen et al., 2005; Jian et al., 2017), and other flame retardants that contain phosphorus (P) and silicon. However, these flame retardants cannot ensure

the flame retardancy of EP and might even release a significant amount of toxic fumes because they cannot easily form char, thereby endangering people's health. Therefore, we need to develop new flame retardants with excellent char-forming ability.

Among the P-based flame retardants, halogen-free spiro P-based flame retardants boast merits, such as high P content, excellent char-forming ability, low toxicity, migration resistance, and durability, which have contributed to their wide applications. Spiro P-based flame retardants consist of three elements, namely, P, oxygen (O), and carbon (C), which give them a stable heterocyclic structure and high thermal stability. With the char-forming property of pentaerythritol, such retardants can inhibit the further combustion of polymer materials and provide flame retardancy in the gas and condensed phases (Zhan et al., 2009; Li et al., 2016; Ma et al., 2019). The molecular structure of their intermediate, spiro P oxychloride, contains a chlorine atom that can be substituted to synthesize multifunctional flame retardants applicable to different flame-retardant systems and can also react with amine group-containing compounds to prepare P–nitrogen (N) concerted self-intumescent flame retardant combining acid, C, and gas sources to allow O isolation, heat insulation, and smoke suppression. Therefore, these retardants boast outstanding char-forming and flame-retardant properties by comparing with additive flame retardant (Huo et al., 2017; Yuan et al., 2017, 2018; Wang C. et al., 2018; Huang et al., 2019; Shang et al., 2019; Ma et al., 2020; Tang et al., 2020a,b).

To date, numerous studies on amino group-containing compounds have been conducted. For example, Huo et al. (2019) prepared a piperidine group-containing flame retardant that can be effectively combined with EP to improve its flame retardancy (Wang X. et al., 2018). Xie et al. (2016) prepared a triazine-based N-alkoxy compound that can effectively improve the flame retardancy of polypropylene film. Existing studies also show that amino group-containing compounds can provide flame retardancy in the gas phase by quenching free radicals (Aubert et al., 2011; Xu et al., 2015; Zhao et al., 2018). Therefore, we can obtain an EP reactive flame retardant with high P content, good char formation, low toxicity, and high curing activity through the reaction between the chlorine atom in the molecular structure of spiro phosphoryl chloride and the N-H in the amino group-containing compounds.

In this study, a novel spiro-P-based reactive flame retardant (SPDPT) was synthesized through the one-pot reaction of P oxychloride, pentaerythritol, and triacetone diamine. SPDPT was used as a co-curing agent for 4′4-diaminodiphenyl sulfone (DDS) to cure EP and produce the desired flame-retardant epoxy thermoset. A series of tests was conducted to examine the curing properties of SPDPT and the mechanical properties, flammability, and thermal stability of the flame-retardant epoxy thermoset.

EXPERIMENTAL TESTS

Subsection

Epoxy resin (DGEBA CYD-128) was purchased from the Baling Petrochemical Branch of Sinopec Group Asset Management Co., Ltd., with an epoxy equivalent of approximately 196 g/eq. Triacetone diamine and DDS were purchased from Aladdin Industrial Corporation. Acetonitrile, P oxychloride, methylene chloride, and pentaerythritol were purchased from Sinopharm Chemical Reagent Co., Ltd.

Synthesis of SPDPT

Spiro-P-based reactive flame retardant was synthesized by using the simple one-pot method, and its synthetic route is shown in **Figure 1**.

In a 500-ml three-necked flask equipped with a magnetic stirrer, a thermometer, and a condenser, 13.6 g (0.1 mol) of pentaerythritol and 168.3 g (1.1 mol) of P oxychloride were added and then heated to 130°C (reflux temperature) until no hydrogen chloride gas is produced, in which case the reaction was stopped and the product was cooled to room temperature. The product was filtered, washed twice with distilled water, washed thrice with dichloromethane, and finally dried in a vacuum oven at 50°C for 24 h.

While introducing N_2 gas, 15.65 g (0.11 mol) of triacetone diamine, 300 ml of acetonitrile, and 14.85 g (0.05 mol) of SPDPC were added into a 500-ml three-necked flask equipped with a magnetic stirrer, an oil seal, and a condenser. After the SPDPC was evenly mixed, the solution was first heated to 30°C for a 3-h reaction and then heated to 50°C for another 3-h reaction, after which the product was washed three times with dichloromethane and finally dried in a vacuum oven at 50°C for 24 h.

Preparation of the Epoxy Thermoset

The SPDPT flame-retardant epoxy thermosets (EP/DDS/SPDPT) with different P contents were obtained through the polymerization among EP, DDM, and SPDPT, where SPDPT is the co-curing agent for DDS, and the sum of the active hydrogen equivalents of DDS and SPDPT is consistent with the epoxy equivalent of EP (see **Table 1**). SPDPT and DDS were added to the EP at a temperature of 110°C, stirred to mix evenly, and vacuum-defoamed. After the solution became transparent, the solution was poured into a mold preheated to 100°C. The mold was subsequently placed in an electric blast drying oven and cured at 130°C, 150°C, 170°C, and 190°C for 2 h After curing, the mold was naturally cooled to room temperature to obtain the SPDPT flame-retardant epoxy thermoset. The preparation process of the pure epoxy thermoset (EP/DDS) was similar to that of the EP/DDS/SPDPT thermoset with no SPDPT added.

Preparation of DSC Epoxy Compound for Test Use

A certain amount of EP and SPDPT (epoxy equivalent in EP is equal to the active hydrogen equivalent in SPDPT) was added and stirred to an appropriate amount of acetone, thereby and, uniformly dispersing the EP and the SPDPT in the acetone. The mixture was then dried at 40°C to obtain the EP/SPDPT compound. The preparation of the EP/DDS and EP/DDS/SPDPT compounds (see **Table 1**) was the same as that of the EP/SPDPT compound.

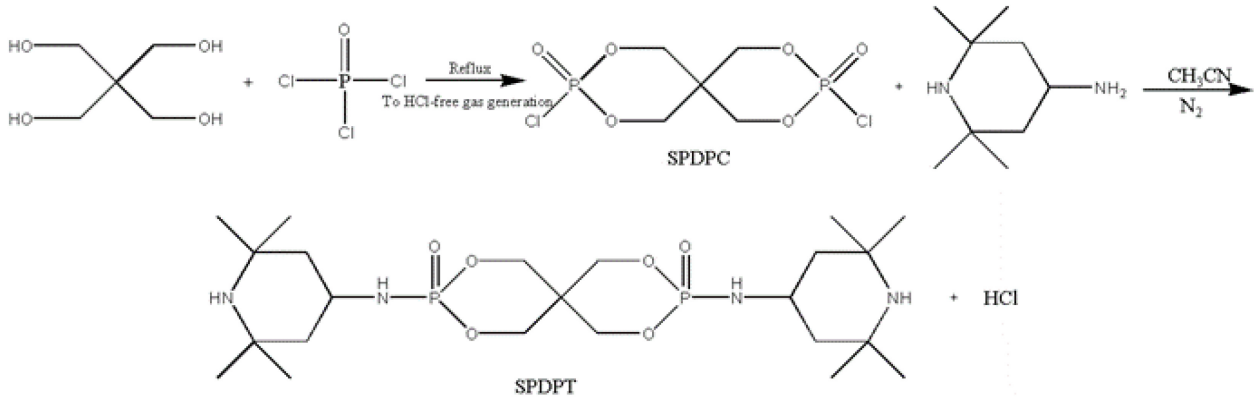

FIGURE 1 | Synthetic route of SPDPT.

Testing and Characterization

Fourier-transform infrared (FTIR) spectroscopy was performed using a United States-made Nicolet 6700 FTIR spectrometer. The samples and KBr were ground, mixed, and pressed into thin sheets (measurement range: 400–4000 m^{-1}).

^{1}H NMR spectroscopy and ^{31}P NMR spectroscopy were performed using an Agilent 400AR NMR spectrometer and deuterated dimethyl sulfoxide (DMSO-d_6).

Elemental analysis was performed using the Germany-made Vario EL cube element analyzer to determine the C, hydrogen, and N contents of the sample.

Differential scanning calorimetry (DSC) was performed using a Perkin-Elmer DSC 4000 differential scanning calorimeter under N atmosphere at a ramp rate of 10°C/min and a temperature range of 25–250°C.

Thermogravimetric analysis (TGA) was performed using a Germany-made NETZSCH STA409PC thermogravimetric analyzer under N atmosphere at a ramp rate of 10°C/min (heating from room temperature to 700°C).

The limiting O index (LOI) was tested pursuant to the ASTM D2863 standard using a JF3 O index meter manufactured by Nanjing Jiangning Analytical Instrument Co., Ltd. The standard size of the sample was 100 mm × 6.5 mm × 3 mm.

The flammability rating (UL 94) was measured pursuant to the GBT2408 2008 standard (the latest Chinese standard) using a NK8017A UL94 vertical burning test machine manufactured by Dongguan Nayu Testing Equipment Co., Ltd. The standard size of the sample was 130 mm × 13 mm × 3 mm.

TABLE 1 | The detailed formulations of EP samples.

Sample	EP (g)	SPDPT (g)	DDS (g)	P content (wt%)
EP/DDS	75.97		24.03	0
EP/DDS/SPDPT-1	75.09	2.16	22.75	0.25
EP/DDS/SPDPT-2	74.21	4.31	21.48	0.5
EP/DDS/SPDPT-3	73.33	6.47	20.20	0.75
EP/DDS/SPDPT-4	72.45	8.62	18.93	1

Tensile property was tested on a GP-TS2000S universal testing machine (at the testing temperature of 25°C, a tensile rate of 5 mm/min), the testing method with reference to GB/T2567-2008.

Flexural property was tested on a GP-TS2000S universal testing machine (at the testing temperature of 25°C, a flexural rate of 2 mm/min), the testing method with reference to GB/T2567-2008.

Impact property was tested on a XJJD-50 impact testing machine (at the testing temperature of 25°C), the testing method with reference to GB/T2570-1995, the specimen size with reference to GB1043-93.

TEST RESULTS

Infrared Analysis of SPDPC and SPDPT

Figure 2 shows the infrared spectra of the intermediate product (e.g., SPDPC) and the final product (e.g., SPDPT). The absorption curve of SPDPC shows that the characteristic absorption peaks of P = O, P-O-C, P-O, and P-Cl appear at 1305, 1023, 858, and 546 cm^{-1}, respectively. On the absorption curve of SPDPT, the characteristic absorption peaks of $-NH_2$ appear at 3430, 3221, and 1626 cm^{-1}; that of P = O appears at 1226 cm^{-1}; that of P-O-C appears at 1023 cm^{-1}; that of P-O appears at 833 cm^{-1}; and that of P-N appears at 1079 cm^{-1}. An obvious characteristic absorption peak of P-Cl (546 cm^{-1}) can be observed on the absorption curve of SPDPC, but this peak does not appear on the absorption curve of SPDPT. Instead, the characteristic absorption peak of P-N (1079 cm^{-1}) appears on the absorption curve of SPDPT, indicating that SPDPC reacts with triacetone diamine to form SPDPT.

NMR Spectroscopy of SPDPC and SPDPT

Figure 3 shows the ^{1}H NMR spectra of the intermediate product (e.g., SPDPC) and the final product (e.g., SPDPT). According to the ^{1}H NMR spectrum of SPDPT, the chemical shifts of imino hydrogen on the piperidine and connecting piperidine rings

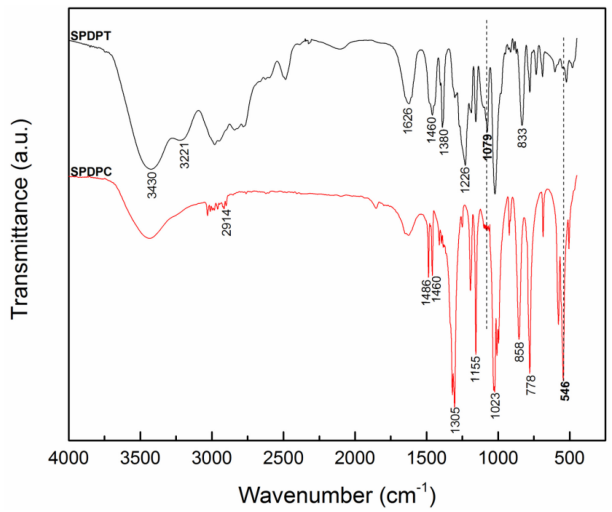

FIGURE 2 | Infrared spectra of SPDPC and SPDPT.

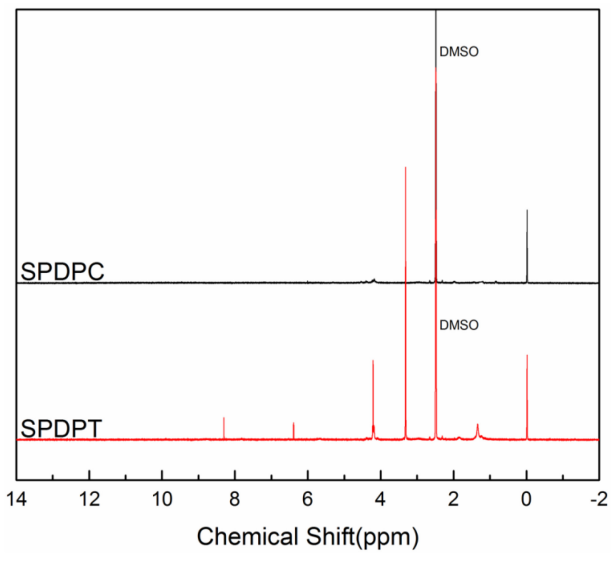

FIGURE 3 | ^{1}H NMR spectra of SPDPC and SPDPT.

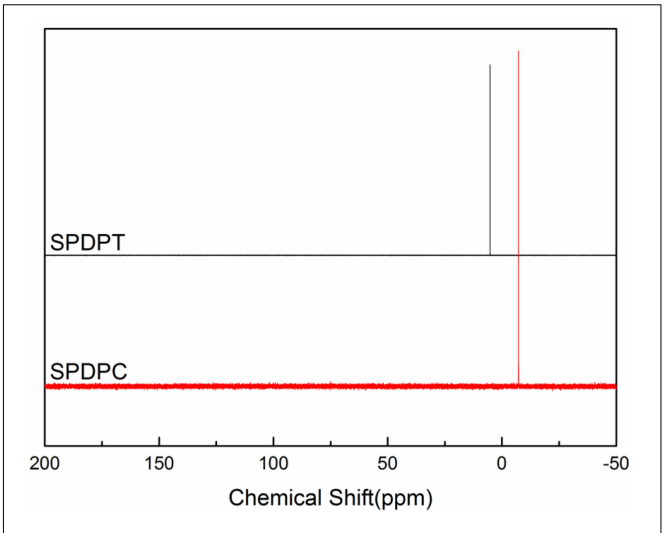

FIGURE 4 | ^{31}P NMR spectra of SPDPC and SPDPT.

TABLE 2 | Elemental analysis of SPDPT.

Element	C	H	N	ratio
Calculate	42.12	6.89	8.77	6:1:1
Found	51.49	8.58	10.45	6:1:1

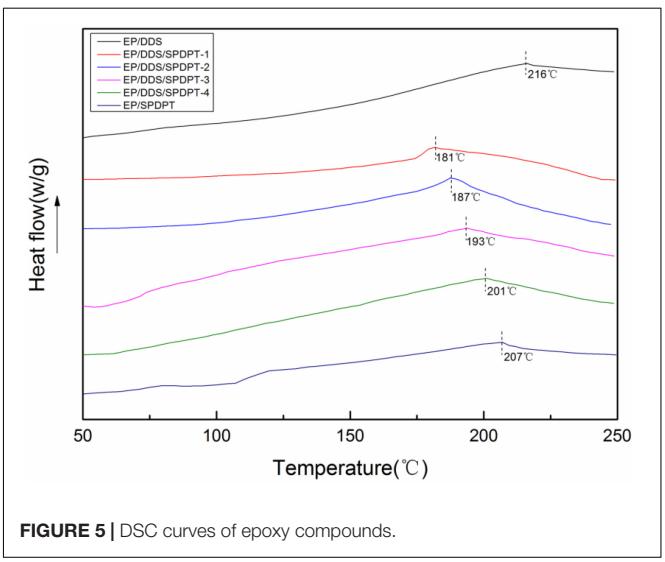

FIGURE 5 | DSC curves of epoxy compounds.

appear at 8.31 and 6.38 ppm, respectively; and the chemical shifts of methylene hydrogen, methyl hydrogen, and methine hydrogen on the piperidine ring appears at 4.22, 3.27–3.33, and 1.29–1.38 ppm, respectively. According to the ^{1}H NMR spectrum of SPDPC, the methylene hydrogen in the spiro ring is at −0.02 ppm and is present in the NMR spectrum of SPDPT, indicating that SPDPC reacted with triacetone diamine to produce SPDPT.

Figure 4 shows the ^{31}P NMR spectra of the intermediate product (e.g., SPDPC) and the final product (e.g., SPDPT). The two spectra differ significantly. The signal peak of SPDPT appears at 5.22 ppm, whereas that of SPDPC appears at −7.29 ppm, indicating that SPDPT and SPDPC are two different P compounds. This finding further points to the fact that SPDPC and triacetone diamine reacted to form a new compound of SPDPT.

SPDPT Elemental Analysis

The chemical structure of SPDPT was further confirmed through elemental analysis, and the results of which are shown in **Table 2**. **Table 2** shows that the measured actual contents of C, hydrogen, and N in SPDPT are almost the same as the theoretical contents.

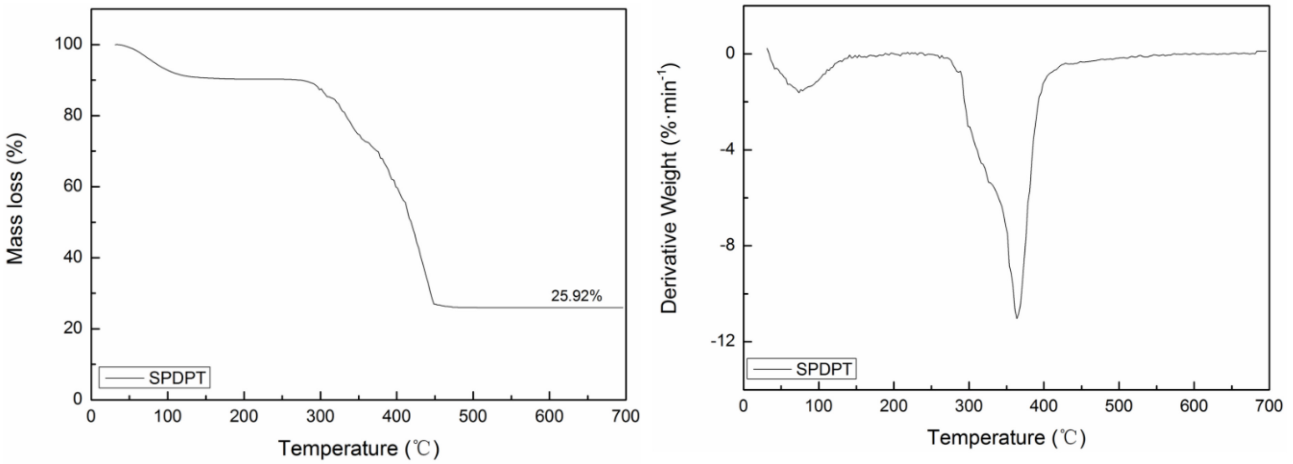

FIGURE 6 | TG and DTG curves of SPDPT.

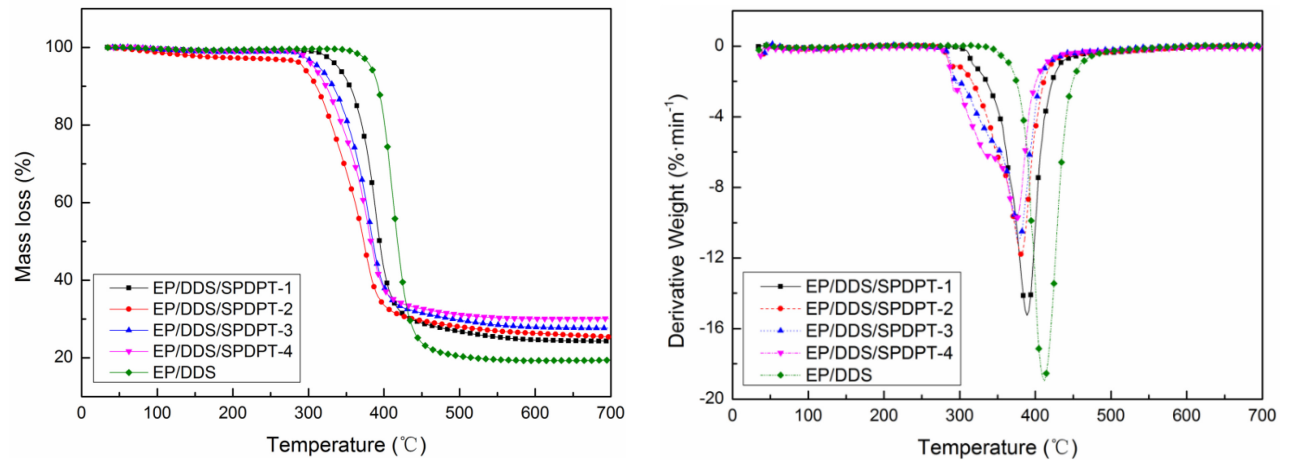

FIGURE 7 | TG and DTG curves of epoxy thermoset.

Reactivity of Epoxy Compound

The curing behavior of the epoxy compounds was measured through DSC. **Figure 5** shows the DSC curves of the EP/DDS, EP/DDS/SPDPT, and EP/SPDPT epoxy compounds. Only one curing exothermic peak appears on each curve. **Figure 5** shows that a significant curing exothermic peak appears on the DSC curve of the EP/SPDPT compound at approximately 207°C, indicating that the imino group in the SPDPT can react with the epoxy group in the EP. That is, SPDPT can cure EP. Moreover, the peak temperature at the curing exothermic peak of the EP/SPDPT compound is apparently lower than that of the EP/DDS compound. The peak temperature at the curing exothermic peak of the EP/DDS/SPDPT compound increases with the SPDPT content because the introduction of the rigid phenanthroline group in the SPDPT enhances the steric hindrance of the SPDPT molecule, thereby weakening the curing activity of SPDPT.

Thermal Stability

The thermal stability of SPDPT and the epoxy thermoset was evaluated under N_2 atmosphere using TGA. The TGA and DTG curves of the SPDPT, EP/DDS, and EP/DDS/SPDPT thermosets are shown in **Figures 6–9**. The characteristic data, such as the 5% mass loss ($T_{5\%}$), the maximum degradation at maximum rate of mass loss (T_{max}), and the C residue yield at 700°C (Y_c), are provided in **Table 3**.

Figure 6 shows that during the decomposition of SPDPT, the $T_{5\%}$ of SPDPT is 285°C, and the residual C of SPDPT at 700°C is 26%, indicating that SPDPT decomposes during combustion and produces a large amount of volatile matter.

For the EP/DDS and EP/DDS/SPDPT thermosets (**Figure 7**), the DTG curve has only one weight loss peak. T_{max} of the EP/DDS/SPDPT thermoset decrease gradually with the increase in the SPDPT content. The residual C yield of the EP/DDS/SPDPT thermoset increases at 700°C with the addition of SPDPT.

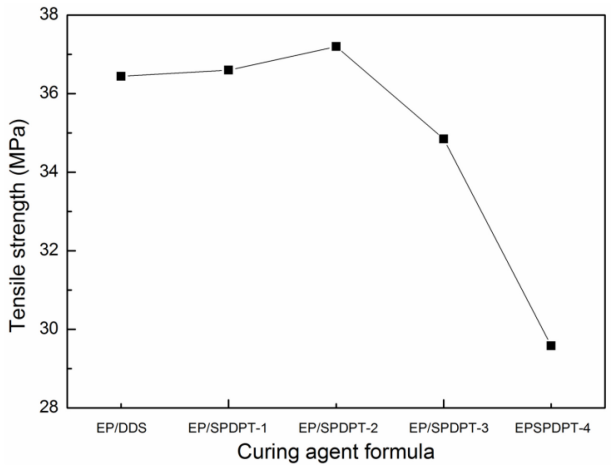

FIGURE 8 | Tensile properties of epoxy thermosets.

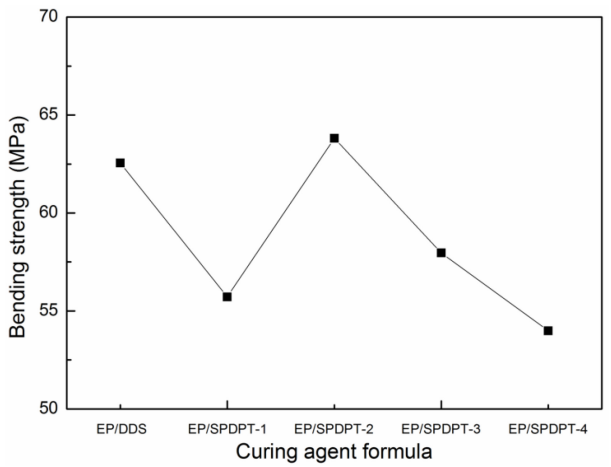

FIGURE 9 | Bending properties of epoxy thermosets.

TABLE 3 | Thermal degradation characteristics of SPDPT and epoxy thermosets.

Sample	T5% (°C)	T_{max} (°C)	Yc (%)
SPDPT	285.5	–	26.0
EP/DDS	361.6	412.4	19.3
EP/DDS/SPDPT/0.25%	322.9	389.4	24.0
EP/DDS/SPDPT/0.5%	284.3	379.8	25.4
EP/DDS/SPDPT/0.75%	297.5	377.2	27.8
EP/DDS/SPDPT/1%	289.1	374.8	30.1

Burning Test

The flammability of the epoxy thermoset was evaluated by LOI and UL-94 vertical burning experiments. **Table 4** shows the corresponding test results.

Table 4 shows that the LOI value of the epoxy thermoset significantly increases from 20.2 for EP/DDS to 26.4 for EP/DDS/SPDPT, with the P content being only 1%. The EP/DDS thermoset failed to pass the UL-94 test, whereas EP/DDS/SPDPT-3 and EP/DDS/SPDPT-4 reached the V-0 rating, and all the EP/DDS/SPDPT thermosets did not show dripping.

TABLE 4 | LOI and UL-94 test results of epoxy thermosets.

Sample code	P (wt%)	LOI (vol%)	UL94 (3 mm)	Dripping
EP/DDS	0	20.2	Failed	Yes
EP/DDS/SPDPT-1	0.25	23.4	V-1	No
EP/DDS/SPDPT-2	0.5	24.1	V-1	No
EP/DDS/SPDPT-3	0.75	25.2	V-0	No
EP/DDS/SPDPT-4	1	26.4	V-0	No

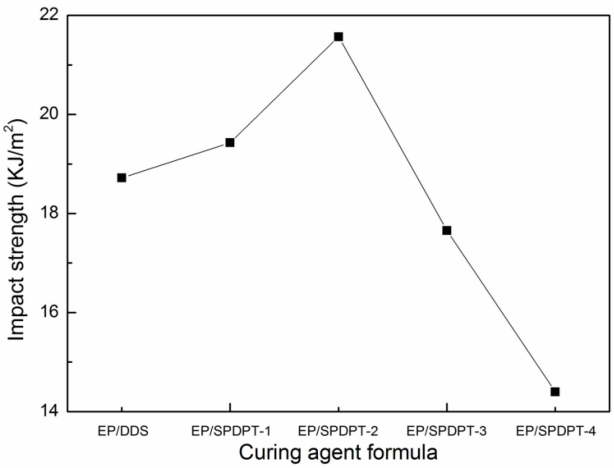

FIGURE 10 | Impact properties of epoxy thermosets.

Mechanical Properties of Epoxy Thermosets

Figure 8 shows the tensile property of the epoxy thermosets. Among the EP/DDS/SPDPT thermosets, EP/DDS/SPDPT-2 (P content = 0.5%) produces the best tensile property of 37.20 MPa.

Figure 9 shows the flexural property of the epoxy thermosets. EP/DDS/SPDPT-2 (P content = 0.5%) demonstrates the best flexural property of 63.82 MPa.

Figure 10 shows the impact property of the epoxy thermosets. EP/DDS/SPDPT-2 (P content = 0.5%) demonstrates the best impact property of 24.57 KJ·m^{-2}.

Figures 8–10 show that the addition of the flame-retardant curing agent SPDPT exerted a certain impact on the mechanical properties of the epoxy thermosets. The tensile, flexural, and impact properties of the EP increased first and then decreased with the increase in the P content in the EP, indicating that the addition of SPDPT can improve the mechanical properties of the EP system.

The tensile property, the flexural strength, and the impact property reached 37.20 MPa, 63.82 MPa, and 21.57 KJ·m^{-2}, respectively.

CONCLUSION

A novel flame-retardant curing agent that contained piperidine groups was successfully synthesized and used as a reactive flame-retardant curing agent to prepare the desired flame-retardant epoxy thermosets. The EP/DDS/SPDPT epoxy thermosets showed a higher C residue yield at 700°C than the EP/DDS sample. the flame retardancy and mechanical properties of the epoxy thermoset will be improved significantly by adding SPDPT at a low P content. As an EP curing agent, the SPDPT can be prepared easily, and the raw material can also be obtained easily. Therefore, SPDPT boasts great application prospects.

DATA AVAILABILITY STATEMENT

All datasets presented in this study are included in the article/supplementary material.

AUTHOR CONTRIBUTIONS

YC and YP: conceptualization. LY: methodology, formal analysis, and writing – original draft preparation. YC: software, resources, supervision, project administration, and funding acquisition. LY and ZH: validation. ZH: investigation. YP: data curation and writing – review and editing. All authors contributed to the article and approved the submitted version.

FUNDING

This research was funded by the National Natural Science Foundation of China, grant number 21376182.

ACKNOWLEDGMENTS

The authors would like to thank the editor and reviewers.

REFERENCES

Aubert, M., Wilén, C., Pfaendner, R., Kniesel, S., Hoppe, H., and Roth, M. (2011). Bis (1-propyloxy-2, 2, 6, 6-tetramethylpiperidin-4-yl)-diazene–An innovative multifunctional radical generator providing flame retardancy to polypropylene even after extended artificial weathering. *Polym. Degrad. Stab.* 96, 328–333. doi: 10.1016/j.polymdegradstab.2010.02.035

Chen, D., Wang, Y., Hu, X., Wang, D., Qu, M., and Yang, B. (2005). Flame-retardant and anti-dripping effects of a novel char-forming flame retardant for the treatment of poly (ethylene terephthalate) fabrics. *Polym. Degrad. Stab.* 88, 349–356. doi: 10.1016/j.polymdegradstab.2004.11.010

Chu, F., Ma, C., Zhang, T., Xu, Z., Mu, X., Cai, W., et al. (2020). Renewable vanillin-based flame retardant toughening agent with ultra-low phosphorus loading for the fabrication of high-performance epoxy thermoset. *Compos. Part B Eng.* 190:107925. doi: 10.1016/j.compositesb.2020.107925

Deng, P., Liu, Y., Liu, Y., Xu, C., and Wang, Q. (2018). Preparation of phosphorus−containing phenolic resin and its application in epoxy resin as a curing agent and flame retardant. *Polym. Adv. Technol.* 29, 1294–1302. doi: 10.1002/pat.4241

Ding, J., Zhang, Y., Zhang, X., Kong, Q., Zhang, J., Liu, H., et al. (2020). Improving the flame-retardant efficiency of layered double hydroxide with disodium phenylphosphate for epoxy resin. *J. Therm. Anal. Calorim.* 140, 149–156. doi: 10.1007/s10973-019-08372-9

Huang, C., Chen, X., Yuan, B., Zhang, H., Dai, H., He, S., et al. (2019). Suppression of wood dust explosion by ultrafine magnesium hydroxide. *J. Hazard. Mater.* 378:120723. doi: 10.1016/j.jhazmat.2019.05.116

Huo, S., Wang, J., Yang, S., Li, C., Wang, X., and Cai, H. (2019). Synthesis of a DOPO-containing imidazole curing agent and its application in reactive flame retarded epoxy resin. *Polym. Degrad. Stab.* 159, 79–89. doi: 10.1016/j.polymdegradstab.2018.11.021

Huo, S., Wang, J., Yang, S., Wang, J., Zhang, B., Zhang, B., et al. (2016). Synthesis of a novel phosphorus-nitrogen type flame retardant composed of maleimide, triazine-trione, and phosphaphenanthrene and its flame retardant effect on epoxy resin. *Polym. Degrad. Stab.* 131, 106–113. doi: 10.1016/j.polymdegradstab.2016.07.013

Huo, S., Wang, J., Yang, S., Zhang, B., Chen, X., Wu, Q., et al. (2017). Synthesis of a novel reactive flame retardant containing phosphaphenanthrene and piperidine groups and its application in epoxy resin. *Polym. Degrad. Stab.* 146, 250–259. doi: 10.1016/j.polymdegradstab.2017.10.015

Jian, R., Wang, P., Xia, L., Yu, X., Zheng, X., and Shao, Z. (2017). Low-flammability epoxy resins with improved mechanical properties using a Lewis base based on phosphaphenanthrene and 2-aminothiazole. *J. Mater. Sci.* 52, 9907–9921. doi: 10.1007/s10853-017-1102-x

Li, H., Liu, J., Zhao, W., Wang, X., and Wang, D. (2016). Synthesis of a novel self-intumescent flame retardant with spiro and triazine structure and its performance for polypropylene. *J. Fire Sci.* 34, 104–119. doi: 10.1177/0734904115621929

Lin, C., Chou, Y., Shiao, W., and Wang, M. (2016). High temperature, flame-retardant, and transparent epoxy thermosets prepared from an acetovanillone-based hydroxyl poly (ether sulfone) and commercial epoxy resins. *Polymer* 97, 300–308. doi: 10.1016/j.polymer.2016.05.035

Luo, Q., Sun, Y., Yu, B., Li, C., Song, J., Tan, D., et al. (2019). Synthesis of a novel DPPA−containing benzoxazine to flame−retard epoxy resin with maintained thermal properties. *Polym. Adv. Technol.* 30, 1989–1995. doi: 10.1002/pat.4631

Luo, Q., Yuan, Y., Dong, C., Liu, S., and Zhao, J. (2015). Intumescent flame retardancy of a DGEBA epoxy resin based on 5, 10-dihydro-phenophosphazine-10-oxide. *RSC Adv.* 5, 68476–68484. doi: 10.1039/c5ra11847f

Ma, S., Hou, Y., Xiao, Y., Chu, F., Cai, T., Hu, W., et al. (2020). Metal-organic framework@polyaniline nanoarchitecture for improved fire safety and mechanical performance of epoxy resin. *Mater. Chem. Phys.* 247:122875. doi: 10.1016/j.matchemphys.2020.122875

Ma, T., Li, L., Liu, T., and Guo, C. (2019). Synthesis of a caged bicyclic phosphates derived anhydride and its performance as a flame−retardant curing agent for epoxy resins. *Polym. Adv. Technol.* 30, 1314–1324. doi: 10.1002/pat.4565

Mestry, S., and Mhaske, S. (2019). Synthesis of epoxy resins using phosphorus-based precursors for flame-retardant coating. *J. Coat. Technol. Res.* 16, 807–818. doi: 10.1007/s11998-018-00157-3

Perret, B., Schartel, B., Stöß, K., Ciesielski, M., Diederichs, J., Döring, M., et al. (2011a). A new halogen−free flame retardant based on 9, 10−dihydro−9−oxa−10−phosphaphenanthrene−10−oxide for epoxy resins and their carbon fiber composites for the automotive and aviation industries. *Macromol. Mater. Eng.* 296, 14–30. doi: 10.1002/mame.201000242

Perret, B., Schartel, B., Stöß, K., Ciesielski, M., Diederichs, J., Döring, M., et al. (2011b). Novel DOPO-based flame retardants in high-performance carbon fibre epoxy composites for aviation. *Eur. Polym. J.* 47, 1081–1089. doi: 10.1016/j.eurpolymj.2011.02.008

Qiu, Y., Qian, L., and Xi, W. (2016). Flame-retardant effect of a novel phosphaphenanthrene/triazine-trione bi-group compound on an epoxy thermoset and its pyrolysis behaviour. *RSC Adv.* 6, 56018–56027. doi: 10.1039/c6ra10752d

Shang, S., Yuan, B., Sun, Y., Chen, G., Huang, C., Yu, B., et al. (2019). Facile preparation of layered melamine-phytate flame retardant via supramolecular self-assembly technology. *J. Colloid Interface Sci.* 553, 364–371. doi: 10.1016/j.jcis.2019.06.015

Shi, Y., Yu, B., Duan, L., Gui, Z., Wang, B., Hu, Y., et al. (2017). Graphitic carbon nitride/phosphorus-rich aluminum phosphinates hybrids as smoke suppressants and flame retardants for polystyrene. *J. Hazard. Mater.* 332, 87–96. doi: 10.1016/j.jhazmat.2017.03.006

Tang, G., Liu, X., Yang, Y., Chen, D., Zhang, H., Zhou, L., et al. (2020a). Phosphorus-containing silane modified steel slag waste to reduce fire hazards of rigid polyurethane foams. *Adv. Powder Technol.* 31, 1420–1430. doi: 10.1016/j.apt.2020.01.019

Tang, G., Liu, X., Zhou, L., Zhang, Z., Deng, D., and Jiang, H. (2020b). Steel slag waste combined with melamine pyrophosphate as a flame retardant for rigid polyurethane foams. *Adv. Powder Technol.* 31, 279–286. doi: 10.1016/j.apt.2019.10.020

Wang, C., Wu, Y., Li, Y., Shao, Q., Yan, X., Han, C., et al. (2018). Flame−retardant rigid polyurethane foam with a phosphorus−nitrogen single intumescent flame retardant. *Polym. Adv. Technol.* 29, 668–676. doi: 10.1002/pat.4105

Wang, P., Xia, L., Jian, R., Ai, Y., Zheng, X., Chen, G., et al. (2018). Flame-retarding epoxy resin with an efficient P/N/S-containing flame retardant: preparation, thermal stability, and flame retardance. *Polym. Degrad. Stab.* 149, 69–77. doi: 10.1016/j.polymdegradstab.2018.01.026

Wang, X., Xu, M., Zhang, Z., Leng, Y., and Li, B. (2018). Synthesis of a novel N-alkoxyamine containing compound and its application as an effective flame retardant for polypropylene film by quenching free radical. *J. Anal. Appl. Pyrolysis* 134, 243–253. doi: 10.1016/j.jaap.2018.06.014

Xie, H., Lai, X., Li, H., and Zeng, X. (2016). Synthesis of a novel macromolecular charring agent with free-radical quenching capability and its synergism in flame retardant polypropylene. *Polym. Degrad. Stab.* 130, 68–77. doi: 10.1016/j.polymdegradstab.2016.05.029

Xu, W., Wang, X., Wu, Y., Li, W., and Chen, C. (2019). Functionalized graphene with Co-ZIF adsorbed borate ions as an effective flame retardant and smoke suppression agent for epoxy resin. *J. J. Hazard. Mater.* 363, 138–151. doi: 10.1016/j.jhazmat.2018.09.086

Xu, W., Wirasaputra, A., Liu, S., Yuan, Y., and Zhao, J. (2015). Highly effective flame retarded epoxy resin cured by DOPO-based co-curing agent. *Polym. Degrad. Stab.* 122, 44–51. doi: 10.1016/j.polymdegradstab.2015.10.012

Yuan, B., Hu, Y., Chen, X., Shi, Y., Niu, Y., Zhang, Y., et al. (2017). Dual modification of graphene by polymeric flame retardant and Ni (OH)2 nanosheets for improving flame retardancy of polypropylene. *Compos. Part A Appl. Sci. Manuf.* 100, 106–117. doi: 10.1016/j.compositesa.2017.04.012

Yuan, B., Sun, Y., Chen, X., Shi, Y., Dai, H., and He, S. (2018). Poorly-/well-dispersed graphene: Abnormal influence on flammability and fire behavior of intumescent flame retardant. *Compos. Part A Appl. Sci. Manuf.* 109, 345–354. doi: 10.1016/j.compositesa.2018.03.022

Zhan, J., Song, L., Nie, S., and Hu, Y. (2009). Combustion properties and thermal degradation behavior of polylactide with an effective intumescent flame retardant. *Polym. Degrad. Stab.* 94, 291–296. doi: 10.1016/j.polymdegradstab.2008.12.015

Zhang, Q., Yang, S., Wang, J., Cheng, J., Zhang, Q., Ding, G., et al. (2019). A DOPO based reactive flame retardant constructed by multiple heteroaromatic groups and its application on epoxy resin: curing behavior, thermal degradation and flame retardancy. *Polym. Degrad. Stab.* 167, 10–20. doi: 10.1016/j.polymdegradstab.2019.06.020

Zhang, Y., Yu, B., Wang, B., Liew, K., Song, L., Wang, C., et al. (2017). Highly effective P–P synergy of a novel DOPO-based flame retardant for epoxy resin. *Indust. Eng. Chem. Res.* 56, 1245–1255. doi: 10.1021/acs.iecr.6b04292

Zhao, J., Dong, X., Huang, S., Tian, X., Song, L., Yu, Q., et al. (2018). Performance comparison of flame retardant epoxy resins modified by DPO–PHE and DOPO–PHE. *Polym. Degrad. Stab.* 156, 89–99. doi: 10.1016/j.polymdegradstab.2018.08.007

Conflict of Interest: The authors declare that the research was conducted in the absence of any commercial or financial relationships that could be construed as a potential conflict of interest.

The reviewer BY declared a shared affiliation, with no collaboration, with one of the authors to the handling editor at the time of review.

frontiers in Materials

ORIGINAL RESEARCH
published: 22 September 2020
doi: 10.3389/fmats.2020.588518

Effect of Graphene Oxide–Modified Cobalt Nickel Phosphate on Flame Retardancy of Epoxy Resin

Qinghong Kong[1], Caijiao Zhang[1], Guolin Zheng[1], Manman Zhang[1], Tao Zhou[1], Junhao Zhang[2]*, Xingmei Guo[2] and Yibing Cai[3]*

[1] School of the Environment and Safety Engineering, Jiangsu University, Zhenjiang, China, [2] School of Environmental and Chemical Engineering, Jiangsu University of Science and Technology, Zhenjiang, China, [3] Key Laboratory of Eco-textiles, Ministry of Education, Jiangnan University, Wuxi, China

OPEN ACCESS

Edited by:
Yongqian Shi,
Fuzhou University, China

Reviewed by:
Gang Tang,
Anhui University of Technology, China
Yuezhan Feng,
Zhengzhou University, China
Chuyuan Huang,
Wuhan University of Technology, China
Wenzong Xu,
Anhui Jianzhu University, China

****Correspondence:***
Qinghong Kong
kongqh@mail.ujs.edu.cn
Junhao Zhang
mailto:jhzhang6@just.edu.cn

Specialty section:
This article was submitted to Polymeric and Composite Materials, Geomorphology and Paleoenvironment, a section of the journal Frontiers in Materials

Received: *29 July 2020*
Accepted: *24 August 2020*
Published: *22 September 2020*

Citation:
Kong Q, Zhang C, Zheng G, Zhang M, Zhou T, Zhang J, Guo X and Cai Y (2020) Effect of Graphene Oxide–Modified Cobalt Nickel Phosphate on Flame Retardancy of Epoxy Resin. Front. Mater. 7:588518. doi: 10.3389/fmats.2020.588518

Synergistic effect is an effective strategy for improving the flame retardancy of epoxy resin (EP). In this work, a novel graphene oxide–cobalt nickel phosphate (GO-$NiCoPO_3$) is successfully synthesized, which is incorporated into an EP matrix for preparing EP/GO-$NiCoPO_3$ nanocomposites. The results show that the limiting oxygen index value of EP/4GO-$NiCoPO_3$ nanocomposites is as high as 30.3%, and UL-94 can reach V-1 rating. The results of micro-combustion calorimetry indicate that the total heat release value and peak of heat release rate of EP/8GO-$NiCoPO_3$ nanocomposites are decreased by 41.9 and 23.8% compared with those of pure EP. This is mainly due to the synergistic barrier effect of GO and $NiCoPO_3$, which together have their own advantages. Meanwhile, EP/GO-$NiCoPO_3$ nanocomposites can form a dense char layer during the burning process and improve the thermal stability of EP/GO-$NiCoPO_3$ nanocomposites.

Keywords: epoxy resin, graphene oxide–cobalt nickel phosphate, thermal stability, flame retardancy, synergistic barrier effect

INTRODUCTION

Epoxy resin (EP) is well known for its excellent mechanical and chemical properties and has been used in various fields such as electronics and insulating materials. (Kong et al., 2017a; Li et al., 2018; Xu et al., 2019; Ding et al., 2020; Nie et al., 2020). However, its severe flammability with toxic gases and smoke during combustion limits its wide application (Zhang et al., 2018; Kong et al., 2019c; Yang et al., 2019). Therefore, searching for efficient and environmentally friendly flame retardants that can reduce the flammability of EP has become the pursuit of many researchers.

In recent years, transition metals and phosphorus-containing compounds have been found to have excellent ability to catalyze the formation of char and catalyze the conversion of harmful substances, arousing wide attention of researchers (Zheng et al., 2017; Sun et al., 2018; Feng et al., 2019; Kong et al., 2019a; Zhang et al., 2019; Zhou et al., 2019). A new flame retardant (P-$MnMo_6$) was synthesized with 9,10-dihydro-9-oxa-10-phosphaphenanthrene-10-oxide (DOPO) with polyoxometalate and added to EP (Peng et al., 2020). The results demonstrated that the peak of heat release rate (PHRR) of EP/P-$MnMo_6$-4 nanocomposites was reduced by 41% and the char yield increased significantly, and CO and smoke emissions were also greatly suppressed. In particular, the addition of ultra-thin layered nanomaterials can increase the viscosity of a polymer and form an insulating char layer during the combustion process, thereby slowing the oxygen overflow rates and reducing the amount of combustible gas (Kong et al., 2018b, Asabina et al., 2019, Kong et al., 2019b). For example, the hybrid NiFe-LDH-MoS_2 was prepared by a simple self-assembly method and blended into EP to

prepare EP/NiFe-LDH-MoS_2 nanocomposites. When 2 wt% NiFe-LDH-MoS_2 was added to EP, the PHRR and total heat release (THR) values were reduced by 66 and 34%, respectively. The output of smoke and toxic gas, such as CO and CO_2, was significantly reduced (Zhou et al., 2017). A multifunctional nanohybrid ($Ti_3C_2T_x$@MCA) was prepared by interacting titanium carbide nanosheets ($Ti_3C_2T_x$, MXene) with melamine cyanurate (MCA) *via* hydrogen bonding interactions. The significantly improved mechanical and fire-safe performances of TPU/$Ti_3C_2T_x$@MCA-3.0 were superior to those of thermoplastic polyurethane (TPU) nanocomposites filled with other nanoadditives (Shi et al., 2020). Therefore, it is possible that layered transition metal phosphide flame retardants could be prepared together with catalytic transition metals and phosphorus element, and applied to polymers, which will inevitably improve the flame retardancy of macromolecule polymers.

Graphene has attracted more and more attention in the flame retardancy of polymers due to its high specific surface area, thermal stability, and unique 2D structure (Cote et al., 2011; Yu et al., 2015; Cai et al., 2016; Xu et al., 2019). In particular, graphene oxide (GO), which has organic groups such as -OH, -COOH, and C-O, can enhance compatibility with a polymer matrix, thereby improving dispersibility in the polymer matrix (Huang et al., 2011; Kong et al., 2018a; Yue et al., 2019). DOPO was covalently bonded to GO and added to an EP matrix for preparing EP/DOPO-rGO nanocomposites. When 10 wt% DOPO-rGO was added, the char yield and limiting oxygen index (LOI) value were increased by 81 and 30%, respectively, and obviously improved the flame retardancy of the EP (Liao et al., 2012). A multifunctional hydrophilic graphene-based hybrid (RGO@$Ni(OH)_2$) containing $Ni(OH)_2$ nanoribbons and reduced GO (RGO) was synthesized, and hexagonal boron nitride sheets were simultaneously added into an EP matrix.

The PHRR, THR, and total smoke production values of EP/hexagonal boron nitride/RGO@$Ni(OH)_2$ nanocomposites were reduced by 33.5, 33.8, and 43.0%, respectively (Feng et al., 2020). A new graphene-based inorganic–organic hybrid flame retardant (GFR) was prepared by hybridization of functionalized GO and phenyl-bis-(triethoxysilylpropyl) phosphoramide; only with the addition of 1 wt% GFR in EP, the char yield was increased by 10.4%, and the PHRR and THR values were decreased by 43 and 44.7%, respectively (Mu et al., 2016).

Therefore, in combination with literature analysis, a type of ultra-thin flame retardant cobalt nickel phosphate ($NiCoPO_3$) nanoplates were successfully synthesized, which were grown on the surface of GO by the surface growth method. Then, the new hybrid flame retardant (GO-$NiCoPO_3$) was incorporated into the EP matrix to prepare EP/GO-$NiCoPO_3$ nanocomposites. Compared with other phosphorus-containing flame retardants, such as phosphorus-containing silane (Tang et al., 2020b), ammonium polyphosphate (Reuter et al., 2020), phosphazene-triazine bi-group (Chen et al., 2020), aluminum diethylphosphinate (Tang et al., 2020c), melamine phenylhypophosphonate (Zhu et al., 2020), and melamine pyrophosphate (Tang et al., 2020a), GO-$NiCoPO_3$ has nanoscale ultra-thin layered structures, which can have a layered barrier effect in the combustion process of polymer composites, and has more organic functional groups to better integrate with polymer composites. GO-$NiCoPO_3$ has low loading in polymers; hence, when only 4 wt% was added to EP, in the UL-94 tests, EP/4 GO-$NiCoPO_3$ nanocomposites passed V-1 rating.

EXPERIMENTAL SECTION

Materials

Graphite powder (spectral pure), potassium permanganate ($KMnO_4$, AR, ≥99.5%), cobalt(II) acetate tetrahydrate ($C_4H_6CoO_4{\cdot}4H_2O$, AR, ≥99.5%), nickel(II) acetate tetrahydrate ($C_4H_6NiO_4{\cdot}4H_2O$, AR, ≥98.0%), sodium pyrophosphate ($Na_4O_7P_2$, AR, ≥99.0%), acetone (C_3H_6O, AR, ≥99.5%), EP (NPEL128), and 4, 4-diaminodiphenyl methane (DDM, ≥98.0%) were purchased by Sinopharm Chemical Reagent Co., Ltd. Sodium nitrate ($NaNO_3$, AR, ≥99.0%) and hydrogen peroxide (H_2O_2, AR, ≥30%) were purchased from Wuxi Jingke Chemical Co., Ltd. Sulfuric acid (H_2SO_4, AR, 95–98%) was provided by Shanghai Jutai Special Reagent Co., Ltd. All chemicals were of analytical grade purity and used without any further purification.

Preparation of $NiCoPO_3$

$C_4H_6NiO_4{\cdot}4H_2O$ (0.4 g), $C_4H_6CoO_4{\cdot}4H_2O$ (0.478 g), $Na_4O_7P_2$ (0.839 g), and 10 ml of water were mixed together. Then, the above mixed solution was stirred at room temperature for 30 min and transferred to a 100-ml stainless steel autoclave lined with polytetrafluoroethylene heated at 180°C for 24 h. The products were washed several times with water and ethanol, and dried at 80°C for 24 h.

Preparation of GO-$NiCoPO_3$

GO was prepared by a modified Hummer's method (Yu et al., 2017). First, $C_4H_6NiO_4{\cdot}4H_2O$ (0.4 g), $C_4H_6CoO_4{\cdot}4H_2O$ (0.478 g), $Na_4O_7P_2$ (0.839 g), and 15 ml (1 g/l) of GO were mixed together. Then, the above mixed solution was stirred at room temperature for 30 min and transferred to a 100-ml stainless steel autoclave lined with polytetrafluoroethylene heated at 180°C for 24 h. The black products were centrifuged and dried under vacuum at 80°C for 24 h.

Preparation of Epoxy Resin/Graphene Oxide–Cobalt Nickel Phosphate Nanocomposites

First, GO-$NiCoPO_3$ was added to acetone and sonicated until completely dispersed; then, EP was added to the above solution and subjected to ultrasound. The homogenous system was stirred at 90°C, DDM was charged into the above system, and stirring was continued until DDM completely dissolved and blended vigorously for 5 min. The homogenized samples were rapidly poured into moulds and, cured at 110, 130, and 150°C/2 h. The preparation procedure of pure EP and EP/$NiCoPO_3$ nanocomposites was exactly the same as the above process. The specific contents are shown in **Table 1**.

Characterization

X-ray powder diffraction (XRD) has a graphite monochromatic diffraction line of Cu Kα, λ = 1.5418 Å, an operating voltage of

TABLE 1 | Ingredients of EP nanocomposites.

Sample	EP (wt%)	GO-$NiCoPO_3$ (wt%)	$NiCoPO_3$ (wt%)
EP	100	0	0
EP/1GO-$NiCoPO_3$	99	1	0
EP/2GO-$NiCoPO_3$	98	2	0
EP/4GO-$NiCoPO_3$	96	4	0
EP/6GO-$NiCoPO_3$	94	6	0
EP/8GO-$NiCoPO_3$	92	8	0
EP/4$NiCoPO_3$	96	0	4

EP, epoxy resin; Go, graphene oxide; $NiCoPO_3$, cobalt nickel phosphate.

40 kV, and current of 100 mA. The diffractometer was of the Japanese Rigaku MAX-RB model. Fourier transform infrared spectra (FTIR) were tested by the KBr tableting method, and the spectral frequency ranges from 400 to 4,000 cm^{-1}. It is a spectrometer of the 6700 model of Nicolet Instrument Co., Ltd. Scanning electron microscopy (SEM) and Transmission electro microscopy (TEM) were used to observe the microstructures and morphology of $NiCoPO_3$ and GO-$NiCoPO_3$. The acceleration voltage was 100 kV, and the transmission electron microscope was of the Japanese JEOL JEM-100SX model.

Thermogravimetric (TG) analysis was carried out using a TG/DSC1 device manufactured by METTLER TOLEDO under a nitrogen atmosphere with a linear heating rate of 10°C min^{-1}. LOI measurements were performed using an oxygen index model instrument (Fire Testing Technology, United Kingdom). The spline size was 130 mm^3 × 6.5 mm^3 × 3.2 mm^3 according to ASTM D 2863-97. Based on ASTM D 3801, the vertical combustion test (UL-94) was carried out in a combustion chamber (Fire Testing Technology, United Kingdom), and the spline size was 130 mm^3 × 12.7 mm^3 × 3.2 mm^3. Micro-combustion calorimetry (MCC) generally involved pulverizing a sample (5 mg) in a nitrogen stream (80 cm^3 min^{-1}). The cleavage product was mixed with a stream of oxygen (20 cm^3 min^{-1}) and then burned at 900°C. The furnace was heated to the desired temperature to obtain heat release parameters, which were measured using a MCC-2 calorimeter (Govmark, United States).

RESULTS AND DISCUSSION

Structure and Performance of Graphene Oxide–Cobalt Nickel Phosphate

The XRD is often used to investigate the lamellar structure and crystallinity of inorganic nanomaterials (Guo et al., 2020; Xue et al., 2020; Zhang et al., 2020). **Figure 1A** presents the XRD pattern of $NiCoPO_3$, which reveals the characteristic peaks at 2θ =

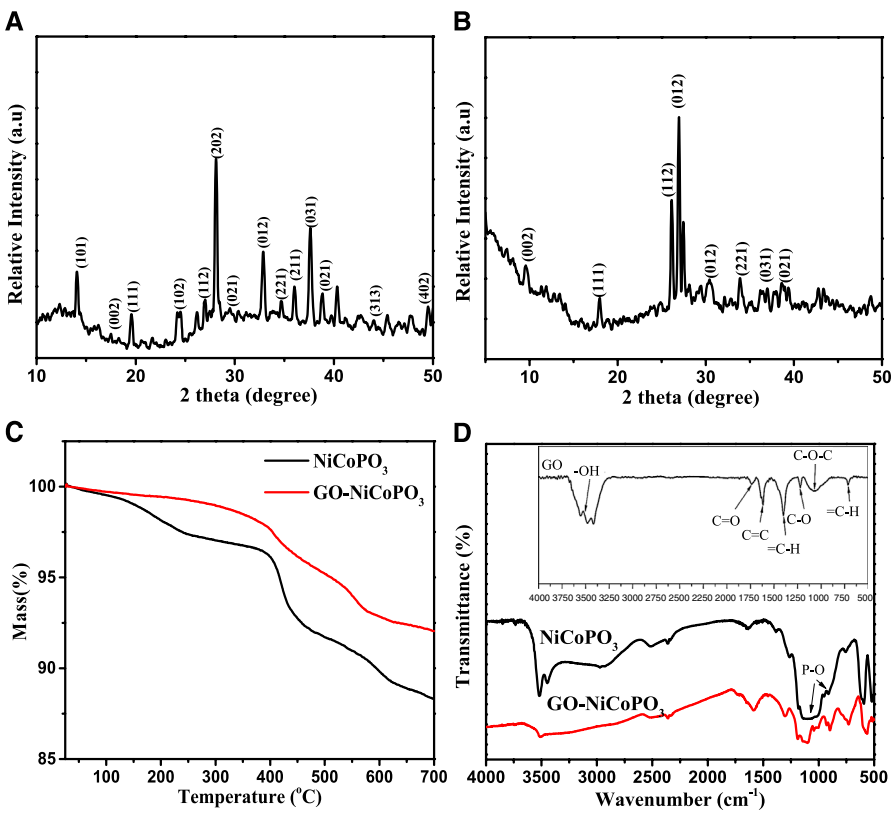

FIGURE 1 | (A) X-ray powder diffraction pattern of $NiCoPO_3$; **(B)** X-ray powder diffraction pattern of GO-$NiCoPO_3$; **(C)** TG curves of $NiCoPO_3$ and GO-$NiCoPO_3$; **(D)** Fourier transform infrared spectra spectra of $NiCoPO_3$ and GO-$NiCoPO_3$; the inset is Fourier transform infrared spectra legend of GO. Go, graphene oxide; $NiCoPO_3$, cobalt nickel phosphate.

13.3°, 17.9°, 26.1°, 26.7°, 26.9°, 27.4°, 29.9°, 33.8°, 38.6°, and 48.5°, corresponding to the orders of $Co_3(PO_4)_2$ on (101), (111), (102), (112), (202), (021), (012), (221), (031), and (402) planes, respectively. Simultaneously, the diffraction peaks are observed at 2θ = 17.5°, 23.5°, 26.0°, 37.2°, and 39.3°, corresponding to the position of $Ni_3(PO_4)_2$ on the (002), (102), (111), (211), and (021) (Li et al., 2017). **Figure 1B** shows the XRD pattern of GO-$NiCoPO_3$, and a weak characteristic diffraction peak of GO appears at 2θ = 9.8°, which may be caused by the low content of GO (Si and Samulski, 2008). GO has hydroxyl groups and carboxyl groups, and can form hydrogen bonds with the surface of $NiCoPO_3$, making the original strong diffraction peak weak. **Figure 1C** shows the TG curves of $NiCoPO_3$ and GO-$NiCoPO_3$. Before 200°C, due to dehydration of $NiCoPO_3$ nanosheets, $NiCoPO_3$, and GO-$NiCoPO_3$ had a little weight loss. After 200°C, $NiCoPO_3$ is decomposed into metaphosphoric acid and metal oxide, and the organic groups of GO also begin to decompose, but the weight loss of GO-$NiCoPO_3$ is less than that of $NiCoPO_3$ in the whole process (Zhu et al., 2010; Huang et al., 2016). The FTIR spectra of $NiCoPO_3$ and GO-$NiCoPO_3$ are shown in **Figure 1D**, and the FTIR legend of GO is embedded in the inset. The peak of 3,500 cm^{-1} corresponds to the -OH stretching vibration of $NiCoPO_3$, and the characteristic peaks of the P-O structure are 1,182, 1,174, and 938 cm^{-1}. For GO-$NiCoPO_3$ nanosheets, the peak at 1,782 cm^{-1} corresponds to the chary C=O stretching vibration peak. The peak at 1,434 cm^{-1} corresponds to the epoxy group C-O, and the peak at 1,055 cm^{-1} corresponds to the alkoxy C-O telescopic vibration peak. This further illustrates the successful preparation of GO-$NiCoPO_3$.

In order to understand the morphology and microstructure of the product in more detail, SEM and TEM tests were performed. The SEM image of $NiCoPO_3$ is presented in **Figure 2A**, which shows that $NiCoPO_3$ has an irregular layered structure of100–200 nm. As can be seen from **Figure 2B**, the surface of GO is wrinkled, and the nanometer scale is about 500 nm (Stobinski et al., 2014). **Figure 2C** shows the SEM image of GO-$NiCoPO_3$. It can be seen that the lamellar structure is darker than $NiCoPO_3$, probably due to the addition of GO to the surface of $NiCoPO_3$. **Figure 2D** shows the TEM image of GO-$NiCoPO_3$. The morphology of GO-$NiCoPO_3$ is substantially smooth and flat, and the edge portion also has a typical lamellar shape.

Thermal Stability of Epoxy Resin/Graphene Oxide–Cobalt Nickel Phosphate Nanocomposites

TG curves were used to further study the effect of GO-$NiCoPO_3$ nanosheets on EP/GO-$NiCoPO_3$ nanocomposites. The TG curves of EP nanocomposites are shown in **Figure 3**, and the key data are listed in **Table 2**. Under the nitrogen atmosphere, pure EP begins to decompose ($T_{5\%}$) at 354°C and the 50% mass loss decomposition temperature ($T_{50\%}$) is 397°C, showing that the main thermal decomposition stage is mainly attributed to oxidation of the main C chain in EP, and the char residual is only 11.8 wt% at 700°C. The addition of GO-$NiCoPO_3$ markedly improves the thermal stability of EP.

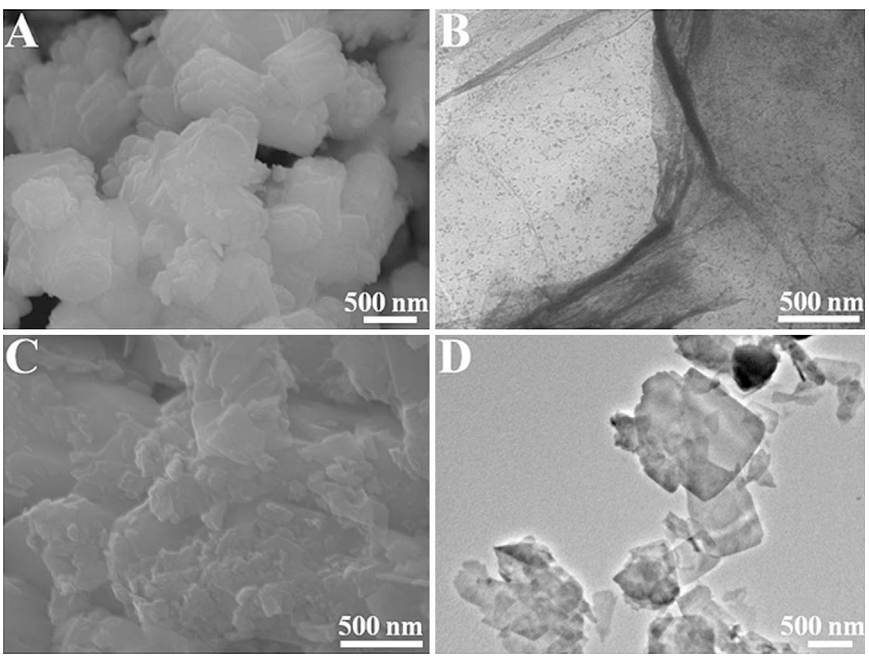

FIGURE 2 | (A) SEM image of $NiCoPO_3$; **(B)** Transmission electron microscopy image of GO; **(C)** SEM image of GO-$NiCoPO_3$; **(D)** Transmission electron microscopy image of GO-$NiCoPO_3$. Go, graphene oxide; $NiCoPO_3$, cobalt nickel phosphate.

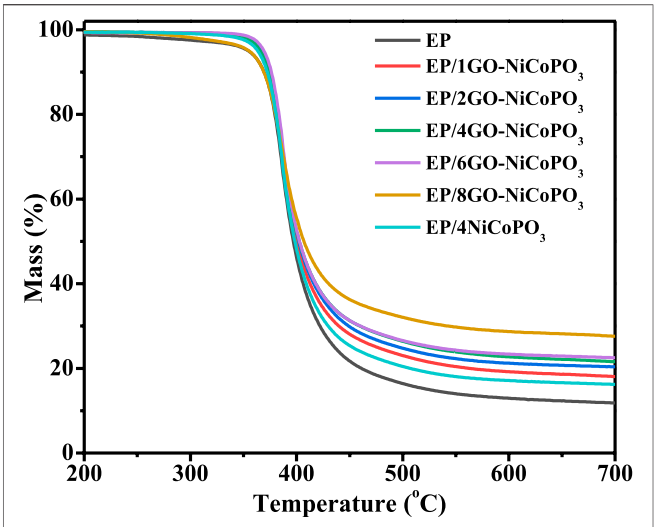

FIGURE 3 | Thermogravimetric curves of pure epoxy resin (EP) and EP nanocomposites.

When 1, 2, 4, 6, and 8 wt% GO-$NiCoPO_3$ nanosheets are added to EP nanocomposites, the $T_{5\%}$ and $T_{50\%}$ are increased to 366, 367, 365, 369, 360, and 400°C, 402, 402, 402, and 406°C, respectively. The amount of residual char in EP/GO-$NiCoPO_3$ nanocomposites is also increased significantly by compared with that of pure EP. Particularly, the residue of EP nanocomposites with 8 wt% GO-$NiCoPO_3$ reaches up to 27.6 wt% at 700°C. Because of the lamellar structure of GO, it has a barrier effect and prolongs the time for the combustible gas to escape from the matrix to the surface of EP/GO-$NiCoPO_3$ nanocomposites (Nine et al., 2017; Shi et al., 2018), so that the Ni ions and Co ions in $NiCoPO_3$ have sufficient time to catalyze the carbonization of EP during the degradation process. The EP/$4NiCoPO_3$ nanocomposites are used as a comparison sample to further verify that the incorporation of GO-$NiCoPO_3$ in EP nanocomposites can improve its thermal stability. The $T_{5\%}$ and $T_{50\%}$ of EP/$4NiCoPO_3$ nanocomposites are 363 and 398°C, and there are about 16.2 wt% char residues at 700°C. Compared to EP/$4NiCoPO_3$ nanocomposites, the $T_{5\%}$ and $T_{50\%}$ values of EP/4GO-$NiCoPO_3$ nanocomposites are obviously improved, reaching 365 and 402°C, respectively, and the residue reaches 21.6% at 700°C. Compared with pure EP, the TG data of EP/$4NiCoPO_3$ and EP/4GO-$NiCoPO_3$ nanocomposites are significantly improved. The above results indicate that $NiCoPO_3$ has excellent performance in catalyzing char formation, but the char layer is loose and weak. The layered GO can increase the viscosity of the polymer and combine the Co, Ni, and P in $NiCoPO_3$ through covalent and non-covalent bonds (Cao et al., 2016; Xu et al., 2016), so that EP nanocomposites can be catalytic formed denser and richer char layer during thermal decomposition (Kong et al., 2018c).

UL-94 vertical burning tests and LOI are commonly used for evaluating the combustion properties of polymer composites. The results are shown in **Table 3**. The pure EP has no rating (NR) in the UL-94 test, and the LOI value is 25.8%. When 1 and 2 wt% GO-$NiCoPO_3$ are added into the EP matrix, the LOI values of EP/GO-$NiCoPO_3$ nanocomposites are increased to 27.1 and 28.3%, respectively. But they still have no UL-94 rating. With GO-$NiCoPO_3$ increasing to 4 and 6 wt%, the LOI values of EP/GO-$NiCoPO_3$ nanocomposites are increased to 30.3 and 29.7%, respectively, and they can reach the V-1 level in UL-94 tests. However, with the amount of GO-$NiCoPO_3$ reaching 8 wt% in the EP matrix, the LOI value of EP/GO-$NiCoPO_3$ nanocomposites is slightly reduced to 29.1%, and it still has no UL-94 rating. This may be caused by the excessive addition of GO-$NiCoPO_3$, which cannot be uniformly dispersed in the EP matrix. The comparative sample EP/$4NiCoPO_3$ nanocomposites have a LOI value of 27.9%, and it has no UL-94 rating, but EP/4GO-$NiCoPO_3$ nanocomposites reach V-1 rating in UL-94 tests. The improvement in UL-94

TABLE 3 | LOI and UL-94 results of pure EP and EP nanocomposites.

Sample	Flame retardancy		
	LOI (vol%)	UL-94 test	
		$t_1 + t_2$ (sec)	Rating
Pure EP	25.7	>50	NR
EP/1GO-$NiCoPO_3$	27.1	68.5	NR
EP/2GO-$NiCoPO_3$	28.3	54.4	NR
EP/4GO-$NiCoPO_3$	30.3	44.0	V-1
EP/6GO-$NiCoPO_3$	29.7	46.5	V-1
EP/8GO-$NiCoPO_3$	29.1	51.2	NR
EP/$4NiCoPO_3$	27.9	63.5	NR

LOI, limiting oxygen index; EP, epoxy resin; Go, graphene oxide; $NiCoPO_3$, cobalt nickel phosphate. Combustion performance of EP/GO-$NiCoPO_3$ nanocomposites.

TABLE 2 | Thermogravimetric data of pure EP and EP nanocomposites.

Sample	$T_{5\%}$ (°C)	$T_{50\%}$ (°C)	Char residues at 700 C (wt%)
Pure EP	354	397	11.8
EP/1Go-$NiCoPO_3$	366	400	18.1
EP/2Go-$NiCoPO_3$	367	402	20.4
EP/4Go-$NiCoPO_3$	365	402	21.6
EP/6Go-$NiCoPO_3$	369	402	22.5
EP/8Go-$NiCoPO_3$	360	406	27.6
EP/$4NiCoPO_3$	363	398	16.2

EP, epoxy resin; Go, graphene oxide; $NiCoPO_3$, cobalt nickel phosphate.

TABLE 4 | Micro-combustion calorimetry data of pure EP and EP/GO-$NiCoPO_3$ nanocomposites.

Sample	PHRR (W/g)	THR (KJ/g)	T_p (°C)
Pure EP	560.9	39.4	417.6
EP/1GO-$NiCoPO_3$	490.4	26.2	422.3
EP/4GO-$NiCoPO_3$	458.6	24.0	415.6
EP/8GO-$NiCoPO_3$	427.1	22.9	420.4
EP/$4NiCoPO_3$	557.8	30.7	417.3

EP, epoxy resin; Go, graphene oxide; $NiCoPO_3$, cobalt nickel phosphate.

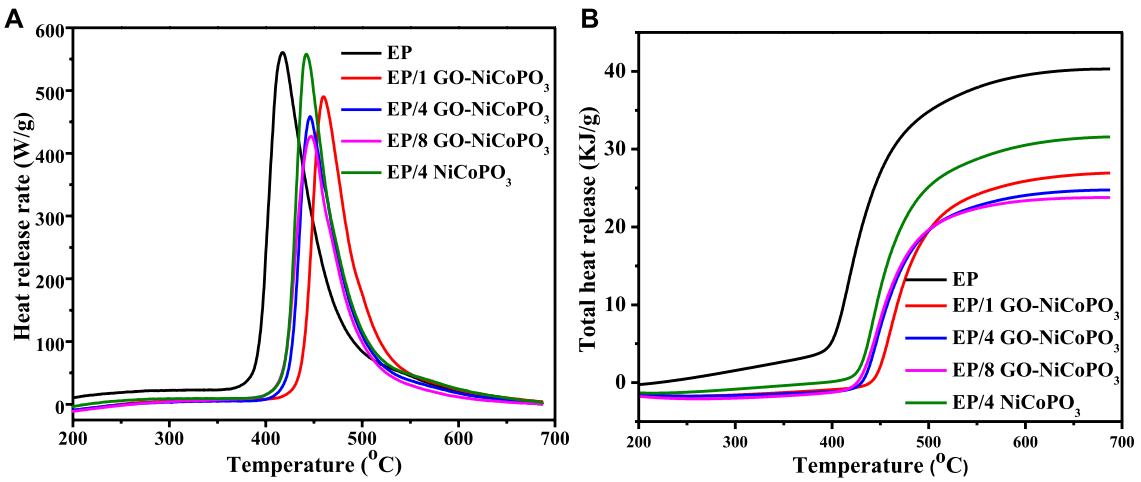

FIGURE 4 | (A) Heat release rate curves of EP/GO-$NiCoPO_3$ nanocomposites; **(B)** Total heat release curves of EP/GO-$NiCoPO_3$ nanocomposites. Go, graphene oxide; $NiCoPO_3$, cobalt nickel phosphate.

rating and LOI values of EP/GO-$NiCoPO_3$ nanocomposites is mainly attributed to the synergistic flame retardant effect of GO and $NiCoPO_3$. On the one hand, GO containing a large number of organic groups (hydroxyl, carboxyl, epoxy, etc.) provides active sites that combine with transition metal ions in $NiCoPO_3$, which not only play a barrier effect for protecting the unburned EP nanocomposites below but also catalytically convert toxic gases to nontoxic gases. On the other hand, the phosphate ions in $NiCoPO_3$ are converted into metaphosphoric acid and polymetaphosphoric acid during the combustion process. Polymetaphosphoric acid has strong dehydration properties, which can dehydrate and char the polymer to form a char film to isolate the air, thereby changing the combustion process and improving the thermal stability of EP (Kong et al., 2017c; Wu et al., 2018; Guo et al., 2019).

MCC tests were performed to further verify the combustion performance of EP/GO-$NiCoPO_3$ nanocomposites. The MCC tests were used to evaluate the potential fire hazard of EP/GO-$NiCoPO_3$ nanocomposites by measuring the HRR, the PHRR, and the THR (Shi et al., 2019). Detailed data are listed in **Table 4**, and the HRR and THR curves of pure EP and EP/GO-$NiCoPO_3$ nanocomposites are shown in **Figure 4**. The PHRR value of pure EP is 560.9 W/g. Compared with pure EP, when 1, 4, and 8 wt% GO-$NiCoPO_3$ are added into the EP matrix, the PHRR values are decreased to 490.4, 458.6, and 427.1 W/g, respectively, reducing about 12.6, 18.2, and 23.9%, respectively. The THR values of EP/1GO-$NiCoPO_3$, EP/4GO-$NiCoPO_3$, and EP/8GO-$NiCoPO_3$ nanocomposites are 26.2, 24, and 22.9 KJ/g, reducing about 33.5, 39.1, and 41.9%, respectively. This fully indicates that GO-$NiCoPO_3$ can promote the formation of a dense and strong char layer on the surface of the polymer and prevent the transfer of external heat and oxygen to the EP matrix, inhibiting polymer combustion and reducing heat release. However, the PHRR value (557.8 W/g) and THR value (30.7 KJ/g) of EP/4$NiCoPO_3$ nanocomposites are higher than those of EP/4 GO-$NiCoPO_3$ and slightly lower than those of pure EP. This may be due to the addition of $NiCoPO_3$; although it has a certain catalytic char formation, the char layer formed is thin and sparse, which has a poor barrier effect so that the heat release amount is not significantly reduced. When $NiCoPO_3$ modified by GO with a rich C structure is added to the EP matrix, the viscosity of the EP/GO-$NiCoPO_3$ polymer increases and reduces the burning rates, which provides sufficient time to catalyze the carbonization of the matrix in the polymer (Wang et al., 2017; Feng et al., 2018). The char layer, whose quantity and quality have been significantly changed, can cover the polymer surface, prevent heat from escaping, inhibit the combustion, and enhance the flame retardant performance of the composites (Zhang et al., 2016; Kong et al., 2017b).

CONCLUSIONS

In summary, $NiCoPO_3$ nanosheets and GO-$NiCoPO_3$ were synthesized by a simple solvothermal method. The TG results showed that the addition of GO-$NiCoPO_3$ promoted char formation and enhanced the thermal stability of the polymer at high temperatures. The LOI and UL-94 data showed that when 4 wt% GO-$NiCoPO_3$ was added, the LOI value was as high as 30.3%, and it reached UL-94 V-1 rating. The MCC results showed that the addition of GO-$NiCoPO_3$ significantly reduced the PHRR and THR values of EP nanocomposites. Compared with pure EP, the THR value of EP/8GO-$NiCoPO_3$ nanocomposites was decreased by 41.9%. These results indicated that GO-$NiCoPO_3$ increased the flame retardancy of EP/GO-$NiCoPO_3$ nanocomposites to some extent. This was mainly due to the fact that GO-$NiCoPO_3$ formed dense carbonaceous protection layers to reduce heat transfer, inhibit combustion, and improve thermal stability of composites.

DATA AVAILABILITY STATEMENT

All datasets presented in this study are included in the article.

AUTHOR CONTRIBUTIONS

QK and JZ conceived and designed the study and experiment plan and wrote the manuscript. CZ drafted the manuscript. MZ and TZ analyzed the experimental results.

FUNDING

This research is funded by the National Natural Science Foundation of China (51603091), Natural Science Foundation of Jiangsu Province (BK20181469), Science and Technology Planning Social Development Project of Zhenjiang City (SSH20190140049), and the Open Project Program of Key Laboratory of Eco-textiles, Ministry of Education, Jiangnan University (No. KLET2006).

REFERENCES

Asabina, E. A., Maiorov, P. A., Pet'kov, V. I., Koval'skii, A. M., and Borovikova, E. Y. (2019). Phosphates of zirconium and metals (Ni, Cu, Co, and Mn) in the oxidation state of +2: synthesis and structure. *Russ. J. Inorg. Chem.* 64, 290–295. doi:10.1134/s0036023619030021

Cai, W., Feng, X., Hu, W., Pan, Y., Hu, Y., and Gong, X. (2016). Functionalized graphene from electrochemical exfoliation for thermoplastic polyurethane: thermal stability, mechanical properties, and flame retardancy. *Ind. Eng. Chem. Res.* 55, 10681–10689. doi:10.1021/acs.iecr.6b02579

Cao, Y., Li, G., and Li, X. (2016). Graphene/layered double hydroxide nanocomposite: properties, synthesis, and applications. *Chem. Eng. J.* 292, 207–223. doi:10.1016/j.cej.2016.01.114

Chen, Y. J., Wu, X. D., and Qian, L. J. (2020). Flame-retardant behavior and protective layer effect of phosphazene-triazine bi-group flame retardant on polycarbonate. *J. Appl. Polym. Sci.* e49523. doi:10.1002/app.49523

Cote, L. J., Kim, J., Tung, V. C., Luo, J. Y., Kim, F., and Huang, J. X. (2011). Graphene oxide as surfactant sheets. *Pure Appl. Chem.* 83, 95–110. doi:10.1351/PAC-CON-10-10-25

Ding, J., Zhang, Y., Zhang, X., Kong, Q., Zhang, J., Liu, H., et al. (2020). Improving the flame-retardant efficiency of layered double hydroxide with disodium phenylphosphate for epoxy resin. *J. Therm. Anal. Calorim.* 140, 149–156. doi:10.1007/s10973-019-08372-9

Feng, Y., Han, G., Wang, B., Zhou, X., Ma, J., Ye, Y., et al. (2020). Multiple synergistic effects of graphene-based hybrid and hexagonal born nitride in enhancing thermal conductivity and flame retardancy of epoxy. *Chem. Eng. J.* 379, 122402. doi:10.1016/j.cej.2019.122402

Feng, Y., Li, X., Zhao, X., Ye, Y., Zhou, X., Liu, H., et al. (2018). Synergetic improvement in thermal conductivity and flame retardancy of epoxy/silver nanowires composites by incorporating "Branch-Like" flame-retardant functionalized graphene. *ACS Appl. Mater. Interfaces* 10, 21628–21641. doi:10.1021/acsami.8b05221

Feng, Y., Yuan, L., Liang, G., and Gu, A. (2019). Phosphorus-free boron nitride/cerium oxide hybrid: a synergistic flame retardant and smoke suppressant for thermally resistant cyanate ester resin. *Polym. Adv. Technol.* 30, 2340–2352. doi:10.1002/pat.4675

Guo, X., Qian, C., Shi, R., Zhang, W., Xu, F., Qian, S., et al. (2019). Biomorphic CoNC/CoO x composite derived from natural chloroplasts as efficient electrocatalyst for oxygen reduction reaction. *Small* 15, 1804855. doi:10.1002/smll.201804855

Guo, X., Qian, C., Wan, X., Zhang, W., Zhu, H., Zhang, J., et al. (2020). Facile *in situ* fabrication of biomorphic Co2P-Co3O4/rGO/C as an efficient electrocatalyst for the oxygen reduction reaction. *Nanoscale* 12, 4374–4382. doi:10.1039/c9nr10785a

Huang, G., Ni, Z., Chen, G., Li, G., and Zhao, Y. (2016). Investigation of irradiated graphene oxide/ultra-high-molecular-weight polyethylene nanocomposites by ESR and FTIR spectroscopy. *Fullerenes Nanotub. Carbon Nanostruct.* 24, 698–704. doi:10.1080/1536383x.2016.1229310

Huang, N. M., Lim, H. N., Chia, C. H., Yarmo, M. A., and Muhamad, M. R. (2011). Simple room-temperature preparation of high-yield large-area graphene oxide. *Int. J. Nanomed.* 6, 3443–3448. doi:10.2147/ijn.s26812

Kong, Q., Sun, Y., Zhang, C., Guan, H., Zhang, J., Wang, D.-Y., et al. (2019a). Ultrathin iron phenyl phosphonate nanosheets with appropriate thermal stability for improving fire safety in epoxy. *Compos. Sci. Technol.* 182, 107748. doi:10.1016/j.compscitech.2019.107748

Kong, Q., Zhang, M., Zhao, S., Yuan, Z., Yu, S., Zhang, F., et al. (2019b). Improving fire safety of epoxy resin with alkyl glycoside modified CuAl-layered double hydroxide. *J. Nanosci. Nanotechnol.* 19, 4571–4577. doi:10.1166/jnn.2019.16495

Kong, Q., Zhang, Y., Zhang, X., Xiang, B., Yi, Y., Zhu, J., et al. (2019c). Functionalized montmorillonite intercalation iron compounds for improving flame retardancy of epoxy resin nanocomposites. *J. Nanosci. Nanotechnol.* 19, 5803–5809. doi:10.1166/jnn.2019.16540

Kong, Q., Wu, T., Liu, H., Zhang, Y., Zhang, M., Cai, Y., et al. (2018a). Graphene oxide nanocoating prevents flame spread on polyurethane sponge. *J. Nanosci. Nanotechnol.* 18, 5105–5112. doi:10.1166/jnn.2018.15284

Kong, Q., Wu, T., Wang, J., Liu, H., and Zhang, J. (2018b). Improving the thermal stability and flame retardancy of PP/IFR composites by NiAl-layered double hydroxide. *J. Nanosci. Nanotechnol.* 18, 3660–3665. doi:10.1166/jnn.2018.14679

Kong, Q., Wu, T., Zhang, J., and Wang, D.-Y. (2018c). Simultaneously improving flame retardancy and dynamic mechanical properties of epoxy resin nanocomposites through layered copper phenylphosphate. *Compos. Sci. Technol.* 154, 136–144. doi:10.1016/j.compscitech.2017.10.013

Kong, Q., Wu, T., Tang, Y., Xiong, L., Liu, H., Zhang, J., et al. (2017a). Improving thermal and flame retardant properties of epoxy resin with organic NiFe-layered double hydroxide-carbon nanotubes hybrids. *Chin. J. Chem.* 35, 1875–1880. doi:10.1002/cjoc.201700313

Kong, Q., Wu, T., Zhang, H., Zhang, Y., Zhang, M., Si, T., et al. (2017b). Improving flame retardancy of IFR/PP composites through the synergistic effect of organic montmorillonite intercalation cobalt hydroxides modified by acidified chitosan. *Appl. Clay Sci.* 146, 230–237. doi:10.1016/j.clay.2017.05.048

Kong, Q., Zhang, H., Zheng, L., Wang, D.-Y., and Zhang, J. (2017c). Effect on thermal and combustion behaviors of montmorillonite intercalation nickel compounds in polypropylene/IFR system. *Polym. Adv. Technol.* 28, 965–970. doi:10.1002/pat.3823

Li, B., Gu, P., Feng, Y., Zhang, G., Huang, K., Xue, H., et al. (2017). Ultrathin nickel-cobalt phosphate 2D nanosheets for electrochemical energy storage under aqueous/solid-state electrolyte. *Adv. Funct. Mater.* 27, 1605784. doi:10.1002/adfm.201605784.

Li, Z., Zhang, J., Dufosse, F., and Wang, D.-Y. (2018). Ultrafine nickel nanocatalyst-engineering of an organic layered double hydroxide towards a super-efficient fire-safe epoxy resin via interfacial catalysis. *J. Mater. Chem.* 6, 8488–8498. doi:10.1039/c8ta00910d

Liao, S.-H., Liu, P.-L., Hsiao, M.-C., Teng, C.-C., Wang, C.-A., Ger, M.-D., et al. (2012). One-step reduction and functionalization of graphene oxide with phosphorus-based compound to produce flame-retardant epoxy nanocomposite. *Ind. Eng. Chem. Res.* 51, 4573–4581. doi:10.1021/ie2026647

Mu, X., Yuan, B., Feng, X., Qiu, S., Song, L., and Hu, Y. (2016). The effect of doped heteroatoms (nitrogen, boron, phosphorus) on inhibition thermal oxidation of reduced graphene oxide. *RSC Adv.* 6, 105021–105029. doi:10.1039/c6ra21329d

Nie, S., Jin, D., Xu, Y., Han, C., Dong, X., and Yang, J.-n. (2020). Effect of a flower-like nickel phyllosilicate-containing iron on the thermal stability and flame retardancy of epoxy resin. *J. Mater. Res. Technol.* 9, 10189. doi:10.1016/j.jmrt.2020.07.021

Nine, M. J., Tran, D. N. H., Tung, T. T., Kabiri, S., and Losic, D. (2017). Graphene-borate as an efficient fire retardant for cellulosic materials with multiple and synergetic modes of action. *ACS Appl. Mater. Interfaces* 9, 10160–10168. doi:10.1021/acsami.7b00572

Peng, C., Chen, T., Zeng, B., Chen, G., Yuan, C., Xu, Y., et al. (2020). Anderson-type polyoxometalate-based hybrid with high flame retardant efficiency for the preparation of multifunctional epoxy resin nanocomposites. *Compos. B Eng.* 186, 107780. doi:10.1016/j.compositesb.2020.107780

Reuter, J., Greiner, L., Kukla, P., and Döring, M. (2020). Efficient flame retardant interplay of unsaturated polyester resin formulations based on ammonium polyphosphate. *Polym. Degrad. Stabil.* 178, 109134. doi:10.1016/j.polymdegradstab.2020.109134

Shi, X., Peng, X., Zhu, J., Lin, G., and Kuang, T. (2018). Synthesis of DOPO-HQ-functionalized graphene oxide as a novel and efficient flame retardant and its application on polylactic acid: thermal property, flame retardancy, and mechanical performance. *J. Colloid Interface Sci.* 524, 267–278. doi:10.1016/j.jcis.2018.04.016

Shi, Y., Liu, C., Duan, Z., Yu, B., Liu, M., and Song, P. (2020). Interface engineering of MXene towards super-tough and strong polymer nanocomposites with high ductility and excellent fire safety. *Chem. Eng. J.* 399, 125829. doi:10.1016/j.cej.2020.125829

Shi, Y., Liu, C., Liu, L., Fu, L., Yu, B., Lv, Y., et al. (2019). Strengthening, toughing and thermally stable ultra-thin MXene nanosheets/polypropylene nanocomposites via nanoconfinement. *Chem. Eng. J.* 378, 122267. doi:10.1016/j.cej.2019.122267

Si, Y., and Samulski, E. T. (2008). Exfoliated graphene separated by platinum nanoparticles. *Chem. Mater.* 20, 6792–6797. doi:10.1021/cm801356a

Stobinski, L., Lesiak, B., Malolepszy, A., Mazurkiewicz, M., Mierzwa, B., Zemek, J., et al. (2014). Graphene oxide and reduced graphene oxide studied by the XRD, TEM and electron spectroscopy methods. *J. Electron. Spectrosc. Relat. Phenom.* 195, 145–154. doi:10.1016/j.elspec.2014.07.003/

Sun, Z., Hou, Y., Hu, Y., and Hu, W. (2018). Effect of additive phosphorus-nitrogen containing flame retardant on char formation and flame retardancy of epoxy resin. *Mater. Chem. Phys.* 214, 154–164. doi:10.1016/j.matchemphys.2018.04.065

Tang, G., Liu, X., Yang, Y., Chen, D., Zhang, H., Zhou, L., et al. (2020a). Phosphorus-containing silane modified steel slag waste to reduce fire hazards of rigid polyurethane foams. *Adv. Powder Technol.* 31, 1420–1430. doi:10.1016/j.apt.2020.01.019

Tang, G., Liu, X., Zhou, L., Zhang, P., Deng, D., and Jiang, H. (2020b). Steel slag waste combined with melamine pyrophosphate as a flame retardant for rigid polyurethane foams. *Adv. Powder Technol.* 31, 279–286. doi:10.1016/j.apt.2019.10.020

Tang, G., Zhou, L., Zhang, P., Han, Z., Chen, D., Liu, X., et al. (2020c). Effect of aluminum diethylphosphinate on flame retardant and thermal properties of rigid polyurethane foam composites. *J. Therm. Anal. Calorim.* 140, 625–636. doi:10.1007/s10973-019-08897-z

Wang, X., Kalali, E. N., Wan, J.-T., and Wang, D.-Y. (2017). Carbon-family materials for flame retardant polymeric materials. *Prog. Polym. Sci.* 69, 22–46. doi:10.1016/j.progpolymsci.2017.02.001

Wu, T., Kong, Q., Zhang, H., and Zhang, J. (2018). Thermal stability and flame retardancy of polypropylene/NiAl layered double hydroxide nanocomposites. *J. Nanosci. Nanotechnol.* 18, 1051–1056. doi:10.1166/jnn.2018.14107

Xu, W., Wang, X., Wu, X., Li, W., and Cheng, C. (2019). Organic-inorganic dual modified graphene: improving the dispersibility of graphene in epoxy resin and the fire safety of epoxy resin. *Polym. Degrad. Stabil.* 165, 80–91. doi:10.1016/j.polymdegradstab.2019.04.023

Xu, W., Zhang, B., Xu, B., and Li, A. (2016). The flame retardancy and smoke suppression effect of heptaheptamolybdate modified reduced graphene oxide/layered double hydroxide hybrids on polyurethane elastomer. *Compos. Appl. Sci. Manuf.* 91, 30–40. doi:10.1016/j.compositesa.2016.09.013

Xu, X., Wang, S., Ma, S., Yuan, W., Li, Q., Feng, J., et al. (2019). Vanillin-derived phosphorus-containing compounds and ammonium polyphosphate as green fire-resistant systems for epoxy resins with balanced properties. *Polym. Adv. Technol.* 30, 264–278. doi:10.1002/pat.4461

Xue, Y., Yu, T., Chen, J., Wan, X., Cai, X., Guo, X., et al. (2020). Fabrication of GeO2 microspheres/hierarchical porous N-doped carbon with superior cyclic stability for Li-ion batteries. *J. Solid State Chem.* 286, 121303. doi:10.1016/j.jssc.2020.121303

Yang, G., Wu, W.-H., Wang, Y.-H., Jiao, Y.-H., Lu, L.-Y., Qu, H.-Q., et al. (2019). Synthesis of a novel phosphazene-based flame retardant with active amine groups and its application in reducing the fire hazard of epoxy resin. *J. Hazard Mater.* 366, 78–87. doi:10.1016/j.jhazmat.2018.11.093

Yu, D., Wen, S., Yang, J., Wang, J., Chen, Y., Luo, J., et al. (2017). RGO modified ZnAl-LDH as epoxy nanostructure filler: a novel synthetic approach to anticorrosive waterborne coating. *Surf. Coating. Technol.* 326, 207–215. doi:10.1016/j.surfcoat.2017.07.053

Yu, Z., Di, H., Ma, Y., He, Y., Liang, L., Lv, L., et al. (2015). Preparation of graphene oxide modified by titanium dioxide to enhance the anti-corrosion performance of epoxy coatings. *Surf. Coating. Technol.* 276, 471–478. doi:10.1016/j.surfcoat.2015.06.027

Yue, X., Li, C., Ni, Y., Xu, Y., and Wang, J. (2019). Flame retardant nanocomposites based on 2D layered nanomaterials: a review. *J. Mater. Sci.* 54, 13070–13105. doi:10.1007/s10853-019-03841-w

Zhang, D., Guo, X., Tong, X., Chen, Y., Duan, M., Shi, J., et al. (2020). High-performance battery-type supercapacitor based on porous biocarbon and biocarbon supported Ni-Co layered double hydroxide. *J. Alloys Compd. Compd.* 837, 155529. doi:10.1016/j.jallcom.2020.155529

Zhang, J., Kong, Q., and Wang, D.-Y. (2018). Simultaneously improving the fire safety and mechanical properties of epoxy resin with Fe-CNTs via large-scale preparation. *J. Mater. Chem.* 6, 6376–6386. doi:10.1039/c7ta10961j

Zhang, J., Kong, Q., Yang, L., and Wang, D.-Y. (2016). Few layered $Co(OH)_2$ ultrathin nanosheet-based polyurethane nanocomposites with reduced fire hazard: from eco-friendly flame retardance to sustainable recycling. *Green Chem.* 18, 3066–3074. doi:10.1039/c5gc03048j

Zhang, Q., Li, Z., Li, X., Yu, L., Zhang, Z., and Wu, Z. (2019). Preparation of cobalt ferrite nanoparticle-decorated boron nitride nanosheet flame retardant and its flame retardancy in epoxy resin. *Nano* 14, 1950063. doi:1010.1142/s1793292019500632

Zheng, L., Wu, T., Kong, Q., Zhang, J., and Liu, H. (2017). Improving flame retardancy of PP/MH/RP composites through synergistic effect of organic CoAl-layered double hydroxide. *J. Therm. Anal. Calorim.* 129, 1039–1046. doi:10.1007/s10973-017-6231-6

Zhou, K., Gao, R., and Qian, X. (2017). Self-assembly of exfoliated molybdenum disulfide (MoS 2) nanosheets and layered double hydroxide (LDH): towards reducing fire hazards of epoxy. *J. Hazard Mater.* 338, 343–355. doi:10.1016/j.jhazmat.2017.05.046

Zhou, T., Wu, T., Xiang, H., Li, Z., Xu, Z., Kong, Q., et al. (2019). Simultaneously improving flame retardancy and dynamic mechanical properties of epoxy resin nanocomposites through synergistic effect of zirconium phenylphosphate and POSS. *J. Therm. Anal. Calorim.* 135, 2117–2124. doi:10.1007/s10973-018-7387-4

Zhu, Y., Murali, S., Cai, W., Li, X., Suk, J. W., Potts, J. R., et al. (2010). Graphene and graphene oxide: synthesis, properties, and applications. *Adv. Mater.* 22, 3906–3924. doi:10.1002/adma.201001068.

Zhu, Z., Lin, P., Wang, H., Wang, L., Yu, B., and Yang, F. (2020). A facile one-step synthesis of highly efficient melamine salt reactive flame retardant for epoxy resin. *J. Mater. Sci.* 55, 12836–12847. doi:10.1007/s10853-020-04935-6

Conflict of Interest: The authors declare that the research was conducted in the absence of any commercial or financial relationships that could be construed as a potential conflict of interest.

frontiers in Chemistry

ORIGINAL RESEARCH
published: 29 September 2020
doi: 10.3389/fchem.2020.587474

Polydopamine-Bridged Synthesis of Ternary h-BN@PDA@TiO_2 as Nanoenhancers for Thermal Conductivity and Flame Retardant of Polyvinyl Alcohol

Xiaodong Wang[1,2]*, *Weizhao Hu*[1] and *Yuan Hu*[1]*

[1] State Key Laboratory of Fire Science, University of Science and Technology of China, Hefei, China, [2] School of Chemistry and Material Engineering, Chaohu University, Chaohu, China

OPEN ACCESS

Edited by:
Yongqian Shi,
Fuzhou University, China

Reviewed by:
Gang Tang,
Anhui University of Technology, China
Yuezhan Feng,
Zhengzhou University, China
Rongkun Jian,
Fujian Normal University, China
Haifeng Pan,
China University of Geosciences Wuhan, China
Hongyu Yang,
Chongqing University, China
Bin Shi Nie,
Anhui University of Science and Technology, China

***Correspondence:**
Xiaodong Wang
053011@chu.edu.cn
Yuan Hu
yuanhu@ustc.edu.cn

Specialty section:
This article was submitted to Polymer Chemistry, a section of the journal Frontiers in Chemistry

Received: 26 July 2020
Accepted: 28 August 2020
Published: 29 September 2020

Citation:
Wang X, Hu W and Hu Y (2020) Polydopamine-Bridged Synthesis of Ternary h-BN@PDA@TiO_2 as Nanoenhancers for Thermal Conductivity and Flame Retardant of Polyvinyl Alcohol. Front. Chem. 8:587474. doi: 10.3389/fchem.2020.587474

In this study, h-BN@PDA@TiO_2 hybrid nanoparticles were prepared and used as functional fillers to prepare PVA nanocomposites, and the effects of hybrid particles on PVA thermal conductivity and flame retardant properties were studied. The results showed that hybrid particles could significantly improve the thermal conductivity and flame retardant performance of PVA composites, and effectively inhibit the release of toxic gases such as combustible pyrolysis products and CO, which enhanced the fire safety of PVA composites. When the addition amount of hybrid particles is 5 wt%, the thermal conductivity of PVA composites is 239.1% higher than that of the pure PVA and the corresponding temperature of PVA composites with a mass loss of 5 wt% was 16.2°C higher than that of the pure PVA. This is due to the barrier effect of h-BN and the protective effect of dense carbon layer catalyzed by TiO_2.

Keywords: hexagonal boron nitride, thermal conductivity, polyvinyl alcohol, flame retardancy, polymer composites

INTRODUCTION

Polymers are widely used in many fields, including aerospace, electronic industry, new energy, insulation materials, decoration, construction, textile, and other fields. However, most polymers do not have flame retardancy, and there is a fire risk during actual use. Fortunately, a large number of studies have proved that adding flame retardants to polymers is an effective way to improve the fire safety of polymeric materials (Shang et al., 2018; Xu et al., 2019; Zhang Q. et al., 2019). Therefore, the performance of flame retardants directly determines the application and development of polymer materials.

With the development of human society, the requirements on material properties are more and more stringent. The concept of "high performance flame retardant" is also increasingly updated, which requires it to have better and more complete performance. The most obvious feature is environmentally friendly, efficient, and multifunctional. It is worth noting that in microelectronics, wearable devices, and other fields, flame retardant, thermal stability and heat conduction properties become the most representative properties of polymer materials used in this field (Cao et al., 2014). However, organic polymeric materials do not have good flame retardancy and thermal conductivity. In order to make the polymer have flame retardancy and thermal conductivity at the same time, it is often necessary to add different functional fillers into the polymer matrix to give the polymer system

good flame retardancy and thermal conductivity. Generally speaking, organic polymeric materials do not have good thermal conductivity, so inorganic materials with high thermal conductivity are usually used as fillers to improve the thermal conductivity parameters of polymer system (Safdari and Al-Haik, 2013); compared with organic flame retardants, inorganic flame retardants are relatively green and pollution-free, but in order to obtain better flame retardant effect, the amount of inorganic flame retardant is usually up to 40%. The mixed use of several kinds of inorganic fillers with different functions often leads to the degradation of the mechanical properties of the polymer. Therefore, composite flame retardants with low filling volume are particularly important for the development of polymer materials. The development of nanotechnology has brought solutions to this problem. Therefore, in order to make the polymer have both flame retardancy and high thermal conductivity, multifunctional nano-hybrid flame retardant is the best choice.

The discovery of graphene subverts the understanding of planar two-dimensional (2-D) structural materials. Therefore, the research boom of 2-D layered nanomaterials with similar structures with graphene has been rising in recent years. Some studies have shown that 2-D layered materials (e.g., MoS_2, GO) can improve the thermal stability and flame retardancy of polymer materials (Huang et al., 2012; Liao et al., 2012; Maddalena et al., 2018; Shi et al., 2019, 2020). The improvement of thermal stability and flame retardant is mainly due to the blocking effect of 2-D layered structure, which can effectively prevent the volatilization of combustible gas and oxygen diffusion, and delay mass loss. As a kind of compound with similar layered structure to graphene, hexagonal boron nitride (h-BN) has good thermal stability and can maintain its layered structure in a relatively stable manner even under thermal conditions; in addition, its special structure can play a barrier effect in the process of polymer combustion (Eichler and Lesniak, 2008; Xu et al., 2013; Weng et al., 2016). Therefore, h-BN can be used as a flame retardant. At the same time, h-BN has a high thermal conductivity, and many researchers use it as a functional filler to improve the thermal conductivity of polymeric materials (Golberg et al., 2010; Feng et al., 2018, 2020; Wang et al., 2018). Therefore, it is very appropriate for our study to use h-BN nanomaterials as functional fillers to enhance the flame retardancy and thermal conductivity of PVA.

As an important metal oxide, titanium dioxide (TiO_2) has attracted great attention from researchers and materials engineers. It has non-toxic, low price, good light stability, thermal stability, and other excellent performance, widely used in water, air purification, surface self-cleaning, self-sterilization, photoelectric devices, and other fields (Uchida et al., 2002; Mor et al., 2005). Existing research results have shown that metal oxides can promote the formation of char residues during the thermal degradation of polymeric materials (Feng et al., 2016). Continuous dense carbon layer can act as a barrier to improve the flame retardancy of polymer materials and reduce the damage of fire. In recent years, TiO_2 has also been gradually applied in the flame retardant field.

Zhang Z. et al. (2019) synthesized CeO_2@TiO_2 functional hybrid materials by a simple method, and blended them into epoxy resins (EP) as a flame retardant to prepare epoxy nanocomposites. The results showed that the addition of hybrid materials can increase the carbon residual rate of the nanocomposite, reduce the peak heat release rate (PHRR), and total heat release (THR), and reduce the fire risk of polymeric materials. At 700°C, the carbon residues content of the composite can reach about 20%, and the PHRR and THR of the sample decrease to 680 kW/m^2 and 32.9 MJ/m^2, respectively. Lam et al. (2011) designed a flame retardant formulation by using nano-TiO_2, N-hydroxymethyl dimethyl phosphate propionamide, and melamine as the main components, and studied its flame retardant effect on cotton fabrics. It was found that the flame-retardant cotton fabric was extinguished immediately after removing the fire source, and no flame spread. The nano-TiO_2 composite formula has a significant effect on reducing the flame propagation speed.

In this paper, h-BN nanosheets were obtained by aqueous phase ultrasonic stripping, and then a polydopamine organic layer was obtained on the surface of BN through dopamine self-polymerization, and TiO_2 was *in situ* grown at the active site provided by the organic layer to prepare core-shell multifunctional hybrid materials (h-BN@PDA@TiO_2). PVA composites were prepared by using hybrid materials as functional fillers and the effects of hybrid materials on the flame retardancy, thermal stability and thermal conductivity of polymers were studied.

MATERIALS AND METHODS

Materials

Ammonium fluotitanate ($(NH_4)_2TiF_6$, CP) and boric acid (H_3BO_3, ≥99.0%) were purchased from Sinopharm Group (China). h-BN (1–2 μm), PVA (PVA1788, Mw = 80,000, alcoholysis degree: 87.0–89.0%), and dopamine hydrochloride (98%) were purchased from Aladdin (China).

Preparation of Hybrid Nanoparticles and PVA Nanocomposites

According to literature (Wang et al., 2020), h-BN nanosheets were prepared by liquid phase ultrasonic method. An appropriate amount of h-BN powder was put into a ceramic crucible and calcined at 700°C for 2 h. Then, the powder was cooled to room temperature and washed. The h-BN suspension was ultrasonic treated in the ice bath for 4 h to obtain the h-BN nanosheets.

Preparation of h-BN@PDA: Sufficient Tris-HCl buffer solution was prepared for use. 100 ml fresh buffer solution and 0.4 g h-BN nanosheets were added to a three-necked flask and dispersed by ultrasound for 60 min. Then, 0.203 g dopamine hydrochloride was added into the solution, and the mixing system was magnetically stirred and reacted for 6 h. After the reaction was finished, the product was washed with deionized water until the pH was neutral and collected after drying. And the collected solid powder was the target product of this stage (h-BN@PDA).

Preparation of h-BN@PDA@TiO_2 nano-hybrid materials: 1.98 g of $(NH4)_2TiF_6$ and 1.853 g of H_3BO_3 were added to 100 ml deionized water and stirred evenly. Then 0.504 g of h-BN@PDA powder was added into the solution. After the pH value was adjusted to 2.8 by hydrochloric acid, the mixture was poured into a three necked bottle and stirred by magnetic force at 50°C for 12 h. At the end of the reaction, the product was repeatedly washed with deionized water until the pH value was 7, and then dried to obtain h-BN@PDA@TiO_2 nano-hybrid materials (**Scheme 1**).

Preparation of PVA composites: Under mechanical agitation, 60 g PVA was added to 300 mL deionized water and heated to 90°C to continue strong stirring until PVA was completely dissolved in the water. Appropriate amount of h-BN@PDA@TiO_2 nano-hybrid materials was transferred to PVA solution, and stirred at high speed for 15 min, followed by magnetic stirring for 2 h. Then, the mixing system was poured into a mold and naturally dried to form a film.

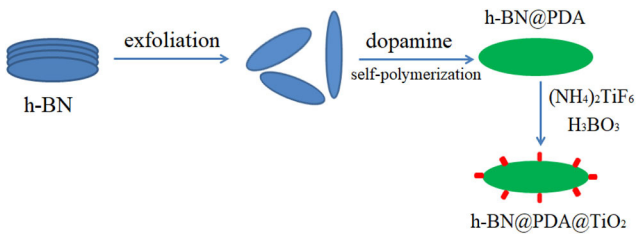

SCHEME 1 | Preparation of h-BN@PDA@TiO_2.

Analysis and Testing

Scanning electron microscope (SEM, SUPRA 55, ZEISS), transmission electron microscopy (TEM, TECNAI G20, FEI), fourier infrared spectrometer (FTIR-650, Tianjin Gangdong), X-ray diffractometer (XRD, D/max-2500ps, Regaku), raman spectroscopy (Raman, DXR 3, Thermo Fisher), material testing machine (Model 2663-901/-902, INSTRON), synchronous thermal analyzer (TG-DSC 3+, METTLER TOLEDO), Thermogravimetric-infrared technology combined technology (TG, 209F3, Netzsch; FT-IR, TENSOR27, Bruker), cone calorimeter (CCT, FTT), X ray photoelectron spectrometer (XPS, PHI-5400, PE), thermal conductivity tester (TCi-3-A, SETARAM), energy spectrometer (EDS, xflash 6130, Bruker) were used for analysis and testing.

The combustion test of composite samples was carried out according to ISO 5660 standard procedures, with 100 × 100 × 3 mm^3 specimens. The thermal conductivity test sample was a circular piece with a diameter of 30 mm and a thickness of 2 mm, and the average value of multiple test data was taken as the result.

RESULTS AND DISCUSSION

Characterization of h-BN@PDA@TiO_2

The morphology of pristine h-BN, h-BN nanosheets, h-BN@PDA, and h-BN@PDA@TiO_2 nano-hybrid particles were analyzed by TEM, as shown in **Figure 1**. It can be seen from **Figure 1a**, pristine h-BN particles are thick and compact, and individual particles are flat and blocky. After stripping, h-BN showed obvious thin flake structure with relatively smooth edge and elliptic shape (**Figure 1b**). **Figure 1c** shows the TEM images of h-BN nanosheets coated with PDA. The surface of h-BN

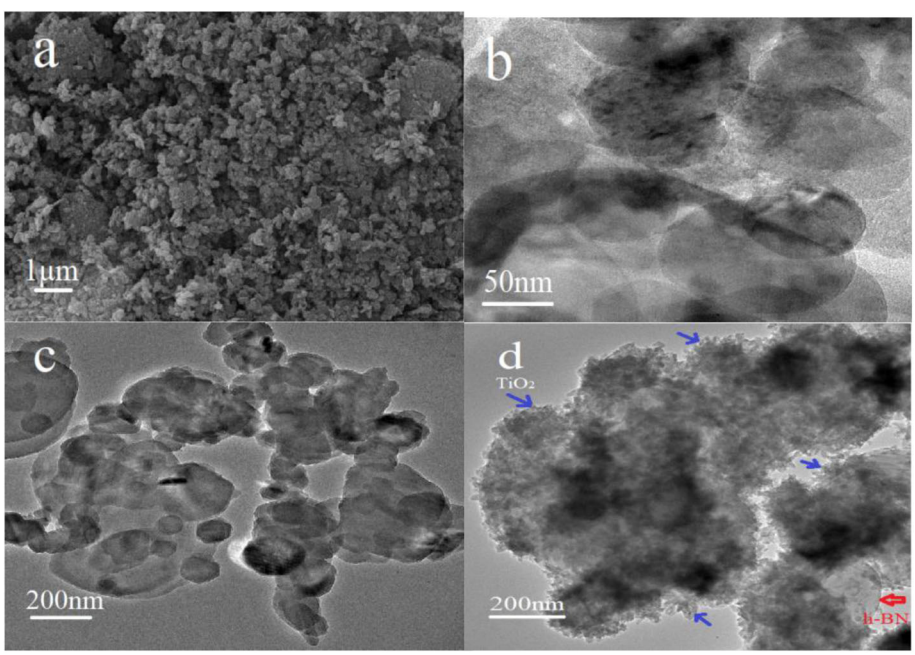

FIGURE 1 | (a) SEM image of pristine h-BN; TEM images of **(b)** h-BN nanosheets; **(c)** h-BN@PDA; **(d)** h-BN@PDA@TiO_2 hybrid particles.

nanosheets becomes fuzzy. There is a thin, continuous coating. This coating is the product of dopamine self-polymerization, which indicates that the nanosheet has been successfully coated by PDA. And it can be seen from **Figure 1d** that a number of protuberances are attached to the surface of h-BN nanosheets, which should be TiO_2 nanoparticles attached by self-assembly on the surface of h-BN@PDA. The h-BN@PDA@TiO_2 nanohybrid particles have typical core-shell structure, in which the h-BN nanosheet is the core and the PDA organic layer and attached TiO_2 particles are the shells. And, in the TEM images, no separate TiO_2 nanoparticles were found except for h-BN@PDA@TiO_2 particles, indicating that TiO_2 was not combined with h-BN nanosheets by physical mixing, but was anchored on the surface of h-BN@PDA in the form of *in situ* growth.

XRD was used to characterize h-BN nanosheets, h-BN@PDA, and h-BN@PDA@TiO_2 particles, and the results are shown in **Figure 2A**. h-BN nanosheets showed obvious diffraction peaks at positions 26.7°, 41.6°, 44.0°, 50.2°, and 55.1°, which correspond to those of JCPDS standard card (NO.34- 042). The difference between h-BN@PDA and h-BN is that there is a PDA organic layer attached to the surface of h-BN nanosheets, which has no influence on the crystal structure of h-BN nanosheets. Therefore, in the XRD spectrum, the diffraction peaks of h-BN@PDA and h-BN are basically consistent. The characteristic peaks of TiO_2 appeared on h-BN@PDA@TiO_2 particles, identified as anatase phase of (101) = 25.2°, (004) = 37.9°, and (200) =48.1°, (105) = 53.8° 2-theta values, which also demonstrated that the TiO_2 particles have successfully grown on the surface of the h-BN nanosheets.

Figure 2B shows the Raman spectra of h-BN, h-BN@PDA, and h-BN@PDA@TiO_2. The spectra of h-BN, h-BN@PDA and h-BN@PDA@TiO_2 showed significant differences. Pure h-BN nanosheets have a sharp characteristic peak at 1,366 cm^{-1}, which is attributed to the E2g phonon mode (Wu et al., 2004; Gorbachev et al., 2011). After functional decoration, there are two broad peaks at 1,363 and 1,588 cm^{-1} in Raman spectra of h-BN@PDA

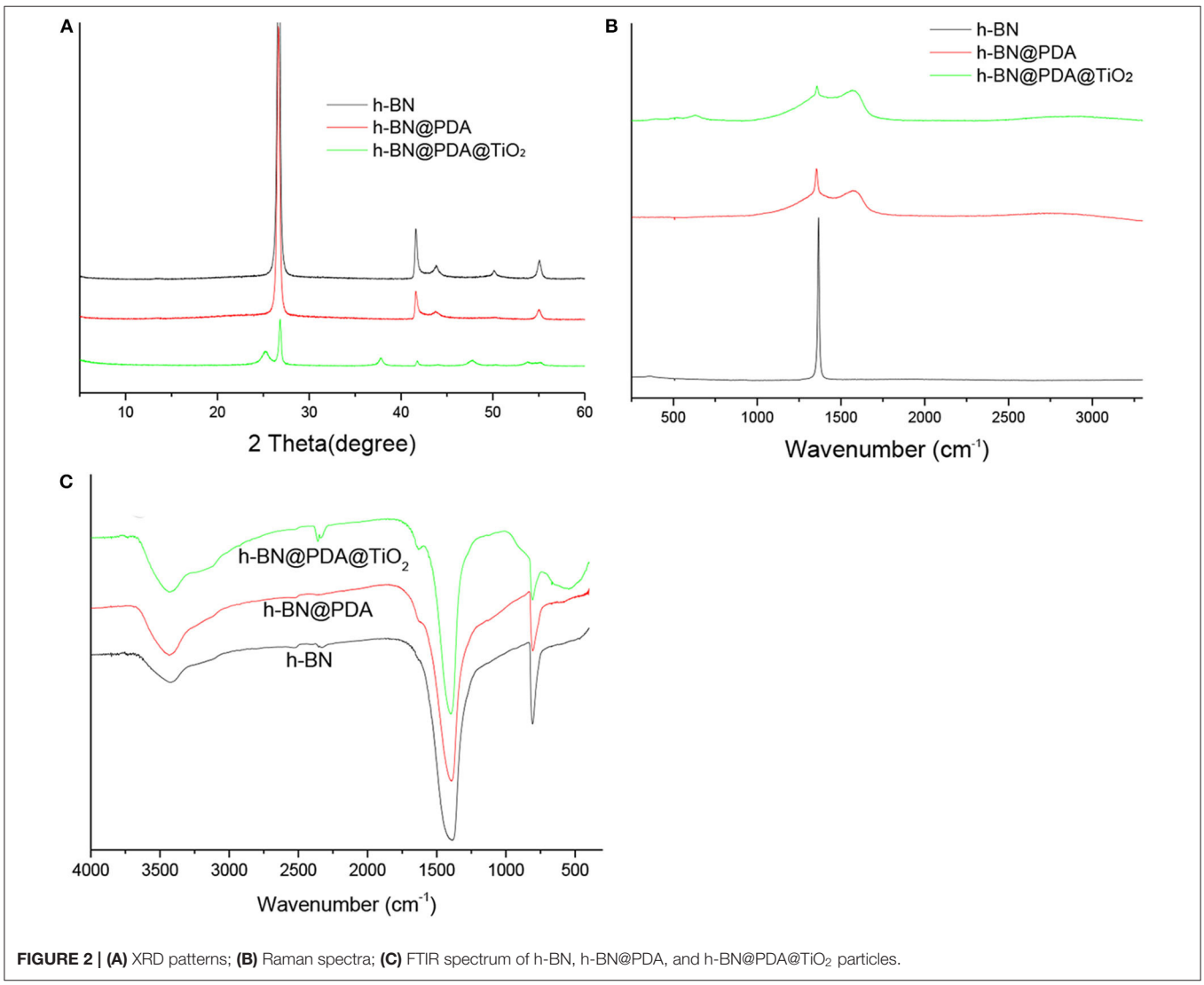

FIGURE 2 | (A) XRD patterns; **(B)** Raman spectra; **(C)** FTIR spectrum of h-BN, h-BN@PDA, and h-BN@PDA@TiO_2 particles.

and h-BN@PDA@TiO_2 hybrid materials, which are consistent with the reported literature and assigned to catechol tensile vibration and deformation in polydopamine structure (Ku et al., 2010). The results also confirmed the successful conversion of dopamine into polydopamine.

The FTIR spectra of h-BN, h-BN@PDA, and h-BN@PDA@TiO_2 are shown in **Figure 2C**. In the FTIR curve of h-BN, the absorption peaks at 1,395 and 804 cm^{-1} correspond to the in-plane stretching vibration peak and out-of-plane bending vibration peak of B-N, respectively. Compared with the FTIR spectra of h-BN, the PDA organic layer on the h-BN nanosheets did not change the FTIR curve significantly. It has been reported that it is difficult to study the surface functional groups of h-BN by FTIR due to the low signal strength of -OH, -NH, and –BN (Zhi et al., 2009). However, when TiO_2 was attached to the surface of h-BN@PDA, the FTIR curve of the hybrid material showed a wide characteristic peak at 562 cm^{-1}, which was attributed to Ti-O vibration peak in TiO_2.

The surface chemical composition of h-BN, h-BN@PDA and h-BN@PDA@TiO_2 was further analyzed by means of XPS. **Figure 3** respectively show the XPS spectra of pure h-BN, h-BN@PDA, and h-BN@PDA@TiO_2. According to literature (Cai et al., 2017), the characteristic peaks at 290.1, 193.5, 402.2, and 537.8 ev on the XPS curve belong to C1s, B1s, N1s, and O1s of h-BN, respectively. It is reasonable that C and O elements appear on the surface of h-BN, and the reason may be that the original powder of h-BN contains impurities. As can be seen from the XPS curve of h-BN@PDA, the characteristic peak strength of C 1s and O 1s in the XPS spectrogram of h-BN coated with PDA is significantly enhanced compared with that of pure h-BN. Meanwhile, in the peak separation of N element, the characteristic peak belonging to NH_2 appears at the position of 399.8 eV. The above results are due to the fact that PDA coating increases the C content on the laminate surface and brings NH_2 group. The characteristic peaks of Ti and O appeared on the XPS spectra of h-BN@PDA@TiO_2, which mainly came from the TiO_2 attached on the surface of h-BN.

Thermal Conductivity Analysis of Nanocomposites

Thermal conductivity plays an important role in the long life and high performance of electronic materials. The simplest and most effective way to improve the thermal conductivity of polymeric materials is to introduce inorganic fillers with high thermal conductivity into the polymer matrix. The prepared h-BN@PDA@TiO_2 hybrid particles were used as fillers to improve the thermal conductivity of PVA. The dispersion of nano-hybrid particles in the PVA matrix can be observed by SEM. As can be seen from **Figure 4b**, the dispersion of nano-particles in the PVA matrix was relatively uniform. In order to compare the thermal conductivity between PVA and PVA nanocomposites, the test samples of the two systems were prepared under the same conditions. **Figure 4a** shows the thermal conductivity of PVA and PVA nanocomposites. It can be seen from the figure that the thermal conductivity of pure PVA is 0.23 $w{\cdot}M^{-1}k^{-1}$. When h-BN@PDA@TiO_2 hybrid nanoparticles were added to PVA, the thermal conductivity of the composite system was significantly higher than that of pure PVA, and increased significantly with the increase of the added amount. When the amount of hybrid particles was increased to 5 wt%, the thermal conductivity of PVA composite reached 0.78w $\bullet m^{-1}k^{-1}$, which was 239.1% higher than that of pure PVA. This significant improvement can be attributed to the extremely high thermal conductivity of h-BN nanosheets. As the amount of hybrid particles added in the PVA matrix increased, the thermal conduction network was gradually formed in the polymer system to facilitate the heat transfer. The functional layer coated on the surface of nanoparticles builds a "bridge" in the two-phase interface of h-BN and the polymer matrix, increasing the contact area between the h-BN nanosheets and PVA and improving the two-phase interface characteristics. This improvement is conducive to phonon transfer, thus reducing the interface thermal resistance between h-BN and PVA matrix and promoting the improvement of thermal conductivity of PVA composite system.

TABLE 1 | TGA analysis of h-BN@PDA@TiO_2/PVA.

Sample (wt%)	$T_{5\%}$ (°C)	$T_{50\%}$ (°C)	Carbon residues at 800°C (wt%)
0	165.5	363.9	4.38
1%	179.8	349.0	6.55
3%	180.2	346.9	6.98
5%	181.7	345.0	9.18
7%	187.3	344.8	11.47

Thermal Stability of PVA Nanocomposites

Thermogravimetric analysis (TGA) is one of the effective methods to analyze the thermal stability of materials. In this study, TGA was used to study the thermal stability of h-BN@PDA@TiO_2/PVA nanocomposites. **Figure 5** shows TGA and DTG curves of PVA nanocomposites, and some important parameters of TGA and DTG curves are summarized in **Table 1**.

It can be seen from **Figure 5** and **Table 1** that $T_{5\%}$ of PVA composites increases gradually with the increase of the amount of nano-hybrid particles. When the additive amount reached 7 wt%, the $T_{5\%}$ of PVA composites reached 187.3°C, which was 21.8°C higher than the pure PVA. This indicates that h-BN@PDA@TiO_2 has the effect of improving the thermal stability of PVA at low temperature, which is mainly attributed to the thermal stability of h-BN nanosheets itself. However, the $T_{50\%}$ of PVA composites was significantly lower than that of pure PVA, which was due to the high thermal conductivity of h-BN and the catalytic action of TiO_2 which promote the early degradation of PVA at high temperature. This early degradation contributes to the formation of protective carbon layer on the surface of PVA earlier, thus improving the thermal stability of the polymer interior. As the addition amount of h-BN@PDA@TiO_2 in PVA gradually increased, the residual amount of carbon residue increased from 4.38% of pure PVA to 11.47% of the addition amount of 7 wt%. Based on the cost, the agglomeration of nanoparticles and

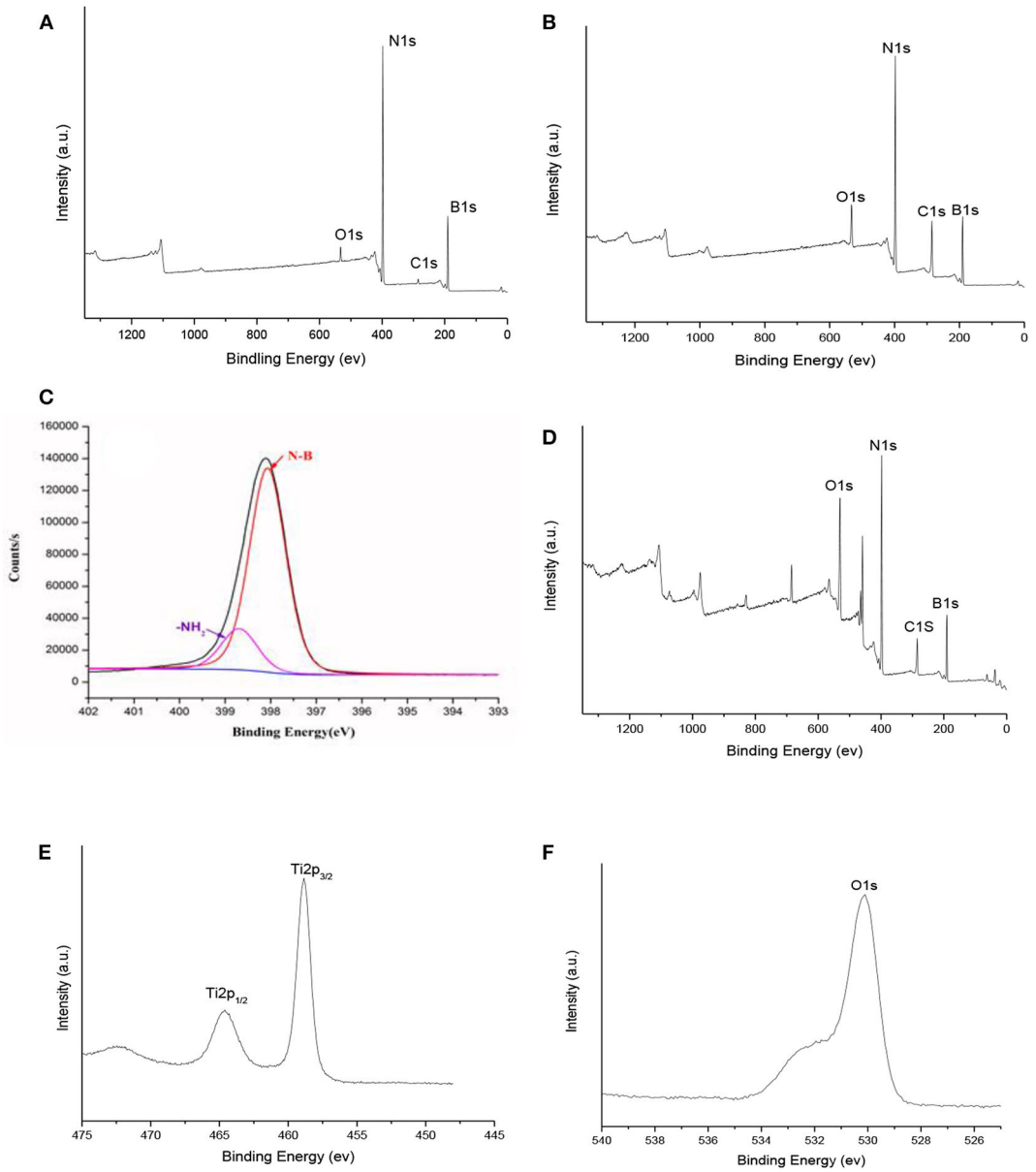

FIGURE 3 | XPS survey scans of **(A)** h-BN; **(B, C)** h-BN@PDA; **(D–F)** h-BN@PDA@TiO_2 particles.

the influence on the thermal stability of PVA, the appropriate addition amount of nano-hybrid particles as a filler is 5 wt%.

Flame Retardant Performance Analysis

The influence of h-BN@PDA@TiO_2 on the flame retardant performance of PVA composites can be obtained by cone test, and the results are shown in **Figure 6**. As can be seen from the figure, the PHRR of pure PVA is 761.39 kW/m^2, while that of h-BN@PDA@TiO_2/PVA (addition amount of hybrid particles: 5 wt%) composite is significantly lower than that of pure PVA. The THR of PVA composite was also lower than that of pure PVA. The improvement of the flame retardancy of PVA composite can be attributed to the following two aspects: on the one hand, the "barrier" effect of h-BN 2-D layer structure can inhibit the release of flammable gases during the combustion of PVA; on the other hand, the carbon layer formed by pyrolysis acts as a barrier. TiO_2 on the surface of hybrid particles can catalyze the formation of carbon, promote the dehydration of PVA into carbon in the combustion process, thus hinder the release of heat and combustible gas and prevent fresh air from entering the combustion area.

SEM was used to analyze the morphology of carbon residue of pure PVA and PVA composite, as shown in **Figure 7**.

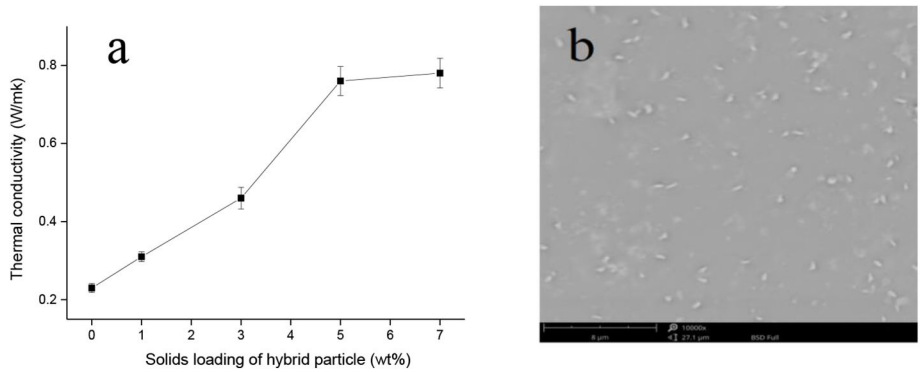

FIGURE 4 | (a) Thermal conductivity and **(b)** SEM image of the fractured surface of PVA composites.

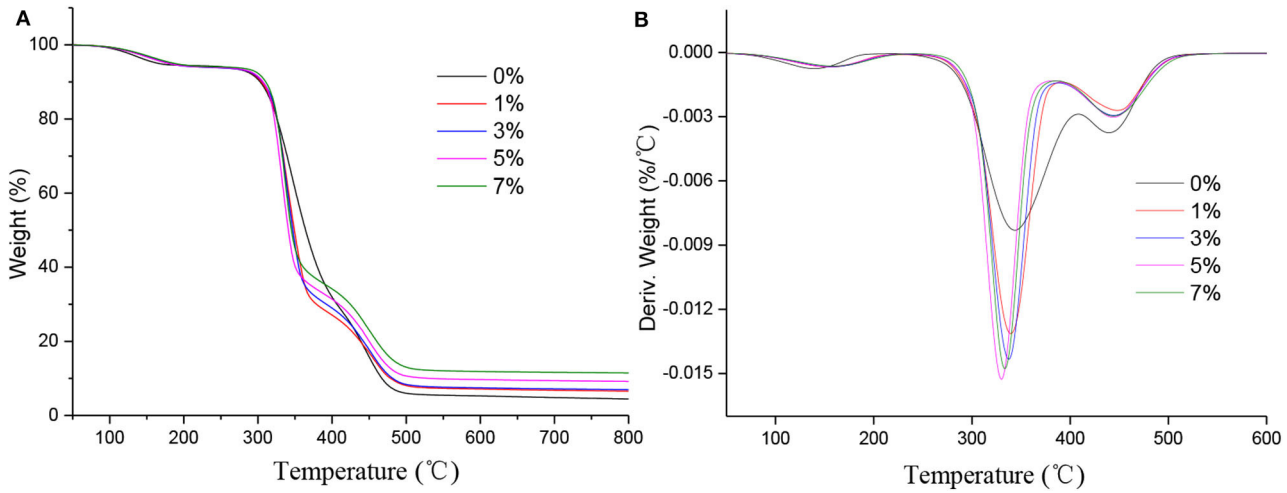

FIGURE 5 | (A) TGA and **(B)** DTG curves of PVA nanocomposites.

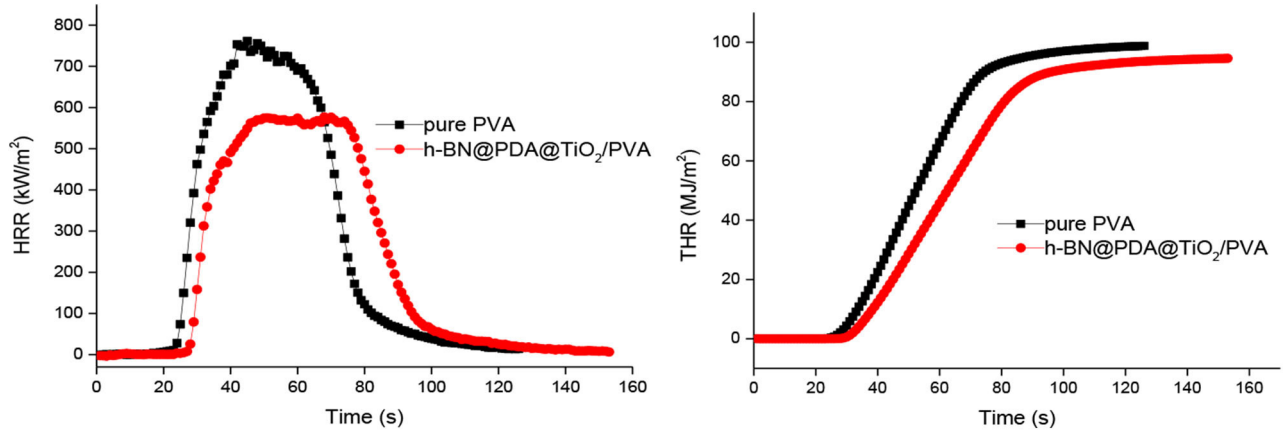

FIGURE 6 | HRR and THR curves of PVA and h-BN@PDA@TiO_2/PVA composites.

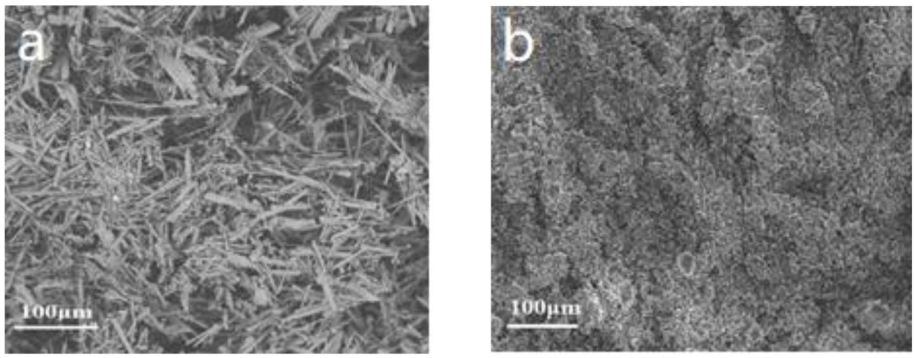

FIGURE 7 | SEM images of carbon residue [**(a)** pure PVA, **(b)** PVA nanocomposite].

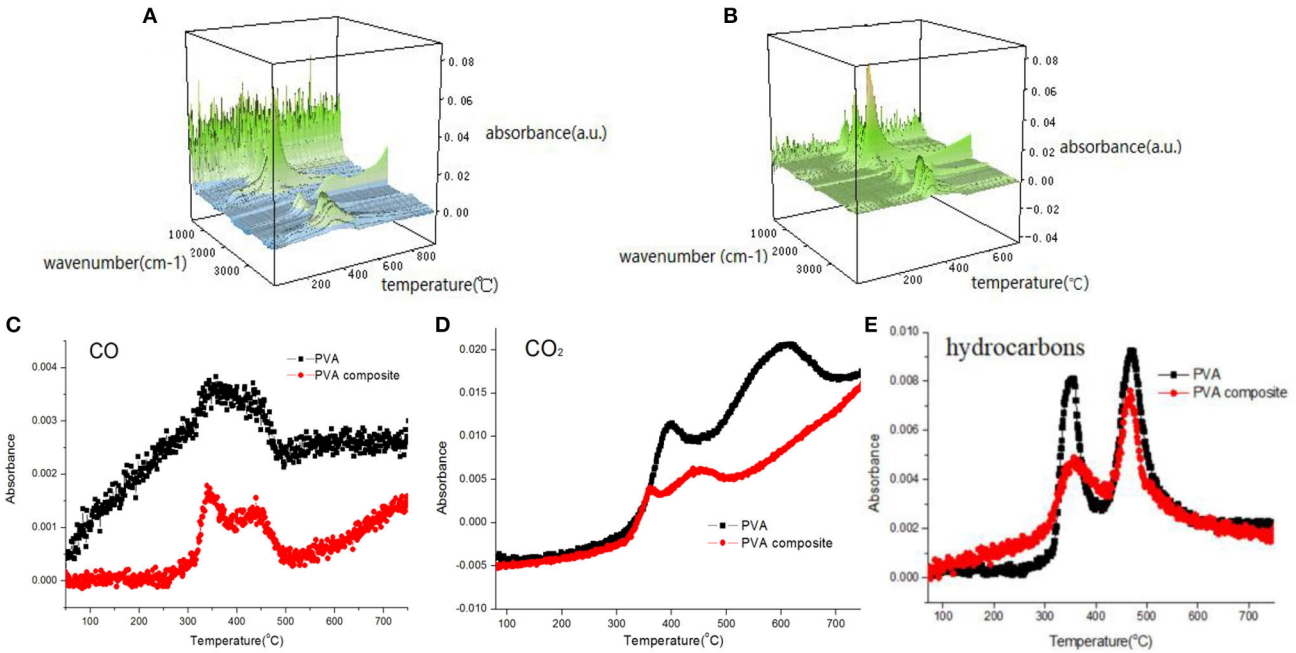

FIGURE 8 | 3D-FTIR spectrum of decomposition products [**(A)** PVA, **(B)** h-BN@PDA@TiO_2/PVA]; absorbance of pyrolysis products for PVA and PVA nanocomposite **(C–E)**.

It can be seen from **Figure 7a** that a large number of holes existed in the carbon residue after pyrolysis of pure PVA, and the carbon layer was not compact. The carbon residue formed by PVA composite pyrolysis was compact and continuous (inset in **Figure 7b**). The reason was that metal oxides in h-BN@PDA@TiO_2 hybrid particles had a strong catalytic carbonization effect, which promoted the production of more carbon residue in the combustion of PVA composites. This also indicated that the addition of h-BN@PDA@TiO_2 hybrid particles was conducive to the formation of a compact carbon layer during PVA pyrolysis, which acted as a "protective shell" for PVA to improve the fire safety of PVA.

Analysis of Gas Phase Products

The gaseous components released during polymer pyrolysis can be tracked and analyzed by means of FT-IR, and then the degradation mechanism of polymer can be studied. The 3D FTIR spectra of PVA and PVA nanocomposites are shown in **Figure 8**. It can be seen from the **Figures 8A,B** that PVA composite has similar infrared characteristic peaks with pure PVA. The attribution decomposition products of these peaks mainly include water (about 3,600–3,700 cm^{-1}), alkane compounds (about 2,800–3,100 cm^{-1}), carbon dioxide (2,300–2,400 cm^{-1}), carbon monoxide (2,180 cm^{-1}), carbonyl compounds (1,740 cm^{-1}) and other organic compounds containing C=C and C-O (1,620 and 1,120 cm^{-1}). **Figures 8C–E**

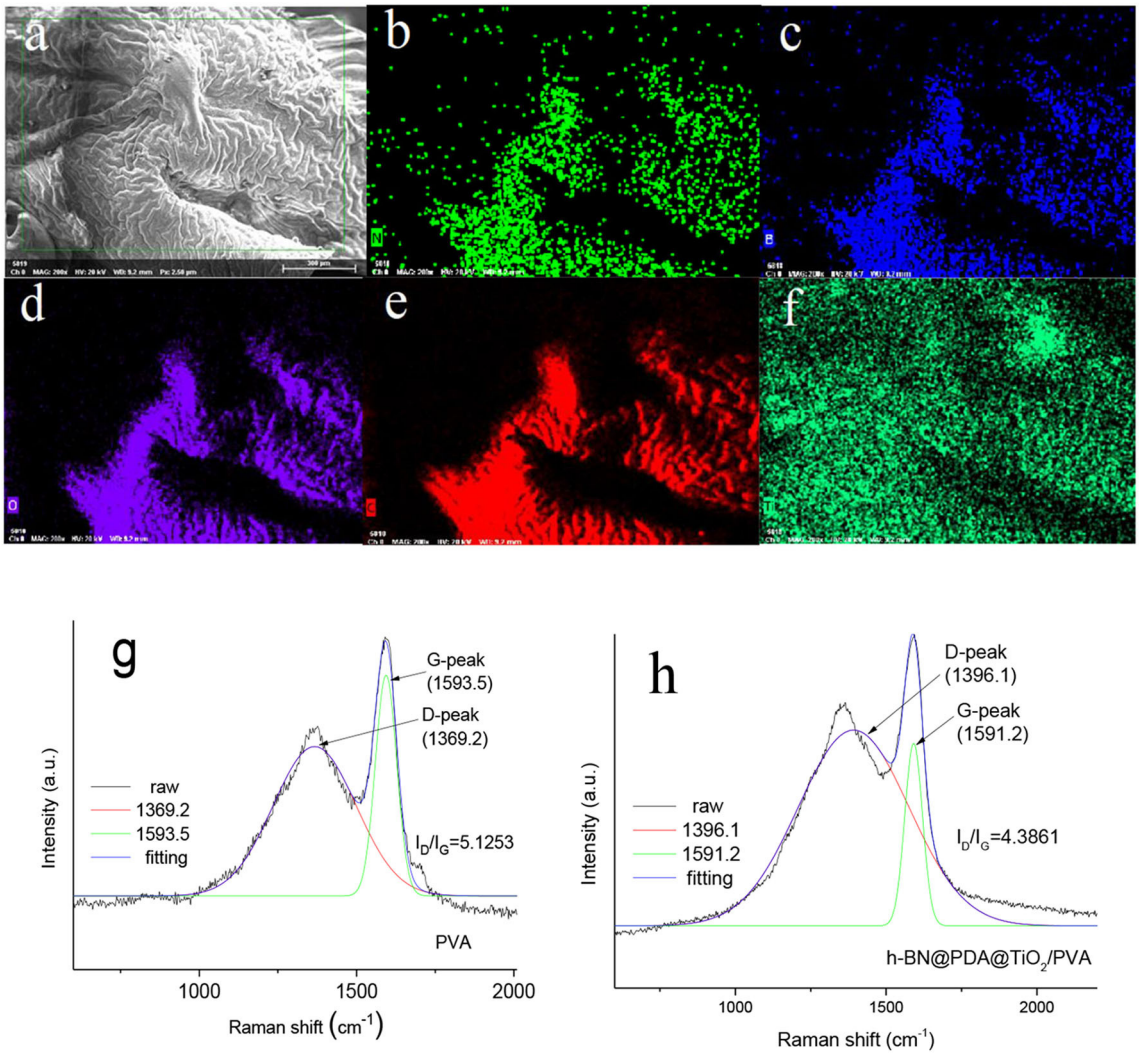

FIGURE 9 | (a–f) Element analysis of carbon residue of PVA composite; **(g, h)** Raman spectrum analysis of PVA and PVA composite carbon residue.

shows the changes of absorbance of pyrolysis products (CO_2, CO, and hydrocarbons). It can be seen that the absorbance strength of pyrolysis products of PVA composite, including combustible volatiles (hydrocarbons and aromatic compounds) and toxic gas (CO), is lower than that of pure PVA sample, indicating that the introduction of h-BN/PDA/TiO_2 reduces the harm brought by pyrolysis products. And, the production of hydrocarbons and aromatic compounds is reduced, which avoids the continuous supply of fuel for the combustion zone. At the same time, as a component of smoke particles, the reduction of the production of aromatic compounds reduces the influence of smoke on visibility in the fire field, which is beneficial to the escape of people. The reduction of CO and other gases is of great significance to the life safety of the escape personnel.

Carbon Residue Analysis

The analysis of the chemical composition of carbon residue is helpful to clarify the solid-phase flame retardant mechanism of h-BN@PDA@TiO_2 during PVA combustion. EDS was used for elemental analysis of carbon residue (inset in **Figure 9**). As can be seen from the **Figures 9a–f** that the carbon residue of PVA composite is rich in elements C, O, B, N, and Ti. It can be considered that C and O are mainly from carbonization products of PVA molecules, while elements B, N, and Ti are mainly from hybrid particles. Moreover, it can be clearly seen that Ti is uniformly dispersed in the outer layer of carbon residue, indicating that metal oxides in the system migrate to the combustion zone of the outer surface of the material during the process of PVA pyrolysis, which plays a better role in the pyrolysis of the polymer into carbon.

Figures 9g,h show Raman spectra of carbon residue of PVA and PVA composites. As can be seen from **Figures 9g,h** Raman spectra of the two samples have similar shapes. And the two peaks of pure PVA carbon residue are 1369.2 and 1,598 cm^{-1}, which correspond to D and G bands. D bands represent the symmetric carbon atom vibration of amorphous carbon, while G bands are caused by the 2-D symmetric stretching vibration of SP2 hybrid fossil carbon atoms. After the addition of h-BN@PDA@TiO_2 hybrid particles, the two peaks of the composite are 1396.1 and 1591.2 cm^{-1}. The graphitization degree of carbon layer residue is usually evaluated by the relative aera ratio of D and G bands (I_D/I_G) (Tang et al., 2019). Generally speaking, the smaller the ratio, the higher the degree of graphitization. The I_D/I_G value of pure PVA is 5.1253. In comparison, the I_D/I_G value of PVA composites has decreased to some extent. This result strongly proves that h-BN@PDA@TiO_2 can promote the graphitization of carbon in the carbon residue.

Combined with gas phase analysis and condensate analysis, we can predict the flame retardant mechanism of hybrid fillers. When affected by high temperature heat source, PVA will decompose to produce combustible gas and burn. The heat generated by combustion will accelerate the decomposition of PVA and produce more combustible gas. At the same time, oxygen entering the flame zone will promote the combustion. The combustion of PVA will lose control and bring great fire risk. When the hybrid nanoparticles with 2-D sheet structure are added to PVA, on the one hand, the 2-D sheet structure of h-BN is conducive to prolong the oxygen and heat transfer path, slow down the diffusion of combustible pyrolysis products, and thus inhibit the extension of combustion region; on the other hand, TiO_2 catalyzes the formation of carbon layer on the surface of PVA., which plays a better protective role on the polymer matrix. The fire safety of PVA is improved by the joint action of the two aspects.

CONCLUSION

In this study, h-BN@PDA@TiO_2 hybrid nanoparticles were prepared and used as functional fillers to prepare PVA nanocomposites, and the effects of hybrid particles on PVA thermal conductivity and flame retardant properties were studied. The results showed that hybrid particles could significantly improve the thermal conductivity of PVA. When the amount of hybrid particles was up to 5 wt%, the thermal conductivity of PVA composite could reach 0.78w • $M^{-1}K^{-1}$, an increase of 239.1% compared with pure PVA. Hybrid particles have an obvious improvement effect on the thermal stability and flame retardant performance of PVA composites, and effectively inhibit the release of toxic gases such as combustible pyrolysis products and CO. As a result, h-BN@PDA@TiO_2 can enhance the fire safety of PVA composite. This is due to the nano-barrier effect of h-BN and the protective effect of dense carbon layer.

DATA AVAILABILITY STATEMENT

All datasets generated for this study are included in the article/supplementary material.

AUTHOR CONTRIBUTIONS

XW worked on the presented work under the guidance of YH. WH assisted in designing and performing experiments. The manuscript was written by XW and WH. All authors contributed to the article and approved the submitted version.

FUNDING

This work was financially supported by the National Natural Science Foundation of China (51991352 and 51874266), the Fundamental Research Funds for the Central Universities (WK2320000043), and the Natural Science Research Project of Department of education of Anhui Province (KJ2019A0686).

REFERENCES

Cai, W., Hong, N., Feng, X., Zeng, W., Shi, Y., Zhang, Y., et al. (2017). A facile strategy to simultaneously exfoliate and functionalize boron nitride nanosheets via Lewis acidbase interaction. *Chem. Eng. J.* 330, 309–321. doi: 10.1016/j.cej.2017.07.162

Cao, J. P., Zhao, X. D., Zhao, J., Zha, J. W., Hu, G. H., and Dang, Z. M. (2014). Improved thermal conductivity and flame retardancy in polystyrene/poly(vinylidene fluride) blends by controlling selective localization and surface modification of SiC nanoparticles. *ACS Appl. Mater. Inter.* 5, 6915–6924. doi: 10.1021/am401703m

Eichler, J., and Lesniak, C. (2008). Boron nitride (BN) and BN composites for high-temperature applications. *J. Eur. Ceram Soc.* 28, 1105–1109. doi: 10.1016/j.jeurceramsoc.2007.09.005

Feng, C., Liang, M., Jiang, J., Zhang, Y., Huang, J., and Liu, H. (2016). Synergism effect of CeO2 on the flame retardant performance of intumescent flame retardant polypropylene composites and its mechanism. *J. Anal. Appl. Pyro.* 122, 405–414. doi: 10.1016/j.jaap.2016.07.006

Feng, Y. Z., Han, G. J., Wang, B., Zhou, X. P., Ma, J. M., Ye, Y., et al. (2020). Multiple synergistic effects of graphene-based hybrid and hexagonal born nitride in enhancing thermal conductivity and flame retardancy of epoxy. *Chem. Eng. J.* 379:122402. doi: 10.1016/j.cej.2019.122402

Feng, Y. Z., Li, X. W., Zhao, X. Y., Ye, Y., Zhou, X., Liu, H., et al. (2018). Synergetic improvement in thermal conductivity and flame retardancy of epoxy/silver nanowires composites by incorporating "branch-like" flame-retardant functionalized graphene. *ACS Appl. Mater. Interfaces* 10, 21628–21641. doi: 10.1021/acsami.8b05221

Golberg, D., Bando, Y., Huang, Y., Terao, T., Mitome, M., Tang, C., et al. (2010). Boron nitride nanotubes and nanosheets. *ACS Nano*. 4, 2979–2993. doi: 10.1021/nn1006495

Gorbachev, R. V., Riaz, I., Nair, R. R., Jalil, R., Britnell, L., Belle, B. D., et al. (2011). Hunting for monolayer boron nitride: optical and Raman signatures. *Small* 7, 465–468. doi: 10.1002/smll.201001628

Huang, G., Chen, S., Tang, S., and Gao, J. (2012). A novel intumescent flame retardant-functionalized graphene: nanocomposite synthesis, characterization, and flammability properties. *Mater. Chem. Phys.* 135, 938–947. doi: 10.1016/j.matchemphys.2012.05.082

Ku, S. H., Lee, J. S., and Park, C. B. (2010). Spatial control of cell adhesion and patterning through mussel-inspired surface modification by polydopamine. *Langmuir* 26, 15104–15108. doi: 10.1021/la102825p

Lam, Y. L., Kan, C. W., and Yuen, C. W. M. (2011). Effect of titanium dioxide on the flame-retardant finishing of cotton fabric. *J. App. Polym. Sci.* 121, 267–278. doi: 10.1002/app.33618

Liao, S. H., Liu, P. L., Hsiao, M. C., Teng, C. C., Wang, C. A., Ger, M. D., et al. (2012). One-step reduction and functionalization of graphene oxide with phosphorus-based compound to produce flame-retardant epoxy nanocomposite. *Ind. Eng. Chem. Res.* 51, 4573–4581. doi: 10.1021/ie210.1002/pat.4646026647

Maddalena, L., Carosio, F., Gomez, J., Saracco, G., and Fina, A. (2018). Layer-by-layer assembly of efficient flame retardant coatings based on high aspect ratio graphene oxide and chitosan capable of preventing ignition of PU foam. *Polym. Degrad. Stabil.* 152, 1–9. doi: 10.1016/j.polymdegradstab.2018.03.013

Mor, G. K., Shankar, K., Paulose, M., Varghese, O. K., and Grimes, C. A. (2005). Enhanced photocleavage of water using titania nanotube arrays. *Nano Lett.* 5, 191–195. doi: 10.1021/nl048301k

Safdari, M., and Al-Haik, M. S. (2013). Synergistic electrical and thermal transport properties of hybrid polymeric nanocomposites based on carbon nanotubes and graphite nanoplatelets. *Carbon* 64, 111–121. doi: 10.1016/j.carbon.2013.07.042

Shang, K., Liao, W., and Wang, Y. Z. (2018). Thermally stable and flame-retardant poly(vinyl alcohol)/montmorillonite aerogel via a facile heat treatment. *Chin. Chem. Lett.* 29, 433–436. doi: 10.1016/j.cclet.2017.10.1002/pat.464608.017

Shi, Y. Q., Liu, C., Duan, Z. P., Yu, B., Liu, M. H., and Song, P. (2020). Interface engineering of MXene towards super-tough and strong polymer nanocomposites with high ductility and excellent fire safety. *Chem. Eng. J.* 399:125829. doi: 10.1016/j.cej.2020.125829

Shi, Y. Q., Liu, C., Liu, L., Fu, L., Yu, B., Lv, Y. C., et al. (2019). Strengthening, toughing and thermally stable ultra-thin MXene nanosheets/polypropylene nanocomposites via nanoconfinement. *Chem Eng J.* 378:122267. doi: 10.1016/j.cej.2019.122267

Tang, G., Liu, X., Zhou, L., Zhang, P., Deng, D., and Jiang, H. (2019). Steel slag waste combined with melamine pyrophosphate as a flame retardant for rigid polyurethane foams. *Adv. Powder Technol.* 31, 279–286. doi: 10.1016/j.apt.2019.10.020

Uchida, S., Chiba, R., Tomiha, M., Masaki, N., and Shir, M. (2002). Application of titania nanotubes to a dye-sensitized solar cell. *Electrochemistry* 70, 418–420. doi: 10.5796/electrochemistry.70.418

Wang, X. D., Yin, Y. J., Li, M., and Hu, Y. (2020). Hexagonal boron Nitride@ZnFe2O4 hybrid nanosheet: an ecofriendly flame retardant for polyvinyl alcohol. *J. Solid State Chem.* 287:121366. doi: 10.1016/j.jssc.2020.121366

Wang, Z., Huang, Y., Zhang, G., Wang, H. Q., Xu, J. Z., Lei, J., et al. (2018). Enhanced thermal conductivity of segregated poly(vinylidene fluoride) composites via forming hybrid conductive network of boron nitride and carbon nanotubes. *Ind. Eng. Chem. Res.* 57, 10391–10397. doi: 10.1021/acs.iecr.8b01764

Weng, Q., Wang, X., Wang, X., Bando, Y., and Golberg, D. (2016). Functionalized hexagonal boron nitride nanomaterials: emerging properties and applications. *Chem. Soc. Rev.* 45, 3989–4012. doi: 10.1039/C5CS00869G

Wu, J., Han, W. Q., Walukiewicz, W., Ager, J. W., Shan, W., Haller, E., et al. (2004). Raman spectroscopy and time-resolved photoluminescence of BN and BxCyNz nanotubes. *Nano Lett.* 4, 647–650. doi: 10.1021/nl049862e

Xu, J., Li, K., Deng, H., Shu, L., Fang, P., Liu,. H., et al. (2019). Preparation of MCA-SiO2 and its flame retardant effects on glass fiber reinforced polypropylene. *Fiber. Polym.* 20, 120–128. doi: 10.1007/s12221-019-8284-6

Xu, M., Liang, T., Shi, M., and Chen, H. (2013). Graphene-like two-dimensional materials. *Chem. Rev.* 113, 3766–3798. doi: 10.1021/cr300263a

Zhang, Q., Wang, X., Tao, X., Li, Z., Li, X., and Zhang, Z. (2019). Polyvinyl alcohol composite aerogel with remarkable flame retardancy,chemical durability and self-cleaning property. *Compos. Com.* 15, 96–102. doi: 10.1016/j.coco.2019.07.003

Zhang, Z., Pan, H., Ma, W., Liang, J., Shen, Q., Zhu,Q., et al. (2019). Synthesis of CeO^2-loaded titania nanotubes and its effect on the flame retardant property of epoxy resin. *Polym. Advan. Technol.* 30, 2136–2142. doi: 10.1002/pat.4646

Zhi, C., Bando, Y., Tang, C., Kuwahara, H., and Golberg, D. (2009). Large-scale fabrication of boron nitride nanosheets and their utilization in polymeric composites with improved thermal and mechanical properties. *Adv. Mater.* 21, 2889–2893. doi: 10.1002/adma.200900323

Conflict of Interest: The authors declare that the research was conducted in the absence of any commercial or financial relationships that could be construed as a potential conflict of interest.

The handling Editor declared a past co-authorship with the authors WH and YH.

frontiers in Materials

ORIGINAL RESEARCH
published: 09 November 2020
doi: 10.3389/fmats.2020.574924

Effect of Bamboo Flour on Flame Retardancy and Smoke Suppression of Polypropylene/Ammonium Polyphosphate Composites

Yide Liu[1], Hongzhou Li[1], Qinghua Chen[1,2]*, Fubin Luo[1] and Changlin Cao[1]*

[1]College of Environmental Science and Engineering, Fujian Normal University, Fuzhou, China, [2]Fujian Polytechnic Normal University, Fuqing, China

In this paper, the flame-retardant Polypropylene (PP) composites were prepared by melt blending. Ammonium Polyphosphate (APP) and bamboo flour (BF) were selected as flame retardant and smoke suppressant of the composite material. Among them, BF as a synergist can effectively improve the flame retardancy and smoke suppression effect of PP/APP composites. The effects of BF on the mechanical properties, crystallization behavior, thermal degradation, flame retardancy, and especially the smoke suppression effect of PP/APP composite materials were studied. thermogravimetric analysis, limiting oxygen index, cone calorimetry, scanning electron microscopy and other characterization methods were used to study the thermal stability, flame retardancy and combustion characteristics of the composites and the microscopic morphology of carbon residue. Experimental results showed that when the total addition amount of APP/BF (2:1) in PP55/APP30/BF15 composite is 45%, the residual carbon had more specific surface area and micro-pores, which causes the composite to have the best smoke suppression effect. The PHRR of the PP55/APP30/BF15 composite was reduced to 308.2 kW/m^2 and the amount of carbon residue was 25%. The continuous carbon layer, formed during combustion can effectively protect the matrix material and prevent the transfer of heat.

Keywords: polypropylene, ammonium polyphosphate, bamboo flour, smoke suppression, flame retardancy

OPEN ACCESS

Edited by:
Bin Yu,
University of Southern Queensland, Australia

Reviewed by:
Jun Sun,
Beijing University of Chemical Technology, China
Wei Yang,
Hefei University, China
Gang Tang,
Anhui University of Technology, China

****Correspondence:***
Hongzhou Li
lihongzhou@fjnu.edu.cn,
Qinghua Chen
cqhuar@fjnu.edu.cn

Specialty section:
This article was submitted to Polymeric and Composite Materials, a section of the journal Frontiers in Materials

Received: *22 June 2020*
Accepted: *18 August 2020*
Published: *09 November 2020*

Citation:
Liu Y, Li H, Chen Q, Luo F and Cao C (2020) Effect of Bamboo Flour on Flame Retardancy and Smoke Suppression of Polypropylene/Ammonium Polyphosphate Composites. Front. Mater. 7:574924. doi: 10.3389/fmats.2020.574924

INTRODUCTION

Polypropylene (PP) is a thermoplastic polymer with excellent comprehensive properties, and it is now widely used in construction, packaging, transportation and furniture (Kumar et al., 2017). Due to the poor heat resistance and the poor flame retardancy of PP, its application is limited to a relatively low temperature (Abu Bakar et al., 2010; Xu et al., 2019). At present, halogen-free flame-retardant technology is a research focus in the field of flame retardancy for environmental and health consideration. In this field, many scholars are focusing on 2D flame retardant materials, such as transition metal compounds because they have excellent catalytic oxidation properties (Kong et al., 2019; Shi et al., 2019; Yu et al., 2020), but the preparation of such flame retardants is usually more complicated and the actual cost of application is higher. In addition, phosphorus-containing flame retardants are often used for flame retardant treatment of polymer because they are rich in phosphorus elements, such as melamine pyrophosphate, aluminum diethylphosphinate, etc.

(Tang et al., 2020b; Tang et al., 2020c). This type of flame retardant usually needs to be compounded with carbon sources such as expanded graphite (Tang et al., 2020a). Most of them are additive-type flame retardants, which require a large amount of addition. Therefore, it will increase the cost of flame-retardant treatment. In summary, the development of low-cost environmentally friendly additive-type flame retardants will be of great significance to actual production.

Phosphorus-based intumescent systems have a wide application range and high flame-retardant efficiency, so they are suitable for polymers flame retardant (Yang et al., 2011; Wang et al., 2012). Ammonium polyphosphate (APP) is a typical representative of halogen-free flame retardants, which has the advantages of high efficiency and is environmentally friendly. In addition, the production process of APP is simple, and it is widely used in the market. Therefore, APP as an intumescent flame retardant is widely used in polymer materials (Zhou et al., 2011; Zhao et al., 2018; Dong et al., 2020; Wu et al., 2020a; Wu et al., 2020b; Xu et al., 2020). When APP is pyrolyzed, it will promote the dehydration of the matrix and be decomposed by heat to form carbides and phosphoric acid, and then cover the surface of the matrix with a carbon layer. At the same time, APP is decomposed by heat to generate NH3 and H2O, which can dilute the concentration of flammable gas in the air, thereby taking effect as a flame retardant (Wang et al., 2020). The addition of APP into the PP matrix can improve the flame retardancy of PP, nevertheless the smoke suppression performance of this composite material is poor. We found that when bamboo flour (BF) and APP were added in PP with a certain proportion, the smoke suppression effect of PP is improved.

Bamboo has a short growth cycle and wide range of planting. Therefore, bamboo resources are abundant. As a biomass material, BF has the advantages of good thermal stability, low cost and degradability (Nie et al., 2013). Because BF has so many advantages, its application is increasingly extensive (Lee et al., 2009; Chattopadhyay et al., 2011; Li et al., 2019; Fang et al., 2020). However, the effect of flame retardancy via adding BF and APP into PP and studying of its smoke suppression performance has rarely been reported.

In this study, BF and APP were used as a compound flame retardant for PP flame retardant modification, and an environmentally friendly PP composite with flame retardancy was prepared by a blending process. Flame retardancy and smoke suppression tests were carried out on the prepared PP composites by the limiting oxygen index (LOI), the vertical burning method (UL-94), and the cone calorimeter test, and the thermal stability of materials by thermogravimetric analysis (TGA). Then, the scanning electron microscopy (SEM) was used to analyze the morphology of the samples after the cone test.

EXPERIMENT

Materials

Polypropylene (PP, PPR-4220, random copolymer, MFI: 0.4 g/10 min) was supplied by China Petrochemical, Co., Ltd. (China). Ammonium polyphosphate (APP, Degree of polymerization ≥1,000) was bought from Shandong Taixing New Material, Co., Ltd. (China). BF was bought from Quanzhou Baixin Biotechnology, Co., Ltd. (China), and the particle size of BF is about 60 μm.

The Preparation of Samples

PP, APP and BF were dried in a blast drying oven (DHG-9070A) at 80°C for 12 h before the experiment. First, APP and BF were added in a small high-speed mixer (FW177) at a fixed speed of 500 rpm and were mixed for 10 min to obtain a compound flame retardant. Second, the samples were prepared by mixing the compound flame retardant with PP in a two-roll mill (ZG-200) at 190°C for 15 min, with a roller speed of 30 rpm. The components of samples are shown in **Table 1**. Third, the right amount of material was weighed and put in a flat vulcanizing machine (ZG-80T), removing the samples after being pressed for 15 min under 10 MPa pressure. Finally, the samples were dried at room temperature for 24 h, and various test splines were cut through a universal sample preparation machine (WZY-240).

Mechanical Properties Test

The tensile strength test and flexural strength test were performed on a CMT-4104 universal mechanical testing machine (produced by Shenzhen Xinsansi Material Testing, Co., Ltd), where the tensile speed is set as 50 mm/min, and the bending speed is 2 mm/min. The simple supported beam impact test was performed on a ZBC500 testing machine (produced by Shenzhen Xinsansi Material Testing, Co., Ltd.).

Cross-Section Topography

The samples were brittle after being frozen in liquid nitrogen and a part of the complete section of the samples was cut out. Then, the sections were subjected to gold spraying treatment and the cross-section morphology was observed at 5 kV by a Regulus 8100 cold field emission scanning electron microscope (produced by Japan Hitachi Company).

DSC Test

The Q20 differential scanning calorimeter (TA Instruments) was used to study the melting and crystallization behavior of the samples. Approximately 7 mg of the sample was weighed and placed in an alumina crucible. First, the samples were heated from 30 to 200°C at a rate of 10°C/min and equilibrated for 5 min to eliminate thermal history under nitrogen atmosphere protection. Then, the temperature was reduced to 30°C at a rate of 10°C/min and equilibrated for 5 min. Finally, the samples were heated to 200°C at a rate of 10°C/min and the DSC curve was recorded.

Flame Retardancy Test

The LOI was measured by a HC-2C oxygen index meter (Nanjing Shangyuan Analysis Instrument Company, China). The LOI test was performed according to the ASTM D2863-77. The LOI refers to the volume fraction concentration of oxygen just supporting combustion in the oxygen and nitrogen mixed gas. The specimen dimensions were 125 mm × 6.5 mm × 3.2 mm and five samples for each group were tested.

TABLE 1 | The components of samples.

Samples	PP	PP70/APP30	PP70/BF30	PP65/APP30/BF5	PP60/APP30/BF10	PP55/APP30/BF15
PP/%	100	70	70	65	60	55
BF/%	0	0	30	5	10	15
APP/%	0	30	0	30	30	30

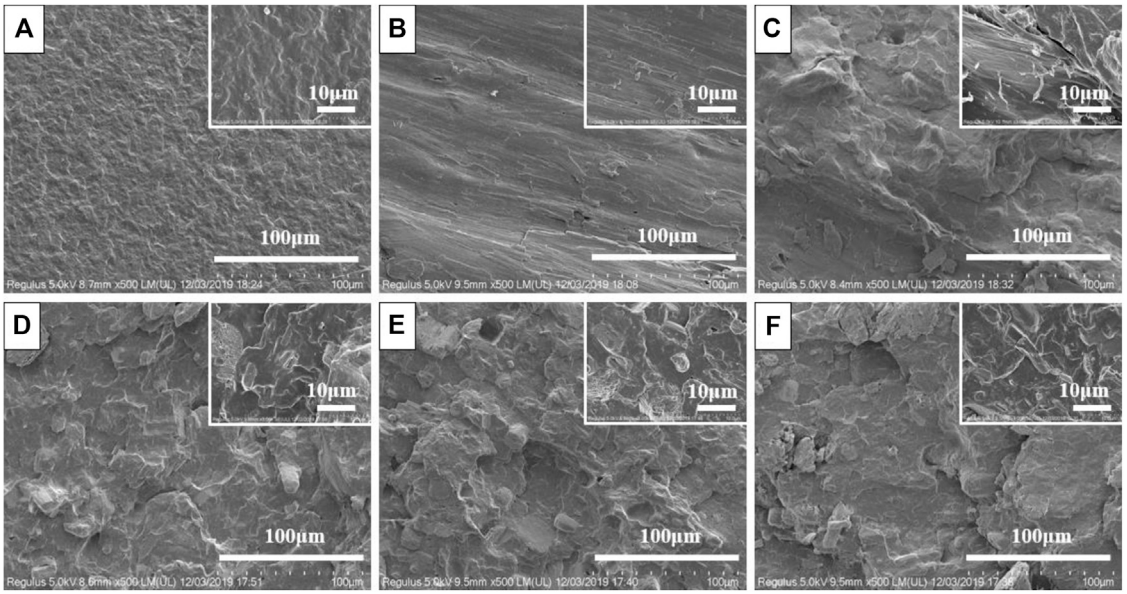

FIGURE 1 | SEM micrographs of PP and composites. (**(A)** PP; **(B)** PP70/APP30; **(C)** PP70/BF30; **(D)** PP65/APP30/BF5; **(E)** PP60/APP30/BF10; **(F)** PP55/APP30/BF15).

The UL-94 vertical burning test was performed on a CZF-4 vertical burning tester (Nanjing Shangyuan Analysis Instrument Company, China), according to ASTM D635-77. The specimen dimensions used for the test were 125 mm × 13 mm × 3.2 mm.

Thermal Stability Test

The TGA was carried out using a SDT Q600 (TA Instruments) thermo-analyzer instrument at a linear heating rate of 10°C/min under a nitrogen atmosphere, and the test temperature ranged from 30 to 700°C. Samples with a mass of about 5–10 mg were weighed in a clean alumina crucible.

Cone Calorimeter Test

The cone calorimeter test is a method that can effectively reflect the fire level. The materials were tested for burning performance using a cone calorimeter (FTT classic, United Kingdom), and the specimen dimensions were 100 mm × 100 mm × 4 mm. The test was carried out under the ISO 5660-1 standard with a heat flow of 35 kW/m^2.

Scanning Electron Microscopy Analysis

The microscopic morphology of the char residues after the cone test was examined by a Regulus 8100 cold field emission scanning electron microscope (produced by Japan Hitachi Company).

RESULTS AND DISCUSSION

Section Characterization

In order to analyze and study the dispersion of flame retardants in PP, the splines were brittlely broken under the condition of liquid nitrogen, and the cross-sectional morphology of the samples was analyzed by SEM. **Figure 1** is the SEM images of the samples at different magnifications. As can be seen from **Figure 1A**, the section of pure PP is relatively flat, with a lamellar structure, and behaves as a typical ductile fracture. After joining APP, the sectional view is shown in **Figure 1B**. The cross section is smooth and tidy, showing a uniform shape which is a typical brittle fracture. As can be seen from **Figure 1C**, fibrous BF is evenly wrapped by PP and disperses well. Comparing **D, E, F** in **Figure 1**, it can be seen that the interface becomes rough and fuzzy when APP and BF were mixed, and some flours were pulled out. This is due to the agglomeration of APP and BF, which reduces the compatibility with the matrix. At the same time, larger roughness caused a larger gap between the flame retardant and the matrix PP. If an external force was applied, these gaps will form stress concentrations.

Mechanical Properties

The tensile strength, flexural strength and impact strength of the samples are shown in **Figure 2-4**, respectively. It can be seen from

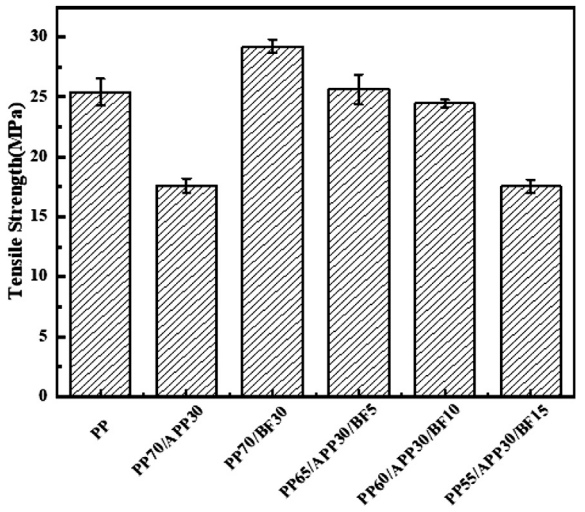

FIGURE 2 | Tensile strength of PP and composites.

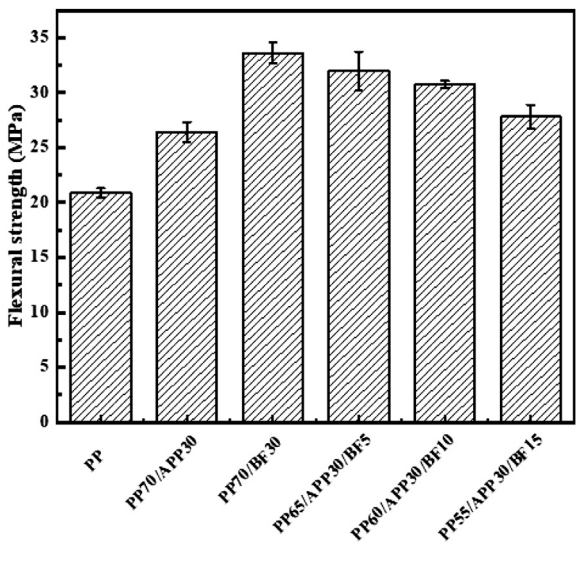

FIGURE 3 | Flexural strength of PP and composites.

Figure 2 that the tensile strength of PP was 25.4 MPa. After adding APP, the tensile strength decreased sharply due to APP agglomeration. When 30% BF was added, the tensile strength of the PP70/BF30 sample reached 29.3 MPa, which might be ascribed to BF having a good strengthening effect. Among the PP65/APP30/BF5, PP60/APP30/BF10, and PP55/APP30/BF15 samples, the mechanical properties of the three samples were decreased when the compound flame retardants were added. This is due to the poor compatibility between flame retardants and the matrix. However, the addition of BF could properly enhance the flexural strength of PP/APP composites, as seen from the result of samples PP65/APP30/BF5, PP60/APP30/BF10, and PP55/APP30/BF15 in **Figure 3**. It is possible that BF

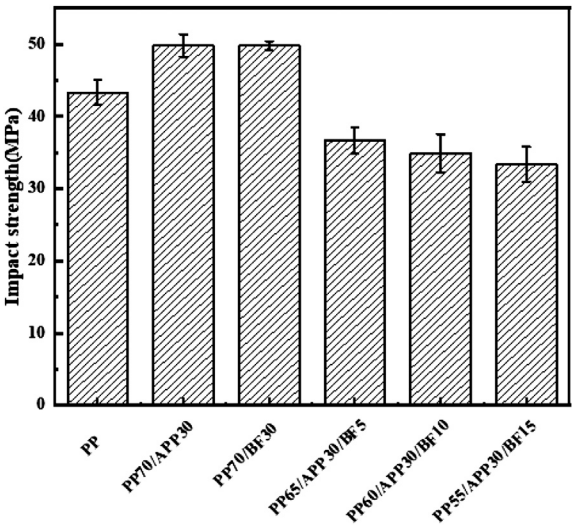

FIGURE 4 | Impact strength of PP and composites.

was arranged in the matrix along the stress direction, resulting in the increase of the bending strength. It can be seen from **Figure 2-4** that the tensile strength and impact strength of the samples PP65/APP30/BF5, PP60/APP30/BF10, and PP55/APP30/BF15 were slightly decreased. This may be because the flame retardants cannot be well dispersed in the matrix, and agglomeration occurs in some places, and stress concentrations formed around the agglomerated particles. At the same time, due to the large particle size of the agglomerated particles, their compatibility with the matrix is poor. Therefore, the tensile strength and impact strength of the composites are reduced.

Thermal Performance

The DSC chart of PP and composite materials is shown in **Figure 5**, and the main data of the samples after DSC tests are listed in **Table 2**. As can be seen from **Figure 5** and **Table 2**, the crystallization temperature and melting temperature of pure PP were 109.6 and 144.7°C, respectively. When APP and BF were added separately, the crystallization temperature and melting temperature of the samples increased. This is due to the heterogeneous nucleation of APP or BF in the PP phase. PP or BF forms a crystal nucleus, which reduces the mobility of the PP molecular chain, thus leading to a higher crystallization temperature and melting temperature of the composite material. When APP and BF are mixed, there may have a hydrogen bonding which weakens heterogeneous nucleation to a certain extent (Kumar and Tumu, 2019; Ding et al., 2020; Yang et al., 2020). As the amount of BF addition increases, the crystallization temperature increased gradually. The crystallization temperatures of the samples PP65/APP30/BF5, PP60/APP30/BF10 and PP55/APP30/BF15 were 108.4, 110.9, and 111.4°C, and there was no significant change in the melting temperature of these samples.

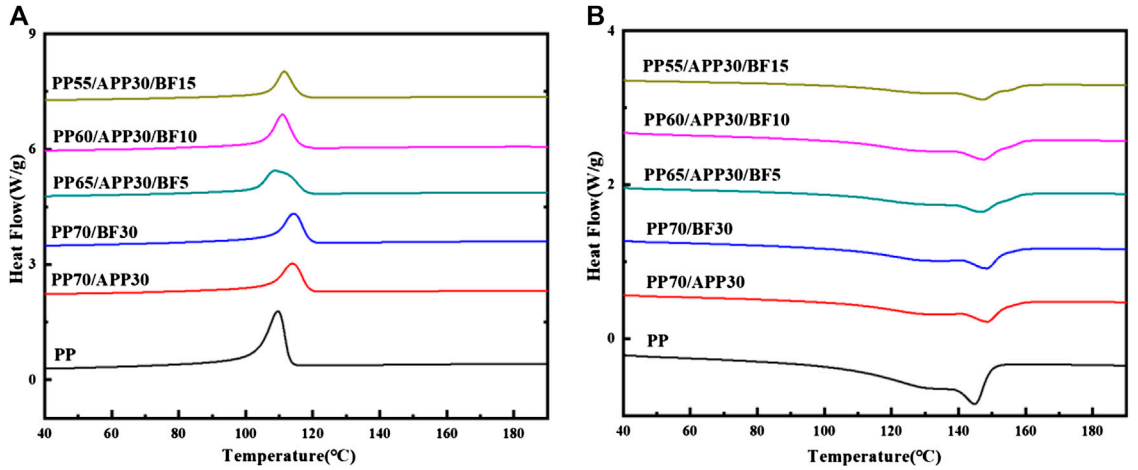

FIGURE 5 | DSC curves of PP and composites. (**(A)** cooling curves; **(B)** heating curves).

TABLE 2 | Main data of DSC tests obtained for PP and composites.

Samples	T_c (°C)	T_m (°C)
PP	109.6	144.7
PP70/APP30	114.1	148.7
PP70/BF30	114.5	148.4
PP65/APP30/BF5	108.4	147.2
PP60/APP30/BF10	110.9	147.7
PP55/APP30/BF15	111.4	147.7

T_c is the crystallization temperature of sample, T_m is the melting temperature of sample.

TABLE 3 | Results of flame-retardant test.

Samples	LOI/vol%	UL-94
PP	21 ± 0.5	No rating
PP70/APP30	33 ± 0.5	No rating
PP70/BF30	20 ± 0.5	No rating
PP65/APP30/BF5	33 ± 0.5	No rating
PP60/APP30/BF10	34 ± 0.5	V-2
PP55/APP30/BF15	32 ± 0.5	V-1

Flame Retardant Properties

The results of LOI and UL-94 vertical burning test are shown in **Table 3**. According to **Table 3**, pure PP had a LOI oxygen index of 21, which is easy to burn in air. The LOI of sample PP70/BF30 was 20, which was lower than the pure PP sample, indicating that the addition of BF promotes the flammability of PP. This result was confirmed by the TTI (time to ignition) value in the subsequent cone test, because the BF is a flammable material which reduces the thermal stability of BF/PP. The LOI values of samples PP65/APP30/BF5, PP60/APP30/BF10, and PP55/APP30/BF15 were 33, 34, and 32, respectively. This indicates that the presence of APP, the LOI value of these samples is not significantly affected as the content of BF increases. It can be seen from the UL-94 grade listed in **Table 3** that adding BF or APP alone does not achieve a higher flame-retardant grade of PP. When the content of APP in the sample is 30%, the UL-94 grade of the sample increased as the content of BF increases. The UL-94 grades of samples PP65/APP30/BF5, PP60/APP30/BF10, and PP55/APP30/BF15 were no rating, V-2, and V-1, respectively. The samples which added both APP and BF showed a dense carbon layer after combustion. This indicates that the addition of BF can effectively improve the flame retardancy of PP/APP composites and promote the formation of charcoal.

Thermal Stability Test

The TGA and DTG curves of samples are shown in **Figure 6**. Pure PP begins to decompose at around 320°C and the maximum decomposition temperature (T_{max}) was 450°C. Due to the poor thermal stability of BF, the PP70/BF30 composite had poor stability. **Figure 7A** shows that the sample PP70/BF30 underwent two stages of the pyrolysis and decomposition of residual carbon. The main peak between 340 and 370°C was assigned to the degradation of a-cellulose (Lewin and Basch, 1978). This sample has almost no residue at 700°C. This result shows that adding BF or APP reduced the initial decomposition temperature of the samples. Because APP is thermally decomposed to form ammonium polymetaphosphate, it promotes the decomposition of BF and the matrix to form a carbon layer covering the surface of the substrate. It can be seen from the DTG curve that when BF or APP was added, the temperature corresponding to the maximum decomposition rate of the sample moves in the direction of a high temperature. The temperature corresponding to the maximum decomposition rate of the PP65/APP30/BF5, PP60/APP30/BF10, and PP55/APP30/BF15 increased to 483, 485, and 491°C, respectively. This is probably due to the fact that when APP and BF were added into PP, the samples formed a highly stable carbon layer under the flame which can protect the matrix from further decomposition. The residue data of the thermogravimetric analysis was consistent with the residue data after the cone test. Pure PP residue content was only 0.5% at 700°C, while the residue content of the PP55/APP30/BF15 sample was as high as 11.4%, as shown in **Table 4**. This indicates that the addition of APP and BF allows PP to form a dense protective carbon layer.

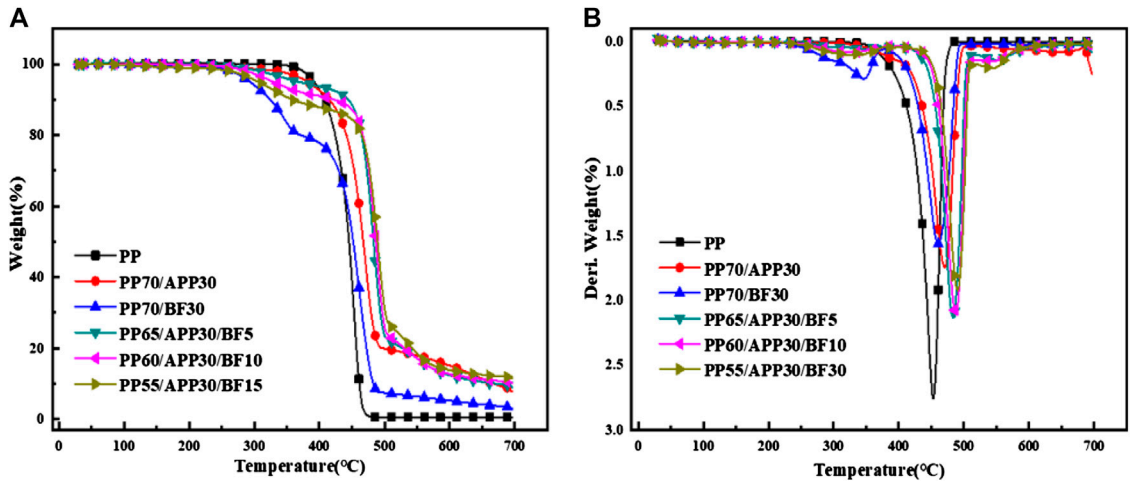

FIGURE 6 | TGA **(A)** and DTG **(B)** curves of PP and composites.

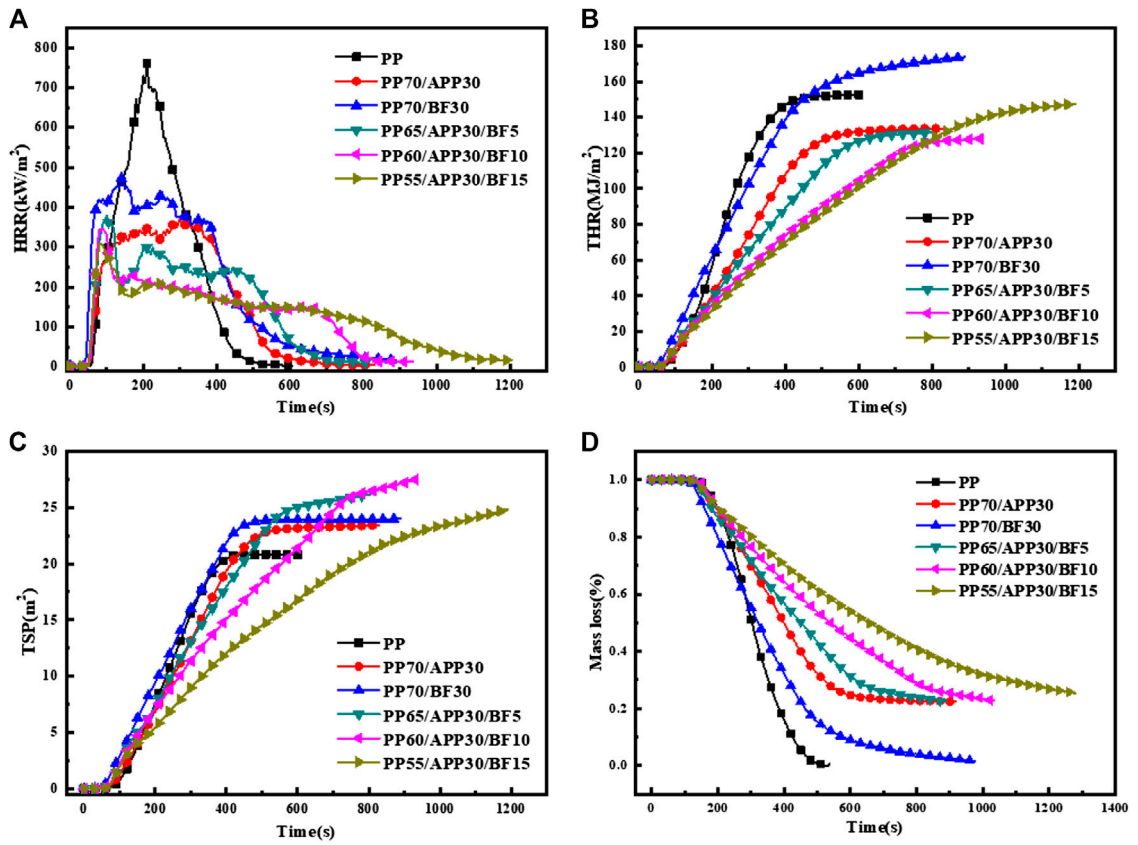

FIGURE 7 | HRR **(A)**, THR **(B)**, TSP **(C)**, and Mass loss **(D)** curves of PP and composites.

Cone Calorimeter Test

The graph of the cone calorimeter test is shown in **Figure 7** and the main data is listed in **Table 5**. The cone calorimeter test can truly reflect the level of material burning and can derive many combustion characteristics (Nie et al., 2008). From **Figure 6A**, it can be seen that the PP sample had a sharp and high peak at a heat flux of 35 kW/m^2, this shows that pure PP will burn quickly and release more heat in a short time. Within 400 s, the peak heat

TABLE 4 | TGA data obtained for PP and composites.

Samples	$T_{1wt\%}$ (°C)	$T_{5wt\%}$ (°C)	T_{max} (°C)	Char residue at 700°C (wt%)
PP	364.38	391.95	451.12	0.5
PP70/APP30	273.25	381.79	472.87	7.8
PP70/BF30	240.43	288.72	464.96	2.6
PP65/APP30/BF5	277.82	361.91	483.82	8.7
PP60/APP30/BF10	261.79	324.48	485.63	9.9
PP55/APP30/BF15	177.99	301.24	491.84	11.4

TABLE 5 | Main data of cone calorimeter test of PP and composites.

Samples	PHRR (kW/m^2)	THR (MJ/m^2)^1	TSP (m^2)^2	Mass loss (%)	TTI (s)
PP	761.6	151.9	20.8	100	60 ± 1
PP70/APP30	373.4	127.1	22.7	78	57 ± 1
PP70/BF30	472.4	156.8	23.9	99	46 ± 1
PP65/APP30/BF5	379.4	112.6	22.6	78	55 ± 1
PP60/APP30/BF10	346.3	90.0	18.4	77	56 ± 1
PP55/APP30/BF15	308.2	86.2	14.5	75	52 ± 1

THR (MJ/m^2)^1 means total heat release of sample at 500 s; TSP (m^2)^2 means total smoke production of sample at 500 s.

release rate (PHRR) reached 761.6 kW/m^2 and the total heat release (THR) was 146 MJ/m^2 (**Figure 6B**). The PHRR of samples PP70/APP30, PP70/BF30, and PP55/APP30/BF15 was reduced to 373.4, 472.4, and 308.2 kW/m^2, respectively. The PP55/APP30/BF15 (APP/BF = 2:1) sample had the lowest PHRR, and this indicates that the BF and APP have an obvious synergistic flame-retardant effect in PP. The result shows that the flame-retardant effect of PP55/APP30/BF15 is the best. This is due to the fact that APP and BF have a certain synergistic effect and a dense carbon layer formed during the combustion process. This carbon layer can effectively block the entry of oxygen and the release of heat, thus reducing the PHRR of the sample. It can be seen from **Figure 6A** that the burning time of PP55/APP30/BF15 was significantly longer than that of pure PP. It is due to the decomposition of transient carbon (Bai et al., 2014). To a certain extent, the addition of APP and BF can effectively inhibit the spread of the flame and reduce the risk factor of fire.

When the test sample is pyrolyzed under the condition of heat radiation, the local concentration of released flammable volatiles reaches the lower limit of flammability, and combustion occurs (Monti and Camino, 2013). **Table 5** shows that the addition of additives reduces the time to ignition (TTI) of the samples. The TTI of the pure PP was 60 s and in the PP70/BF30 sample it was 46 s. The TTI of samples with BF additive alone was 14 s ahead of the pure PP. The addition of BF had the greatest influence on the flame retardancy of all samples and this result was substantiated in the thermogravimetric data. When APP was added, the TTI of the PP55/APP30/BF15 sample was extended and ignited at 52 s. This is due to the presence of an expanded carbon layer in the presence of APP which covered the surface of the substrate and prolonged the ignition time. It can be seen from **Figure 6B** that the THR slope of samples PP65/APP30/BF5, PP60/APP30/BF10, and PP55/APP30/BF15 gradually slows down with the increase of flame-retardant content. Within 500 s, the THR of PP55/APP30/BF15 was only 86.2 MJ/m^2, while in PP it was 151.9 MJ/m^2. Compared with PP, the THR of PP55/APP30/BF15 decreased 43.3%. The slope of the THR curve can reflect the spread fire of samples. This result proves that the combination of APP and BF can effectively inhibit the generation of heat.

When a fire occurs, the mortality caused by smoke is more than that caused by flame. According to reports, about 50% of those trapped in a fire were killed by inhaling toxic gases instead of from fire damage (Manfredi et al., 2006; Manfredi et al., 2010). The initial 500 s is of great significance for escaping a fire (Araby et al., 2018; Kruger et al., 2019; Blais et al., 2020). The total smoke production (TSP) curve, as shown in **Figure 6C,** indicates that the TSP values of samples where flame retardant were added, are more than, or close to those of the pure PP within 500 s except for the PP55/APP30/BF15 sample. The TSP value of the PP55/APP30/BF15 sample was 14.5 m^2 which is 30.3% lower than PP. Decreasing the value of TSP can improve the smoke suppression effect. The reason "why the smoke suppression effect of the PP55/APP30/BF15 sample is so significant" (Dong et al., 2012; Sun et al., 2020; de Juan et al., 2020) is that the synergistic action of BF and APP in the combustion process is within 500 s. This process formed a dense and porous structure of sintered carbon. This was confirmed by the SEM image of the carbon residue after the cone test. This result shows that APP and BF added in PP significantly promotes the formation of residues. Cone test results show that the residue content of the PP55/APP30/BF15 sample reached 25%, but the pure PP had no residue formation. It can be seen from **Figure 6D** that the PP55/APP30/BF15 sample has the lowest mass loss and the highest residual amount. This indicates that the APP/BF system effectively forms an expanded and dense carbon layer. The carbon layer protects the underlying substrate from rapid degradation and reduces the release of combustible gases during combustion. Thereby, the residual carbon after burning was increased.

Microscopic Characterization

The digital photos of samples after the cone calorimeter test are shown in **Figure 8**. There was almost no residue after the combustion of pure PP as shown in **Figure 8A**. This is because PP is a polyolefin compound and will burn completely when it is ignited. APP can promote PP to form a continuous and expanded carbon layer as shown in **Figure 8B**. However, the addition of BF into PP only formed a small amount of gray charcoal, as shown in **Figure 8C**. When the content of APP is 30%, as the content of BF increases, the carbon layer becomes denser and denser. There are no macro-cracks in the carbon layer, as shown in **Figure 8E**. When combustion occurs, APP will decompose to produce acidic substances such as polyphosphoric acid, which quickly dehydrates the carbon source (BF) into char. The formed carbon layer is continuous and dense, which can be observed in **Figure 8**. The results in **Figure 8** show that the addition of BF and APP into PP can effectively promote char formation. BF and APP had a good synergistic flame-retardant effect and had a certain cross-linking effect.

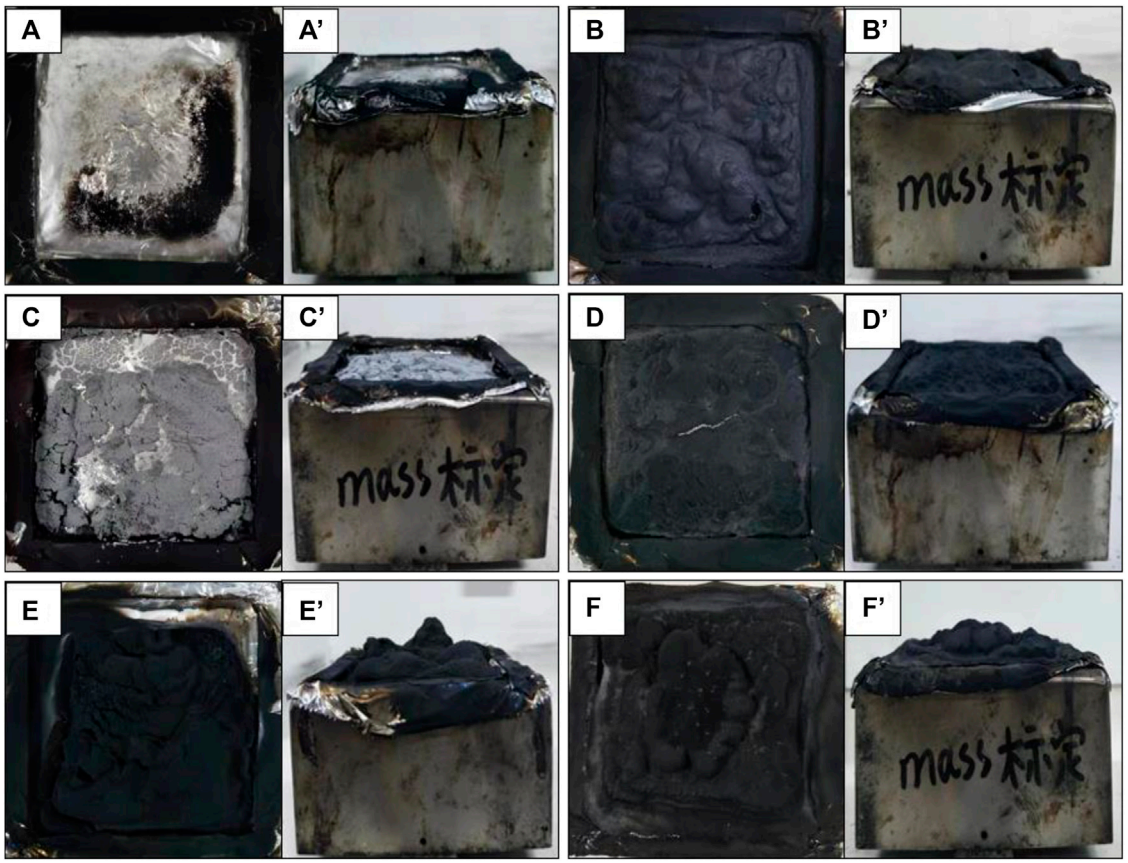

FIGURE 8 | Digital photo of surface intumescent carbon layer of PP and composites after cone calorimeter test. (**(A,A')** PP; **(B,B')** PP70/APP30; **(C,C')** PP70/BF30; **(D,D')** PP65/APP30/BF5; **(E,E')** PP60/APP30/BF10; **(F,F')** PP55/APP30/BF15).

In order to observe the microscopic morphology of the carbon layer, residue after the cone calorimeter test was observed by SEM. Since there was almost no residue formation after the cone test of pure PP, no observation was made for pure PP. It can be seen from **Figure 9** that although the microstructure of the carbon residue of the PP70/APP30 sample was relatively smooth and continuous, the carbon layer as a whole was brittle. It can be seen from **Figure 9B** that by adding 30% BF alone, the carbonation effect of the sample was poor, and the continuous carbon layer did not form.

After compounding BF 5, 10, 15, and 30% into APP, it can be seen from the SEM image that the continuity and compactness of the carbon layer are gradually increased in **Figures 9C–E**. The pores in the carbon layer became smaller and smaller. The morphology of the carbon residue shows a rough and convex appearance. These protrusions had many micropores which greatly increased the specific surface area of the carbon layer. At the same time, a cross-linking network was formed between the protrusions, so the stability of the carbon layer was improved. The carbon layer can effectively suppress the spread of heat. As shown in **Figure 9E**, the existence of many microporous structures in the carbon layer may be a significant cause of the smoke suppression effect, because these micro-holes may absorb part of the smoke.

CONCLUSIONS

A series of flame-retardant PP composites with a certain ratio of BF and APP were prepared. BF was used as a synergistic smoke suppressant. The influence of BF and APP as flame retardants on PP was studied. The addition of BF alone will improve the comprehensive mechanical properties of PP. However, when the APP and BF were mixed, the particles will agglomerate due to the higher amount of the addition. They will reduce some mechanical properties of PP. DSC results showed that the addition of BF in PP produced heterogeneous nucleation and affected the crystallization behavior of the composites. When the ratio of APP to BF was 2:1 and the total addition amount was 45%, the smoke suppression effect was most significant. The amount of carbon residue reached 25%. TGA and DTG data show that the PP55/APP30/BF15 sample had the highest amount of carbon residue with 11.4%, while pure PP had almost no carbon residue generation. The results of cone calorimetry show that the PHRR, THR, and mass loss of the PP55/APP30/BF15 sample were significantly lower than that of the pure

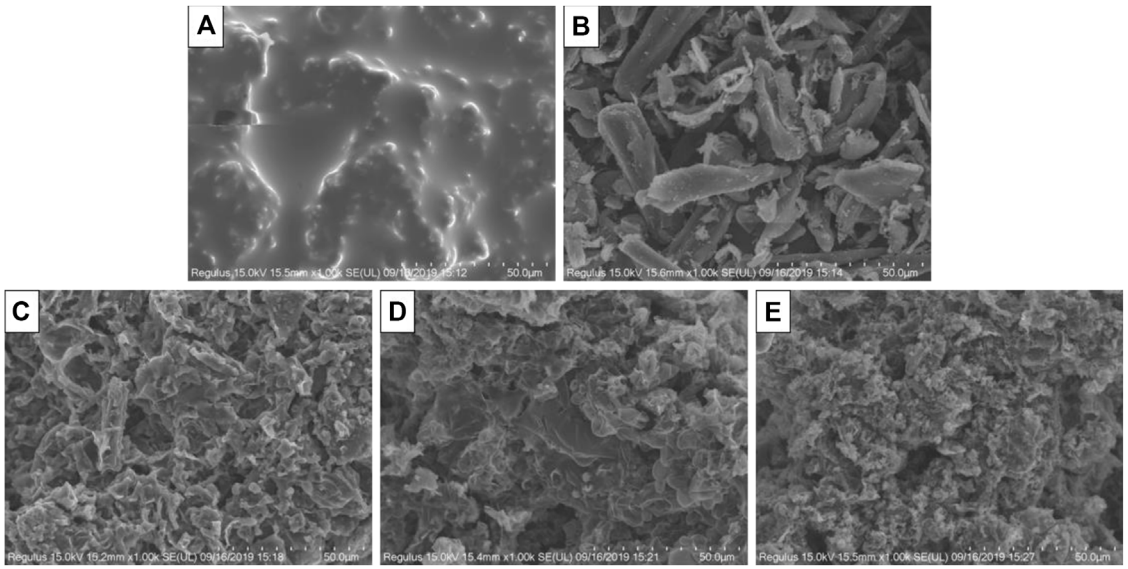

FIGURE 9 | SEM of surface carbon layer of composites after cone calorimeter test. (**(A)** PP70/APP30; **(B)** PP70/BF30; **(C)** PP65/APP30/BF5; **(D)** PP60/APP30/BF10; **(E)** PP55/APP30/BF15).

PP, from 761.6 to 308.2 kW/m^2, from 151.9 to 86.2 MJ/m^2, and from 100 to 75%, respectively. The SEM and the digital photos of residual carbon show that the PP55/APP30/BF15 sample formed a dense and continuous carbon layer, which hinders the transfer of heat and flammable gases into the matrix. The carbon layer had many convex structures, which contains many tiny holes that may absorb a large amount of smoke. Thus, the PP55/APP30/BF15 sample exhibited a better smoke suppression effect. Therefore, it substantiates that the combination of APP and BF is a potential application for PP with flame retardancy and smoke suppression.

DATA AVAILABILITY STATEMENT

All datasets presented in this study are included in the article/supplementary material.

AUTHOR CONTRIBUTIONS

YL and HL designed and performed the experiment, YL wrote the paper, HL, QC, FL, and CC edited the paper.

FUNDING

This work was supported by the foundation of Quangang Petrochemical Research Institute, Fujian Normal University (No. 2018YJY03); the Science and Technology Development Projects of the Central Committee Guidance Local (2018L3015); the Startup Fund from Fujian Normal University; the Fujian Provincial Department of Science and Technology (2018Y4002); and the National Natural Science Foundation of China (51903049).

REFERENCES

Abu Bakar, M. B., Mohd Ishak, Z. A., Mat Taib, R., Rozman, H. D., and Mohamad Jani, S. (2010). Flammability and mechanical properties of wood flour-filled polypropylene composites. *J. Appl. Polym. Sci.* 116 (5), 2714–2722. doi:10.1002/app.31791

Araby, S., Wang, C.-H., Wu, H., Meng, Q., Kuan, H.-C., Kim, N. K., et al. (2018). Development of flame-retarding elastomeric composites with high mechanical performance. *Compos. Appl. Sci. Manuf.* 109, 257–266. doi:10.1016/j.compositesa.2018.03.012

Bai, G., Guo, C., and Li, L. (2014). Synergistic effect of intumescent flame retardant and expandable graphite on mechanical and flame-retardant properties of wood flour-polypropylene composites. *Construct. Build. Mater.* 50, 148–153. doi:10.1016/j.conbuildmat.2013.09.028

Blais, M. S., Carpenter, K., and Fernandez, K. (2020). Comparative room burn study of furnished rooms from the United Kingdom, France and the United States. *Fire Technol.* 56 (2), 489–514. doi:10.1007/s10694-019-00888-8

Chattopadhyay, S. K., Khandal, R. K., Uppaluri, R., and Ghoshal, A. K. (2011). Bamboo fiber reinforced polypropylene composites and their mechanical, thermal, and morphological properties. *J. Appl. Polym. Sci.* 119 (3), 1619–1626. doi:10.1002/app.32826

De Juan, S., Zhang, J. H., Acuna, Pablo., Nie, S. B., and Liu, Z. Q. (2020). An efficient approach to improving fire retardancy and smoke suppression for intumescent flame-retardant polypropylene composites via incorporating organo-modified sepiolite. *Fire Mater.* 43 (8), 961–970. doi:10.1002/fam.2757

Ding, C. X., Pan, M. Z., Chen, H., Zhang, S., and Mei, C. (2020). An anionic polyelectrolyte hybrid for wood-polyethylene composites with high strength and fire safety via self-assembly. *Construct. Build. Mater.* 248, 1–12. doi:10.1016/j.conbuildmat.2020.118661

Dong, H., Yuan, B., Qi, C., Li, K., Shang, S., Sun, Y., et al. (2020). Preparation of piperazine cyanurate by hydrogen-bonding self-assembly reaction and its application in intumescent flame-retardant polypropylene composites. *Polym. Adv. Technol.* 31 (5), 1027–1037. doi:10.1002/pat.4837

Dong, Y. Y., Gui, Z., Hu, Y., Wu, Y., and Jiang, S. H. (2012). The influence of titanate nanotube on the improved thermal properties and the smoke

suppression in poly (methyl methacrylate). *J. Hazard Mater.* 209, 34–39. doi:10.1016/j.jhazmat.2011.12.048.

Fang, L., Lu, X. Z., Zeng, J., Chen, Y., and Tang, Q. (2020). Investigation of the flame-retardant and mechanical properties of bamboo fiber-reinforced polypropylene composites with melamine pyrophosphate and aluminum hypophosphite addition. *Materials* 13 (2), 479. doi:10.3390/ma13020479

Kong, Q. H., Sun, Y. L., Zhang, C. J., Guan, H., Zhang, J., Wang, D.-Y., et al. (2019). Ultrathin iron phenyl phosphonate nanosheets with appropriate thermal stability for improving fire safety in epoxy. *Compos. Sci. Technol.* 182, 107748. doi:10.1016/j.compscitech.2019.107748

Krüger, S., Schartel, B., Schubert, M., and Schoch, R. (2019). Wood plastic composites: how do flame retardant influence the smoke gas composition in case of fire?. *Bautechnik* 96 (6), 438–449. doi:10.1002/bate.201900020

Kumar, A., and Tumu, V. R. (2019). Physicochemical properties of the electron beam irradiated bamboo powder and its bio-composites with PLA. *Compos. B. Engg.* 175, 107098. doi:10.1016/j.compositesb.2019.107098

Kumar, N., Mireja, S., Khandelwal, V., Arun, B., and Manik, G. (2017). Light-weight high-strength hollow glass microspheres and bamboo fiber based hybrid polypropylene composite: a strength analysis and morphological study. *Compos. B. Eng.* 109, 277–285. doi:10.1016/j.compositesb.2016.10.052

Lee, S.-Y., Chun, S.-J., Doh, G.-H., Kang, I.-A., Lee, S., and Paik, K.-H. (2009). Influence of chemical modification and filler loading on fundamental properties of bamboo fibers reinforced polypropylene composites. *J. Compos. Mater.* 43 (15), 1639–1657. doi:10.1177/0021998309339352

Lewin, M., and Basch, A. (1978). *Structure, pyrolysis, and flammability of cellulose*. New York, NY: Plenum Press, Vol. 2: 1–41.

Li, W., He, X., Zuo, Y., Wang, S., and Wu, Y. (2019). Study on the compatible interface of bamboo fiber/polylactic acid composites by *in-situ* solid phase grafting. *Int. J. Biol. Macromol.* 141, 325–332. doi:10.1016/j.ijbiomac.2019.09.005

Manfredi, L. B., Rodríguez, E., Wladyka-Przybylak, M., and Vázquez, A. (2010). Thermal properties and fire resistance of jute-reinforced composites. *Compos. Interfaces.* 17 (5–7), 663–675. doi:10.1163/092764410x513512

Manfredi, L. B., Rodríguez, E. S., Wladyka-Przybylak, M., and Vázquez, A. (2006). Thermal degradation and fire resistance of unsaturated polyester, modified acrylic resins and their composites with natural fibres. *Polym. Degrad. Stab.* 91 (2), 255–261. doi:10.1016/j.polymdegradstab.2005.05.003

Monti, M., and Camino, G. (2013). Thermal and combustion behavior of polyethersulfone-boehmite nanocomposites. *Polym. Degrad. Stab.* 98 (9), 1838–1846. doi:10.1016/j.polymdegradstab.2013.05.010

Nie, S., Hu, Y., Song, L., He, Q., Yang, D., and Chen, H. (2008). Synergistic effect between a char forming agent (CFA) and microencapsulated ammonium polyphosphate on the thermal and flame retardant properties of polypropylene. *Polym. Adv. Technol.* 19 (8), 1077–1083. doi:10.1002/pat.1082

Nie, S., Liu, X., Wu, K., Dai, G., and Hu, Y. (2013). Intumescent flame retardation of polypropylene/bamboo fiber semi-biocomposites. *J. Therm. Anal. Calorim.* 111 (1), 425–430. doi:10.1007/s10973-012-2422-3

Shi, Y. Q., Liu, C., Liu, L., Fu, L., Yu, B., Lv, Y., et al. (2019). Strengthening, toughing and thermally stable ultra-thin MXene nanosheets/polypropylene nanocomposites via nanoconfinement. *Chem. Eng. J.* 378, 122267. doi:10.1016/j.cej.2019.122267

Sun, L. C., Xie, Y. J., Ou, R, X., Guo, C. G., Hao, X. L., et al. (2020). The influence of double-layered distribution of fire retardants on the fire retardancy and mechanical properties of wood fiber polypropylene composites. *Constr. Build Mater.* 242, 1–8. doi:10.1016/j.conbuildmat.2020.118047.

Tang, G., Liu, X., Yang, Y., Chen, D., Zhang, H., Zhou, L., et al. (2020a). Phosphorus-containing silane modified steel slag waste to reduce fire hazards of rigid polyurethane foams. *Adv. Powder Technol.* 31 (4), 1420–1430. doi:10.1016/j.apt.2020.01.019

Tang, G., Liu, X., Zhou, L., Zhang, P., Deng, D., and Jiang, H. (2020b). Steel slag waste combined with melamine pyrophosphate as a flame retardant for rigid polyurethane foams. *Adv. Powder Technol.* 31 (1), 279–286. doi:10.1016/j.apt.2019.10.020

Tang, G., Zhou, L., Zhang, P., Han, Z., Chen, D., Liu, X., et al. (2020c). Effect of aluminum diethylphosphinate on flame retardant and thermal properties of rigid polyurethane foam composites. *J. Therm. Anal. Calorim.* 140 (2), 625–636. doi:10.1007/s10973-019-08897-z

Wang, J. S., Xue, L., Zhao, B., Lin, G., Jin, X., Liu, D., et al. (2020). Flame retardancy, fire behavior, and flame retardant mechanism of intumescent flame retardant EPDM containing ammonium polyphosphate/pentaerythrotol and expandable graphite. *Materials* 12 (24), 4035. doi:10.3390/ma12244035

Wang, L., Yang, W., Wang, B., Wu, Y., Hu, Y., Song, L., et al. (2012). The impact of metal oxides on the combustion behavior of ethylene-vinyl acetate coploymers containing an intumenscent flame retardant. *Ind. Eng. Chem. Res.* 51 (23), 7884–7890. doi:10.1021/ie202502s

Wu, K., Wang, X. Y., Xu, Y. H., and Guo, W. (2020a). Flame retardant efficiency of modified para-aramid fiber synergizing with ammonium polyphosphate on PP/EPDM. *Polym. Degrad. Stab.* 172, 1090605. doi:10.1016/j.polymdegradstab.2019.109065

Wu, Q., Guo, J., Fei, B., Li, X., Sun, J., Gu, X., et al. (2020b). Synthesis of a novel polyhydroxy triazine-based charring agent and its effects on improving the flame retardancy of polypropylene with ammonium polyphosphate and zinc borate. *Polym. Degrad. Stab.* 175, 109–123. doi:10.1016/j.polymdegradstab.2020.109123

Xu, S., Zhang, M., Li, S., Yi, M., Shen, S., Zeng, H., et al. (2019). Non-isothermal decomposition kinetic of polypropylene/hydrotalcite composite. *J. Nanosci. Nanotechnol.* 19 (11), 7493–7501. doi:10.1166/jnn.2019.16675

Xu, X. D., Dai, J. F., Ma, Z. W., Liu, L., Zhang, X., Liu, H., et al. (2020). Manipulating interphase reactions for mechanically robust, flame-retardant and sustainable polylactide biocomposites. *Compos. B. Eng.* 190, 107903. doi:10.1016/j.compositesb.2020.107930

Yang, J. W., Ji, G. Z., Gao, Y., Fu, W., Irfan, M., Mu, L., et al. (2020). High-yield and high-performance porous biochar produced from pyrolysis of peanut shell with low-dose ammonium polyphosphate for chloramphenicol adsorption. *J. Clean. Prod.* 264, 121516. doi:10.1016/j.jclepro.2020.121516

Yang, W., Lu, H., Tai, Q., Qiao, Z., Hu, Y., Song, L., et al. (2011). Flame retardancy mechanisms of poly(1,4-butylene terephthalate) containing microencapsulated ammonium polyphosphate and melamine cyanurate. *Polym. Adv. Technol.* 22 (12), 2136–2144. doi:10.1002/pat.1735

Yu, B., Yuen, A. C. Y., Xu, X., Zhang, Z. C., Yang, W., Lu, H., et al. (2020). Engineering MXene surface with POSS for reducing fire hazards of polystyrene with enhanced thermal stability. *J. Hazard Mater.* 401, 123342. doi:10.1016/j.jhazmat.2020.123342

Zhao, Z., Jin, Q., Zhang, N., Guo, X., and Yan, H. (2018). Preparation of a novel polysiloxane and its synergistic effect with ammonium polyphosphate on the flame retardancy of polypropylene. *Polym. Degrad. Stab.* 150, 73–85. doi:10.1016/j.polymdegradstab.2018.02.007

Zhou, L., Guo, C., and Li, L. (2011). Influence of ammonium polyphosphate modified with 3-(Methylacryloxyl) propyltrimethoxy silane on mechanical and thermal properties of wood flour-polypropylene composites. *J. Appl. Polym. Sci.* 122 (2), 849–855. doi:10.1002/app.34069

Conflict of Interest: The authors declare that the research was conducted in the absence of any commercial or financial relationships that could be construed as a potential conflict of interest.

frontiers in Chemistry

ORIGINAL RESEARCH
published: 10 February 2021
doi: 10.3389/fchem.2020.627642

Functionalized CNTs with DOPO and Silicon Containing Agents: Effective Reinforcer for Thermal and Flame Retardant Properties of Polystyrene Nanocomposites

Congling Shi, Xiaodong Qian, Jingyun Jing and Honglei Che*

Beijing Key Lab of MFPTS, China Academy of Safety Science and Technology, Beijing, China

DOPO and silicon containing agents modified multiwalled carbon nanotubes (MCNTs) were synthesized through sol-gel process and MCNTs are introduced into polystyrene (PS) through *in situ* polymerization. TEM observations and FTIR results of MCNTs demonstrated that the MCNT nanofillers were coated with the organic/inorganic flame retardant compound. Moreover, the TEM results of the composites indicate that MCNTs dispersed in polystyrene PS matrix uniformly due to the modification. The PS/MCNTs composites showed improved thermal stability as well as flame retardant properties in comparison with PS/CNTs composites, which are due to the good dispersion of MCNT in the PS matrix. MCNTs in the PS matrix can also reduce the peak heat release rate, total heat release and improve the smoke suppression performance. The improved flame retardant properties are attributed to the char reinforcing effect of CNTs, which can provide enough time for MCNTs and organic/inorganic compound to trap the degradation of polymer chains and catalyze the formation of char. The char layers can not only serve as an efficient insulating barrier to reduce the exposure of PS matrix to heat source but also retard the releasing of combustible gas.

Keywords: nanocomposites, polystyrene, flame retardants, CNTs, DOPO

OPEN ACCESS

Edited by:
Bin Yu,
University of Southern Queensland, Australia

Reviewed by:
Saihua Jiang,
South China University of Technology, China
Bibo Wang,
University of Science and Technology of China, China

****Correspondence:***
Xiaodong Qian
wjxyqxd@hotmail.com

Specialty section:
This article was submitted to Polymer Chemistry, a section of the journal Frontiers in Chemistry

Received: *09 November 2020*
Accepted: *30 December 2020*
Published: *10 February 2021*

Citation:
Shi C, Qian X, Jing J and Che H (2021) Functionalized CNTs with DOPO and Silicon Containing Agents: Effective Reinforcer for Thermal and Flame Retardant Properties of Polystyrene Nanocomposites. Front. Chem. 8:627642. doi: 10.3389/fchem.2020.627642

INTRODUCTION

Since 1991, carbon nanotubes (CNTs) have became a major interest of research all over the world. The properties of CNTs include the resistance to acid, high adsorption capacity and possibility to control surface chemistry. Those special properties make CNTs applicable to a wide range of potential applications, taking electronics, polymer nanocomposites and medical devices for example (Esawi et al., 2007; Gao et al., 2009; Zhang et al., 2018; Ali et al., 2019). Among various polymer nanocomposites, taking the advantage of the flame retardant effect of CNTs is one of the most promising research directions (Hapuarachchi et al., 2010; Ji et al., 2018). Kashiwagi found that CNTs can reduce the heat release rate of polypropylene at very low CNTs loading, and the network structured layers of CNTs can act as excellent thermal insulation char layers to protect the underlying polypropylene from external heat and radiation (Kashiwagi et al., 2005). However, the agglomeration of CNTs usually results in the reduced flame retardant and mechanical properties, which are due to

strong Vander Waals forces and π–π interactions among CNTs. As a result, one of the major challenges for preparing polymer composites is to disperse the CNTs in the polymer matrices individually.

As for polymer composites based on CNTs, many methods have been developed to improve the dispersion of CNTs in the polymers composites through surface modification. Among those methods, the covalent and noncovalent functionalization are common modification method (Kim et al., 2006; Gupta et al., 2015). Generally, the noncovalent functionalization of CNTs can confer the special properties of CNTs without changing the structural characteristics, but the dispersion of CNTs in the polymer composites is usually not very ideal (Huang et al., 2019a; Huang et al., 2019b). As for the covalent functionalization, the solubility and compatibility of CNTs in the polymer matrix can be improved significantly, and various functional organic groups can be adopted to modified CNTs, resulting in the uniform dispersion of CNTs in the polymer composites.

The organic/inorganic hybrids materials based on silicon are generally prepared through the sol-gel reaction. As for the organosilane, the organic groups can be varied according their application. As for the flame retardancy, the organic groups of organosilane can be changed to phosphorus based groups (SforA et al., 1999; Kurayama et al., 2010). Among the phosphorus based flame retardants, 9,10-dihydro-9-oxa-10-phosphaphenanthrene-10-oxide (DOPO) and its derivative have attracted great attention in the field of flame retardant due to their high flame retardant efficiency to polymer materials and high thermal stability (Perret et al., 2011; Salmeia. et al., 2015). In the previous work, novel organic/inorganic flame retardants based on silicane and DOPO was designed, and the flame retardants play their flame retardant roles in not only condensed phase but also gases phase (Qian et al., 2013). Due to the existence of silane structure, the novel organic/inorganic flame retardants can be use as a good modifier for the inorganic fillers.

As a common engineering plastics, polystyrene (PS) has outstanding properties such as low density, excellent mechanical properties, chemical resistance and easy processing molding. Due to those outstanding properties, PS has been broadly used in various fields such as decoration, transportation, etc., (Qian et al., 2000; Jürgen et al., 2009; Shi et al., 2019) However, PS is high flammability, which limits its further application in the areas with high fire safety requirements. In order to improve its flame retardant properties of PS, various flame retardants such as ammonium polyphosphate, aluminum phosphate and decabromodiphenyl ethane have been incorporated into the PS matrix (Wang et al., 2002; Braun et al., 2004; Li et al., 2020). Due to the environmental problems, researchers have been exploring novel halogen-free flame retardants such as novel phosphorus based flame retardants or nano-fillers flame retardants.

In this manuscript, DOPO and silicon containing agents modified MCNTs were prepared through sol-gel process and the MCNTs was incorporated into PS matrix through free radical addition polymerization. The TEM results of the composites indicate that MCNTs distributed within the PS matrix uniformly. Compared with PS/CNTs composites, PS/MCNTs composites showed improved thermal stability and flame retardant properties, which are due to the improved dispersion and flame retardant effect of DOPO and silicon containing agents.

EXPERIMENTAL SECTION

Materials

Vinyl trimethoxysilane was purchased from Shenmao new material Co., (Guangzhou, China). 9,10-Dihydro-9-oxa-10-phosphaphenanthrene-10-oxide (DOPO) was supplied by Shandong Mingshan Fine Chemical Industry Co., Ltd. (Shandong, China). Styrene and azodiisobutyronitrile (AIBN) were purchased from Sinopharm Chemical Reagent Co., Ltd. (Shanghai, China). Moreover, carbon nanotubes (CNTs) were supplied by Chengdu Organic Chemicals Co., Ltd.

Preparation of Multiwalled Carbon Nanotubes

The DOPO-VTS was synthesized according to our previous report (Qian et al., 2013). In a 250 ml three-necked flask, CNTs (2 g), DOPO-VTS (5 g) and THF (100 ml) were mixed. After the mixtures were saturated with nitrogen atmosphere in case of mechanical mixing, the temperature of the mixtures was increased to 60°C. After stirring for 12 h, 2 g vinyltrimethoxysilane (A171) was added to the mixtures by drop addition, then the mixtures of ammonia (1 ml) and water (10 ml) were dropped into the three-necked flask. After that, the black powders were obtained by filtration. Moreover, the black powders were purified by washing with THF for several times and dried at 60°C in vacuum for 12 h. The black powders named MCNTs were obtained (2.2 g). **Scheme 1A** illustrates the synthesis routs of MCNTs.

Preparation of Flame Retardant Polystyrene Composites

Generally, MCNTs (2.0 g) and styrene monomers (98.0 g) were added into a three-necked flask and kept in ultrasonic state for 120 min. After MCNTs are dispersed well in the mixtures, AIBN (0.2 g) was added and the mixtures were kept stirring at 80°C for 60 min until viscous paste formed. Then, the mixtures were transferred into a mold and kept heating at 60°C for 48 h. Scheme 1B illustrates the synthesis routs of PS/MCNTs composites. Then the PS/MCNTs are obtained and other composites are prepared by the same way according to **Table 1**.

Characterization

The FTIR spectroscopy was recorded with Nicolet 6700 FT-IR spectrophotometer and the wavelength range of the FTIR spectroscopy was 4000–500 cm^{-1}.

The structures of MCNTs and the dispersions of CNTs in the composites were investigated by transmission electron microscopy (TEM) (JEOL JEM-2100 instrument).

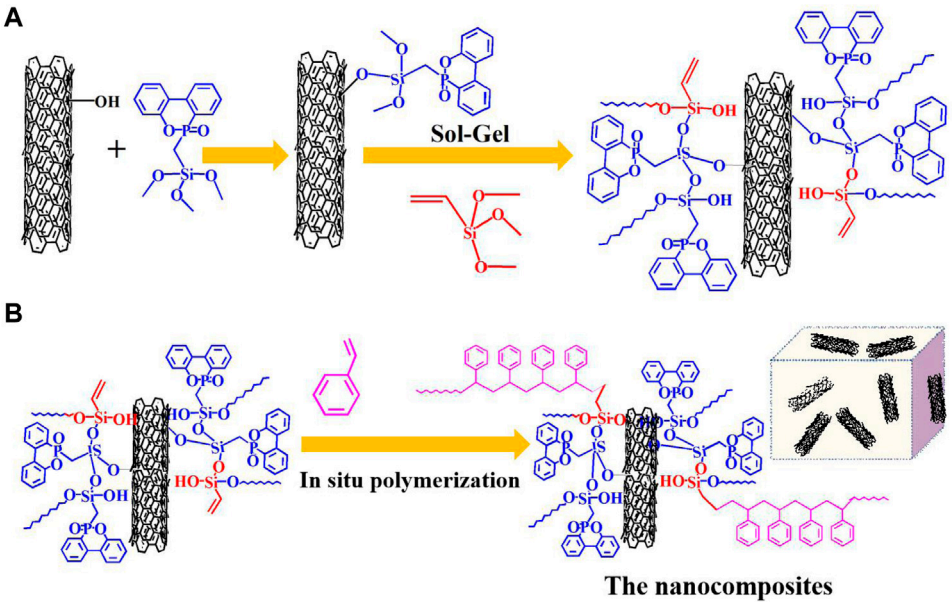

SCHEME 1 | Preparation of MCNTs and PS/MCNTs composites: **(A)** preparation routes of MCNTs; **(B)** preparation routes of PS/MCNTs composites.

TABLE 1 | The compositions, TGA and cone data of the composites.

Samples	Nanofillers (wt.%)	pHRR (W/g)	THR (kJ/g)	$T_{10\%}$°C	$T_{50\%}$°C	Char residues (%)
PS	0	1,003	120	331	375	0.96
PS/CNTs	2	932	121	350	396	0.97
PS/MCNTs-1	1	896	121	354	402	1.16
PS/MCNTs-2	2	745	111	361	403	3.09

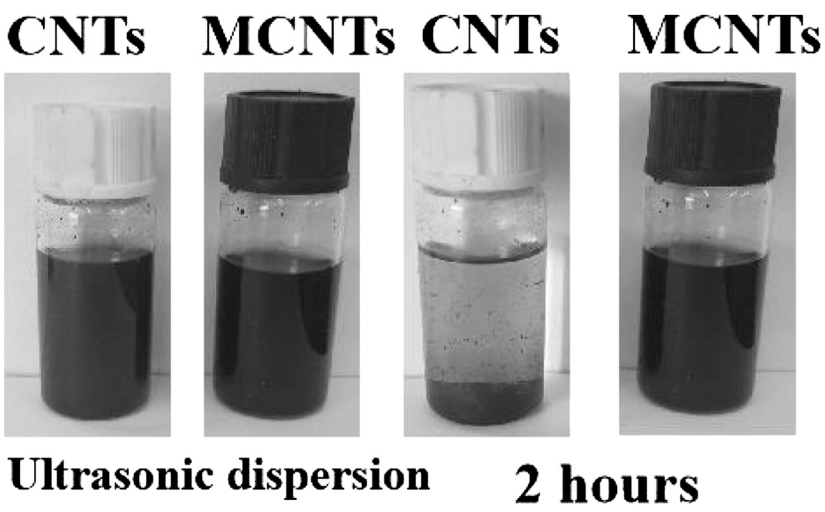

FIGURE 1 | Digital photos of CNTs and MCNTs dispersion in THF at different time.

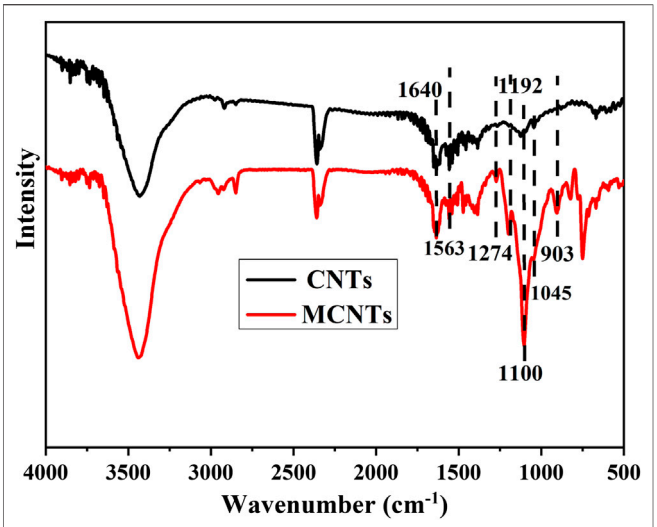

FIGURE 2 | FTIR of CNTs and MCNTs.

The thermal stability of the composites was investigated by TGA Q5000 IR thermal gravimetric analyzer (TA Instruments). About 4~10 mg of the composites was heated from room temperature to 800°C.

The flame retardant proerties of the polymer composites was studied by cone calorimeter according to ISO 5660. The heat flux is 50 $kW{\cdot}m^{-1}$ and the dimensions of the samples are 100 × 100 × 3 mm^3 (Yu et al., 2016; Shi et al., 2019a; Shi et al., 2019b; Shi et al., 2019c; Lin et al., 2020; Yu et al., 2021). The samples are tested three times and the average value is selected.

The char layers were investigated by Raman spectroscopy measurements (SPEX-1403 laser Raman spectrometer) at room temperature.

RESULTS AND DISCUSSION

Characterizations of Carbon Nanotubes and Multiwalled Carbon Nanotubes

The dispersion of CNTs and MCNTs in organic solvent can reflect the surface modification performance, the decentralized states of CNTs and MCNTs in tetrahydrofuran (THF) were investigated at different time. **Figure 1** shows the dispersion state of CNTs and MCNTs at a concentration of 1 $mg{\cdot}ml^{-1}$ after sonication in THF. The DOPO based organic/inorganic compounds on the surface of CNTs have significant influence on the dispersibility of MCNTs in THF. After ultrasonic treatment, the CNTs and MCNTs were well-dispersed in THF, exhibiting the black color. After 2 h, the CNTs precipitated at the bottom while MCNTs were well-dispersed in THF, which are due to the attractive force between the polar organic groups on the surface of MCNTs and organic solution. **Figure 2** shows the FTIR spectra of MCNTs and CNTs. As for the MCNTs, the peaks for the stretching vibrations of P-O-Ph appear at both 1,045 cm^{-1} and 903 cm^{-1}, the peaks at 1,274 cm^{-1} are due to the stretching vibrations of P=O, and the peak at 1,640 cm^{-1} corresponds to the C=C bonds in the DOPO structures. Moreover, the characteristic peak for P-Ph bonds appeared at 1,563 cm^{-1} and the peaks at around 1,100 cm^{-1} are due to Si-O-C and Si-O-Si bonds (Ciesielski et al., 2008; Wang et al., 2011; Lu et al., 2017). The peaks at 1,560 cm^{-1} are due to the characteristic peak of benzene ring in the DOPO structures, indicating the graft modification of organic/inorganic compound containing DOPO structures and C=C bonds onto the surface of MCNTs.

Morphology of Carbon Nanotubes, Multiwalled Carbon Nanotubes and the Polystyrene/Multiwalled Carbon Nanotubes Composites

The TEM images of CNTs and MCNTs are presented in **Figure 3**. As for CNTs, it has curved shape. After the modification (**Figure 3B**), it is found that the diameters of CNTs increased compared with CNTs. The TEM results provide the direct evidence for modification of CNTs with DOPO based flame retardants. The properties of the CNTs based composites depend strongly on the dispersion and interface interaction between CNT and the polymer matrix. Therefore, TEM was adopted to investigate the dispersion state of the MCNTs in the composites, as shown in **Figure 4**. It's found that the boundary of MCNTs are obscure and the MCNTs are dispersed well in the PS matrix, which are due to the modification of CNTs with the organic/inorganic flame retardants. Generally, the uniform dispersion characteristics of MCNTs in the PS matrix are due to the good interfacial interaction between the MCNTs and polystyrene molecular chains. The organic/inorganic groups on the surface of CNTs have good interaction with the polystyrene molecular chains due to the formation of covalent bond, resulting in the uniform dispersion of CNTs in the polystyrene matrix.

Thermo-Oxidation Decomposition Performance of the Composites

The thermo-oxidation properties of PS and its composites were investigated by TGA under air conditions in **Figure 5** and the corresponding data are collected in **Table 1**. The 10% weight loss temperatures are regarded as the onset temperatures ($T_{10\%}$) while the 50% weight loss temperature are on behalf of due to half degradation temperatures ($T_{50\%}$). The TEM results of PS/MCNTs composites indicate that there are no agglomerates of MCNTs in the PS matrix. Due to the high thermal conductivity of CNTs, the heat usually focus on the domains, resulting in the asymmetric distribution of temperature. As for pure PS, the T10% of PS/MCNTs composites is higher than those of pure PS. Furthermore, it can be observed that there are no residues at 500°C for pure PS, while the corresponding char residues for PS/MCNTs-2 composites at 500°C increase to 3.09wt%. Moreover, the half degradation temperatures ($T_{50\%}$) of MCNTs modified PS composites are improved significantly. Only 2.0 wt% MCNTs in the composites result in 28°C increase of T50%. The TGA results indicate that the improved thermo-oxidative stability of the composites against the thermal oxidation are due to the stable

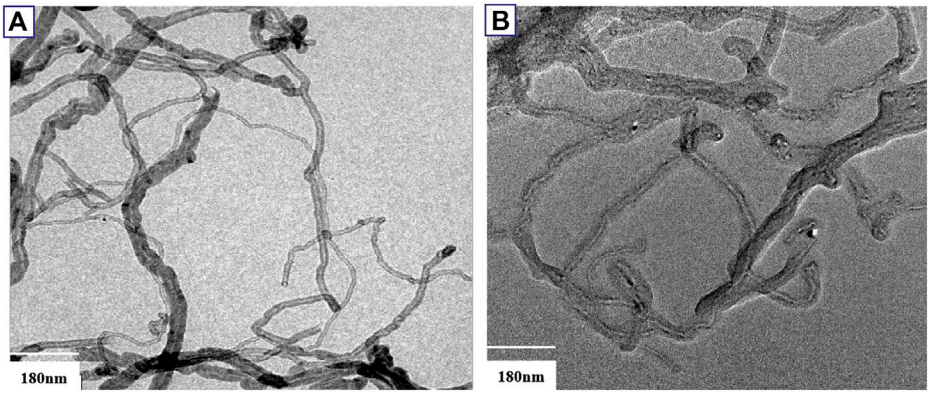

FIGURE 3 | TEM images of CNTs **(A)** and MCNTs **(B)**.

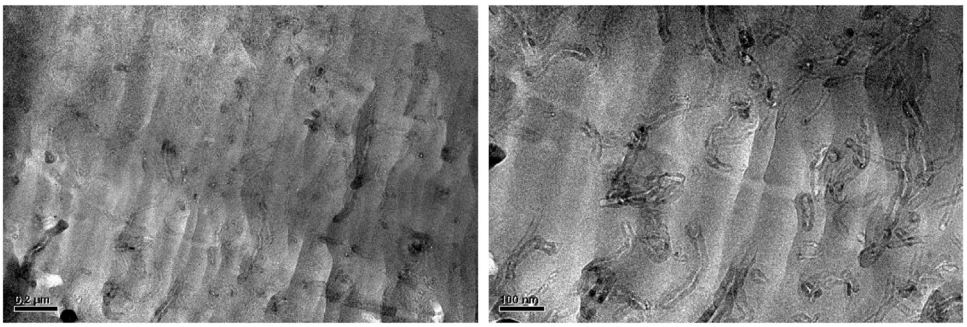

FIGURE 4 | a: TEM images of the PS/MCNTs composites.

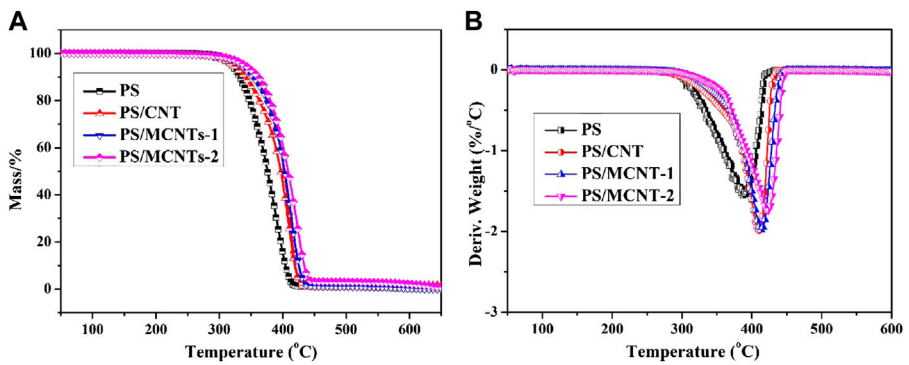

FIGURE 5 | TGA/DTG profiles for PS and its composites as function of temperature under air atmosphere.

char layers formed during the thermal degradation process, attributing to the good dispersion of MCNTs and the organic/inorganic flame retardants on the surface of CNTs (Xing et al., 2016). Generally, the MCNTs can act as high-temperature stabilizers and the organic/inorganic flame retardants can catalyze the formation of stable char layers. Moreover, the physical barrier effect of char layers can provide enough time for MCNTs and DOPO based compounds to trap the degrading polymer radicals and inhibit thermo-oxidative degradation, resulting good flame retardant efficiency.

The Fire Hazards of the Composites

The fire hazards of materials are investigated by the cone calorimeter, which can show important fire risk parameters such as heat release rate (HRR) and total heat release (THR). The HRR and THR curves of neat PS and its composites at the

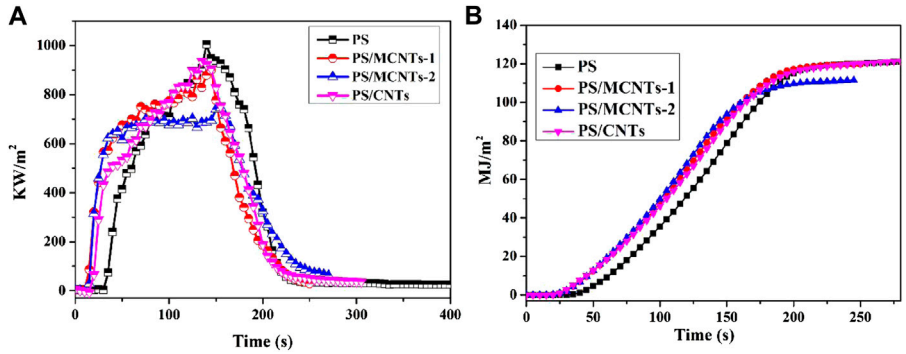

FIGURE 6 | Cone calorimeter test results: HRR and THR curves of PS and its composites.

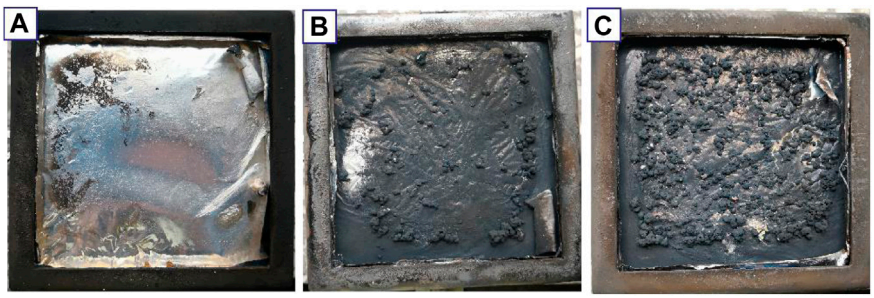

FIGURE 7 | Digital photo of the char residues of PS **(A)**, PS/CNTs **(B)** and PS/MCNTs **(C)**

heat flux of 50 kW/m^2 are shown in **Figure 6**, and the corresponding data are summarized in **Table 1**. As for PS, it has high pHRR (1,003 kW·m^{-2}) value, and the HRR peak is at 139.2 s. The incorporation of CNTs or MCNTs into PS resulted in the reduced pHRR value and flatter HRR curves. It can be found that the pHRR of PS/CNTs composites decreases from 1,003 to 929 kW·m^{-2}, which is a small decrease. Moreover, the incorporation of CNTs into PS composites has few effects on the reduction of THR. It's found that the incorporation of MCNTs has better effect on the reduction of pHRR due to the modification of CNTs with the organic/inorganic compound. The THR is further reduced after the 2 wt% of MCNTs was introduced. PS/MCNTs-2 composites have the lowest THR value, which is 7.5% reduction compared with virgin PS. Therefore, the reduced pHRR and THR values of the composites are due to the stable char layers, which can not only prevent the releasing of combustible gas but also the heat release.

The Investigation of the Char Layers

The improved fire safety properties of PS/CNTs and PS/MCNTs composites are probably due to the good carbonization effect and the char reinforcing effect of CNTs. From the TGA results, it is obvious that MCNTs can improve the char residues and the thermal stability of PS, which is in accordance with the high residual chars after the cone calorimeter test. From **Figure 7**, it is obvious that PS/MCNTs composites have higher char residues after the cone calorimeter test. The stable char layers with MCNTs are good for CNTs and DOPO based organic/organic flame retardants to trap the degrading polymer radicals and

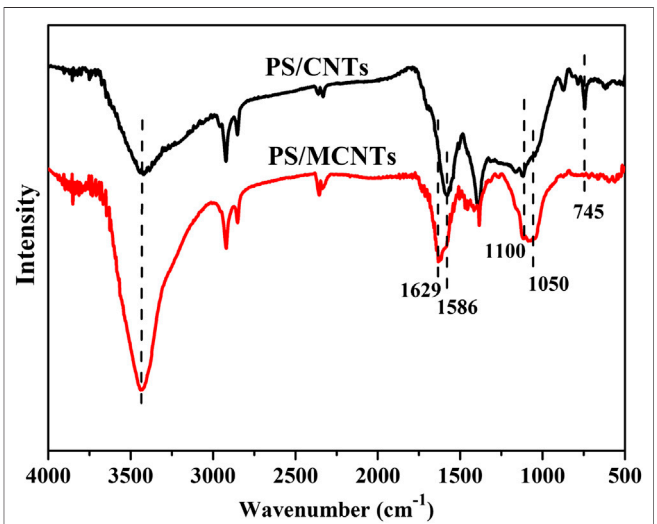

FIGURE 8 | FTIR of the char residues the char residues of PS/CNTs and PS/MCNTs composites.

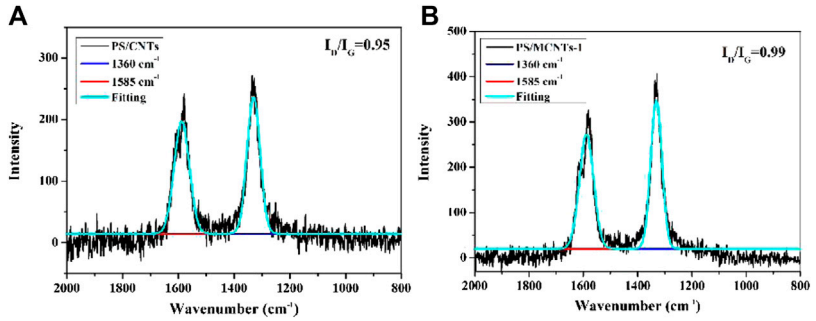

FIGURE 9 | Raman spectra of the char residues of PS/CNTs and PS/MCNTs-1 composites.

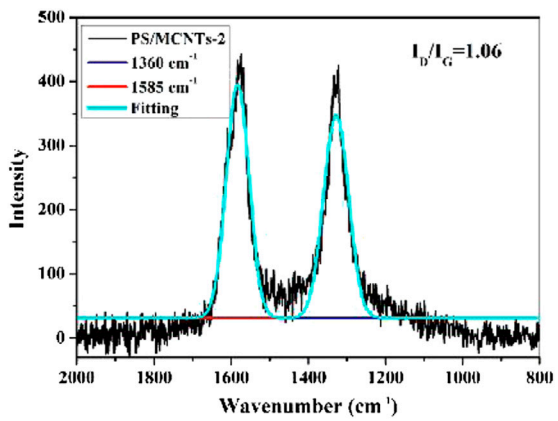

FIGURE 10 | Raman spectra of the char residues of PS/MCNTs-2 composites.

inhibit the further thermal degradation of the composites. Generally, the char layer resulting from the carbonization reaction can act as an insulating barrier to reduce the exposure of PS matrix to an external heat source, resulting in improved flame retardant properties.

The FTIR spectra of the char residues of PS and its composites after cone calorimeter test are shown in **Figure 8**. Compared with the char residues of PS/CNTs composites, the broad peaks of the PS/MCNTs composites at around 1,100 cm^{-1} for the stretching vibration of P=O appears. Moreover, the intensity of the peak at 1,050 cm^{-1} (P-O-P, P-O-C or Si-O-Si bonds) became strength, indicating the formation of the phosphorus-silicon based char layers. Meanwhile, the peak at 1,586 cm^{-1} for the stretching vibrations of C=C in the aromatic compounds of PS/CNTs composites shifts to higher wavenumber, indicating the DOPO based flame retardants influence the structure of char residues (Wu et al., 2009; Qian et al., 2012). Generally, the FTIR results of the char indicate that stable char layers based on the silicon and phosphorus are formed, and the stable char layers can act as an efficient barrier layers to retard the flammable gases from releasing and PS matrix from the exposure of heat.

Raman spectroscopy is used to analyze carbonaceous materials, as shown in **Figure 9**. The Raman spectroscopy of the char layers usually exhibits two strong peaks at about 1,360 and 1,585 cm^{-1}. The peak at 1,360 cm^{-1} (the D band) corresponds to disordered graphite or glassy carbon, and the peak at 1,585 cm^{-1} (G band) is due to the aromatic layers of crystalline graphite. Generally, the graphitization degree of the char layers is evaluated by the ratio of the intensity of the D and G bands (I_D/I_G), and the lower ratio of I_D/I_G indicate higher graphitization degree of the char layers (Brian et al., 2005; Sadezky et al., 2005; Shi et al., 2020; Zhang, et al., 2020). As shown in **Figure 10**, the I_D/I_G ratio follows PS/CNTs < PS/MCNTs-1 < PS/MCNTs-2, indicating that the highest graphitization degree is PS. However, the TGA results indicate that the incorporation of MCNTs can improve the char residues significantly at high temperature. Based on the Raman spectra and TGA results, it can be concluded that the MCNTs could only catalyze the formation of more glassy carbon as the composites thermally decompose.

CONCLUSION

In the present work, CNTs was modified by organic/inorganic silicon based compound through sol-gel process, PS/CNTs and PS/MCNTs composites with different particles contents have been prepared successfully through *in situ* polymerization. The TEM results indicate that the MCNTs disperse well in the PS matrix due to the improved interface interaction between PS and MCNTs. The incorporation of MCNTs into the PS matrix can improve the thermal and flame retardant properties of PS. The homodispersion of MCNTs in the PS matrix and the flame retardant element on the surface of MCNTs are the two main factors for the improved thermal stability and flame retardants properties. The PS/MCNTs composites form a stable silicon and phosphorus based char layers. It's believed that the stable char layers can not only serve as an efficient insulating barrier to reduce the exposure of PS matrix to heat but also retard the releasing of the flammable gases.

DATA AVAILABILITY STATEMENT

The raw data supporting the conclusions of this article will be made available by the authors, without undue reservation.

AUTHOR CONTRIBUTIONS

All authors listed have made a substantial, direct, and intellectual contribution to the work and approved it for publication.

FUNDING

This work was financially supported by Natural Science Foundation of China (Grant No. 21704111), National high-level talent special support plan project (Grant No. WRJH201801), Fundamental Research Funds for China Academy of Safety Science and Technology (Grant No. 2020JBKY02), National key research and development program (Grant No. 2017YFC0805000). National Key Research and Development Program of China (2018YFC0809005, the Science and Technology Program of Guangzhou (201806010113).

REFERENCES

Ali, I., Alharbi, O. M. L., Alothman, Z. A., Al-Mohaimeed, A. M., and Alwarthan, A. (2019). Modeling of fenuron pesticide adsorption on CNTs for mechanistic insight and removal in water. *Environ. Res.* 170, 389–397. doi:10.1016/j.envres.2018.12.066

Braun, U., and Schartel, B. (2004). Flame retardant mechanisms of red phosphorus and magnesium hydroxide in high impact polystyrene. *Macromol. Chem. Phys.* 205, 2185–2196. doi:10.1002/macp.200400255

Brian, J. D., Ruf, H. J., Evans, C. M., Cress, C. D., and Raffaelle, R. P. (2005). Purity assessment of single-wall carbon nanotubes, using optical absorption spectroscopy. *J. Phys. Chem. B.* 109, 9952–9965. doi:10.1021/jp044990c

Ciesielski, M., Schäfer, A., and Döring, M. (2008). Novel efficient DOPO-based flame-retardants for PWB relevant epoxy resins with high glass transition temperatures. *Polym. Adv. Technol.* 19, 507–515. doi:10.1002/pat.1090

Esawi, A., and Morsi, K. (2007). Dispersion of carbon nanotubes (CNTs) in aluminum powder. *Compos. Part A-Appl. S.* 38, 646–650. doi:10.1016/j.compositesa.2006.04.006

Gao, B., Chen, G. Z., and Puma, G. L. (2009). Carbon nanotubes/titanium dioxide ($CNTs/TiO_2$) nanocomposites prepared by conventional and novel surfactant wrapping sol–gel methods exhibiting enhanced photocatalytic activity. *Appl. Catal. B. Environ.* 89, 503–509. doi:10.1016/j.apcatb.2009.01.009

Gupta, V. K. (2015). Study on the removal of heavy metal ions from industry waste by carbon nanotubes: effect of the surface modification: a review. *Crit. Rev. Environ. Sci. Technol.* 7, 93–118. doi:10.1080/10643389.2015.1061874

Hapuarachchi, T., and Peijs, T. (2010). Multiwalled carbon nanotubes and sepiolite nan-o-clays as flame retardants for polylactide and its natural fibre reinfor-ced composites. *Compos. Part A-Appl. S.* 41, 954–963. doi:10.1016/j.compositesa.2010.03.004

Huang, Y., Jiang, S., and Liang, R. (2019a). Thermal-triggered insulating fireproof layers: a novel fire-extinguishing MXene composites coating. *Chem. Eng. J.* 2019, 391. doi:10553410.1016/j.cej.2019.123621

Huang, Y., Jiang, S., Liang, R., Liao, Z., and You, G. (2019b). A green highly-effective surface flame-retardant strategy for rigid polyurethane foam: transforming UV-cured coating into intumescent self-extinguishing layer. *Compos. Part A: App. Ence and Manuf.* 125, 105534. doi:10.1016/j.composite

Ji, X. Y. (2018). Synergistic effect of flame retardants and carbon nanotubes on flame retarding and electromagnetic shielding properties of thermoplastic polyurethane. *Compos. Sci. Technol.* 163, 49–55. doi:10.1016/j.compscitech.2018.05.007

Jürgen, S. (2009). Recent transition metal catalysts for syndiotactic polystyrene. *Prog. Polym. Sci.* 34, 688–718. doi:10.1016/j.progpolymsci.2009.04.002

Kashiwagi, T., Du, F., Douglas, J. F., Winey, K. I., Harris, R. H., and Shields, J. R. (2005). Nanoparticle networks reduce the flammability of polymer nanocomposites. *Nat. Mater.* 4, 928. doi:10.1038/nmat1502

Kim, J. A. (2006). Effects of surface modification on rheological and mechanical properties of CNT/epoxy composites. *Carbon* 44, 1898–1905. doi:10.1016/j.carbon.2006.02.026

Kurayama, F., Suzuki, S., Oyamada, T., Furusawa, T., Sato, M., and Suzuki, N. (2010). Facile method for preparing organic/inorganic hybrid capsules using amino-functional silane coupling agent in aqueous media. *J. Colloid Interface Sci.* 349, 70–76. doi:10.1016/j.jcis.2010.05.039

Li, M. E. (2020). A facile and efficient flame-retardant and smoke-suppressant resin coating for expanded polystyrene foams. *Compos. B. Eng.* 185, 107797. doi:10.1016/j.compositesb.2020.107797

Lin, B., Yuen, A. C. Y., Li, A., Zhang, Y., Chen, T. B. Y., Yu, B., et al. (2020). MXene/chitosan nanocoating for flexible polyurethane foam towards remarkable fire hazards reductions. *J. Hazard Mater.* 381, 120952. doi:10.1016/j.jhazmat.2019.120952

Lu, L., Guo, N., and Qian, X. (2017). Thermal degradation and combustion behavior of intumescent flame-retardant polypropylene with novel phosphorus-based flame retardants. *J. Appl. Polym. Sci.* 135 (10), 45962. doi:10.1002/APP.45962

Perret, B. (2011). Novel DOPO-based flame retardants in high-performance carbon fibre epoxy composites for aviation. *Eur. Polym. J.* 47, 1081–1089. doi:10.1016/j.eurpolymj.2011.02.008

Qian, D. (2000). Load transfer and deformation mechanisms in carbon nano-tube-polystyrene composites. *Appl. Phys. Lett.* 76, 28–68. doi:10.1063/1.126500

Qian, X. D. (2013). Thermal degradation and flammability of novel organic/inorganic epoxy hybrids containing organophosphorus-modified oligosiloxane. *Thermochim. Acta* 552, 87–97. doi:10.1016/j.tca.2012.11.010

Qian, X. D. (2012). Thermal properties of novel 9,10-Dihydro-9-oxa-10-phosphaphenanthrene 10-Oxide-based organic/inorganic hybrid materials prepared by sol–gel and UV-curing processes. *Ind. Eng. Chem. Res.* 51, 85–94. doi:10.1021/ie2017493

Sadezky, A. (2005). Raman microspectroscopy of soot and related carbonaceous materials: spectral analysis and structural information. *Carbon* 43, 1731–1742. doi:10.1016/j.carbon.2005.02.018

Salmeia, K. A., and Gaan, S. (2015). An overview of some recent advances in DOPO-derivatives: chemistry and flame retardant applications. *Polym. Degrad. Stabil.* 113, 119–134. doi:10.1016/j.polymdegradstab.2014.12.014

SforA, M. L., Yoshida, I. V. P., and Nunes, S. P. (1999). Organic–inorganic membranes prepared from polyether diamine and epoxy silane. *J. Membr. Sci.* 159, 197–207. doi:10.1016/S0376-7388(99)00059-9

Shi, Y. Q., Liu, C., and Duan, Z. P. (2020). Interface engineering of MXene towards super-tough and strong polymer nanocomposites with high ductility and excellent fire safety. *Chem. Eng. J.* 399, 125829. doi:10.1016/j.cej.2020.125829

Shi, Y. Q., Liu, C., and Fu, L. B. (2019a). Hierarchical assembly of polystyrene/graphitic carbon nitride/reduced graphene oxide nanocomposites toward high fire safety. *Compos. Part B.* 179, 107541. doi:10.1016/j.compositesb.2019.107541

Shi, Y. Q., Liu, C., and Fu, L. B. (2019b). Sodium alginate-templated synthesis of $g\text{-}C_3N_4$/carbon spheres/Cu ternary nanohybrids for fire safety application. *J. Colloid Interface Sci.* 539, 1–10. doi:10.1016/j.jcis.2018.12.051

Shi, Y. Q., Liu, C., and Liu, L. (2019c). Strengthening, toughing and thermally stable ultrathin MXene nanosheets/polypropylene nanocomposites via nanoconfinement. *Chem. Eng. J.* 378, 122267. doi:10.1016/j.cej.2019.122267

Wang, J. Q. (2002). An XPS study of the thermal degradation and flame retard-ant mechanism of polystyrene-clay nanocomposites. *Polym. Degrad. Stabil.* 77, 249–252. doi:10.1016/S0141-3910(02)00055-1

Wang, X. (2011). Synthesis and characterization of a DOPO-substitued organophosphorus oligomer and its application in flame retardant epoxy resins. *Prog. Org. Coating* 71, 72–82. doi:10.1016/j.porgcoat.2010.12.013

Wu, K. (2009). Synthesis and characterization of a functional polyhedral oligomeric silsesquioxane and its flame retardancy in epoxy resin. *Prog. Org. Coating* 65, 490–497. doi:10.1016/j.porgcoat.2009.04.008

Xing, W., Yang, W., Yang, W., Hu, Q., Si, J., Lu, H., et al. (2016). Functionalized carbon nanotubes with phosphorus- and nitrogen-containing agents: effective reinforcer for thermal, mechanical, and flame-retardant properties of polystyrene nanocomposites. *ACS Appl. Mater. Interfaces* 8, 26266–26274. doi:10.1021/acsami.6b06864

Yu, B., Yuen, A. C. Y., Xu, X., Zhang, Z. C., Yang, W., Lu, H., et al. (2021). Engineering MXene surface with POSS for reducing fire hazards of polystyrene with enhanced thermal stability. *J. Hazard Mater.* 401, 123342. doi:10.1016/j.jhazmat.2020.123342

Yu, B., Xing, W., and Guo, W. (2016). Thermal exfoliation of hexagonal b-oron nitride for effective enhancements on thermal stability, flame retarda-ncy and smoke suppression of epoxy resin nanocomposites via sol-gel pro-cess. *J. Mater. Chem.* 4, 7330–7340. doi:10.1039/C6TA01565D

Zhang, D., Guo, X., Tong, X., Chen, Y., Duan, M., Shi, J., et al. (2020). High-performance battery-type supercapacitor based on porous biocarbon and biocarbon supported Ni-Co layered double hydroxide. *J. Alloys Compd.* 837, 155529. doi:10.1016/j.jallcom.2020.155529

Zhang, J. H., Kong, Q. H., and Wang, D. Y. (2018). Simultaneously improving fire safety and mechanical properties of epoxy resin by Fe-CNTs via large-scale preparation. *J. Mater. Chem.* 6 (15), 6376–6386. doi:10.1039/C7TA10961J

Conflict of Interest: The authors declare that the research was conducted in the absence of any commercial or financial relationships that could be construed as a potential conflict of interest.

frontiers in Materials

ORIGINAL RESEARCH
published: 26 February 2021
doi: 10.3389/fmats.2020.629284

Flame Retarded Rigid Polyurethane Foams Composites Modified by Aluminum Diethylphosphinate and Expanded Graphite

Yuxiang Hu[1], Zijian Zhou[2], Shuisheng Li[1], Dong Yang[1], Shui Zhang[1] and Yakang Hou[1]*

[1]China Construction Fifth Engineering Division Co., Ltd., Changsha, China, [2]School of Architecture and Civil Engineering, Anhui University of Technology, Ma'anshan, China

Rigid polyurethane foam (RPUF) was an organic porous material, which was applied in many fields for excellent thermal insulation and mechanical properties, especially in building insulation. However, the poor fire performance significantly suppresses its further application. In this work, aluminum diethylphosphinate (ADP) combined with expanded graphite (EG) to form a synergistic flame retarded system, which was introduced to fabricate flame retarded rigid polyurethane foam composites (FR-RPUF) by one-step water-blown method. Furthermore, thermal insulation, thermal stability, fire performance, and decomposition products of RPUF and FR-RPUF composites were systematically investigated. It was found that FR-RPUF composites possessed LOI of 25.9 vol% with V-1 rating in UL-94 test when 10 php of ADP and 20 php of EG were added, which were better than RPUF composites with ADP or EG added alone. MCC test showed that RPUF/ADP24/EG6 had the lowest PHRR value of 159.85 W/g, which was 52.01 W/g lower than that of pure RPUF. Gas phase products investigation implied that the combination of ADP and EG could decrease toxic and combustible gases intensities, thus significantly enhancing fire safety of FR-RPUF composites. SEM test indicated that ADP and EG promoted the formation of dense and continuous char residue, which significantly inhibited heat and substance transfer in combustion, thus significantly enhancing fire performance of FR-RPUF composites.

Keywords: flame retarded, rigid polyurethane foams, aluminum diethylphosphinate, expanded graphite, thermal stability

OPEN ACCESS

Edited by:
Yongqian Shi,
Fuzhou University, China

Reviewed by:
Bihe Yuan,
Wuhan University of Technology, China
Gang Tang,
Anhui University of Technology, China
Weizhao Hu,
University of Science and Technology of China, China
Yuezhan Feng,
Zhengzhou University, China

****Correspondence:***
Dong Yang
ydcscec@hotmail.com

Specialty section:
This article was submitted to Polymeric and Composite Materials, a section of the journal Frontiers in Materials

Received: *14 November 2020*
Accepted: *16 December 2020*
Published: *26 February 2021*

Citation:
Hu Y, Zhou Z, Li S, Yang D, Zhang S and Hou Y (2021) Flame Retarded Rigid Polyurethane Foams Composites Modified by Aluminum Diethylphosphinate and Expanded Graphite. Front. Mater. 7:629284. doi: 10.3389/fmats.2020.629284

INTRODUCTION

Rigid polyurethane foams (RPUF), as a novel organic porous material, are widely applied in building, pipeline engineering, refrigerator, and other fields for its excellent thermal insulation performance and mechanical properties (Hejna et al., 2018; Wang et al., 2018; Li et al., 2020; Wang et al., 2020). However, RPUF is easily to be ignited and released kinds of toxic and combustible gases, which would result in heavy casualties in the fire (Barkoula et al., 2008; Liu and Wang, 2018). This shortcoming significantly restricts the further application of RPUF and RPUF composites in many fields, especially in building constructions. Thus, many researchers try to enhance flame retardancy of RPUF (Wang et al., 2018; Bhoyate et al., 2019). Usually, additive and reactive strategies are the common ways to enhance fire performance of RPUF and its composites. Reactive flame retarded

RPUF is fabricated by involving phosphorus-containing diols and polyols. This strategy is often limited for high cost and poor storage stability of phosphorus-containing diols and polyols. The most used way in engineering for fire retardancy of RPUF is additive strategy, which only simply incorporates flame retardant particles in the formation process of RPUF. Some typical flame retardants, such as expandable graphite (EG), ammonium polyphosphate (APP), aluminum hypophosphite (AHP), melamine polyphosphate (MPP), and steel slags (SS), are introduced to fabricate flame retarded RPUF composites. Chen et al. prepare RPUF/EG composites and systematically research structure and flame retardancy of the composites. It is found that 15 phr EG loading endowed LOI of 22.2 vol% for the composites with significantly decreased PHRR and THR value (Chen et al., 2019). Cheng et al. prepare polyurea microencapsulated ammonium polyphosphate (POAPP), which is further applied into RPUF/POAPP composites. It is observed that RPUF/POAPP20 with 20 wt% POAPP loading possessed LOI of 24.8 vol% with 33.9% decrease of PHRR value compared with virgin RPUF (Cheng et al., 2020). Tang et al. combine melamine polyphosphate with steel slag; 2.5 wt% of steel slag and 7.5 wt% of MPP made RPUF composites reach LOI of 24.0 vol% (Tang et al., 2020).

Metal hypophosphate, as a novel flame retardant, is widely used in enhancing fire performance of polymers, including polylactides, thermoplastic polyurethane, and polyamide (Tang et al., 2012; Zhou et al., 2019; Pan et al., 2020). Tang et al. report flame retarded polyurethane foam composites based on aluminum diethylphosphinate (ADP), in which 30 php ADP loading makes RPUF composites possess LOI of 23.0 vol% (Tang et al., 2020). However, because of porous structure, it is very hard to enhance fire performance of RPUF composites, and high loading of flame retardant will inhibit foam formation and be harmful to thermal insulation of the composites. Thus, it is meaningful to fabricate flame retardant RPUF composites with lower flame retardant loading. Synergism strategy can be a good way for solving this problem and many researches about synergistic effect in RPUF system are reported. Chen et al. systematically investigate synergistic effect of ionic liquid modified expandable graphite/3-(N-diphenyl phosphorous) amino-propyl triethoxysilane (IL-EG/DPES) in RPUF composites. It is reported that RPUF composites with 10 phpp IL-EG and10 phpp DPES presented best compressive strength and flame retardancy compared with RPUF with only DPES or IL-EG added (Chen et al., 2020). Han et al. (2020) fabricate flame retardant RPUF composites based on diethyl bis(2-hydroxyethyl) aminomethylphosphonate (DBHP) and organoclay (OMMT). It is found that the RPUF composites with OMMT and DBHP loading possessed significantly raised LOI value and UL94 rating, reduced heat release rate and total heat release, and increased char yields (Han et al., 2020). Akdogan et al. report the synergistic effect of expandable graphite (EG) and ammonium pentaborate octahydrate (APB) in RPUF composites. The flame retarded RPUF composite with 15 wt EG and 5 wt% APB loading possesses PHRR reduction of 57.5% and THR reduction of 42.8% compared with those of virgin RPUF (Akdogan et al., 2020).

Expandable graphite (EG) often plays its flame retardant role by generating worm-like structure, which could suppress mass and substance transfer in condensed phase. Metal hypophosphate salts (MHP) exhibit flame retardancy for generating lots of PO· radicals, which could quench H· and HO in gas phase. The combination of flame retardant effect in condensed phase and gas phase often results in excellent fire retardancy. However, there are a few reports about EG/MHP system applied in RPUF composites. In this work, expandable graphite (EG) is combined with aluminum diethylphosphinate (ADP) to form a novel synergistically flame retarded system, which is further introduced in RPUF. A series of RPUF/ADP/EG composites are fabricated by one-step water-blown method. Thermal stability, thermal insulation property, fire retardancy, and combustion properties of RPUF/ADP/EG composites are characterized by thermogravimetric analysis (TG), thermal conductivity meter, limiting oxygen index (LOI), and UL-94 vertical burning test, microscale combustion calorimetry (MCC), and cone calorimetry (CONE). The gaseous products of the composites are investigated by TG-FTIR. And also, the char residues of composites are researched by X-ray photoelectron spectroscopy (XPS) and scanning electron microscope (SEM).

EXPERIMENTAL SECTION

Materials

LY-4110 (viscosity: 2,500 mPa·s, hydroxyl number: 430 mg KOH/g, purity ≥99 wt%), triethylenediamine (A33, Purity 33 wt%), and silicone surfactant (AK880599, purity ≥99 wt %) were provided by Jiangsu Luyuan New Materials Co., Ltd, China. Polyaryl polymethylene isocyanate (PAPI, purity ≥99.9 wt%) was provided by Wanhua Chemical Group Co., Ltd, China. Dibutyltin dilaurate (LC, purity ≥99 wt%) was obtained from Air Products and Chemicals, Inc. Triethanolamine (TEOA, 99.9 wt%) was purchased from Sinopharm Chemical Reagent Co., Ltd, China. Distilled water used as a chemical blowing agent was made in our laboratory. Aluminum diethylphosphinate (ADP, purity ≥99 wt%) was purchased from Qingdao Fuslin Chemical Technology Co., Ltd. Expanded graphite (EG, Purity ≥99 wt%) was obtained from Qingdao Xingyuan Colloidal Graphite Co., Ltd. All the chemicals were used without treatment.

Preparation of Rigid Polyurethane Foam Composites

RPUF composites were fabricated by free-rise method; the formulation of the composites was listed in **Table 1**. All the raw materials except PAPI were mixed in a 1,000 ml plastic beaker by high speed mechanical stirrer for 20 s. Then, PAPI was poured into the mixture with vigorous stirring for another 10 s and quickly poured into a mold. The obtained foam was cured at 80°C for 5 h to complete the further polymerization reaction. The samples were cut into suitable size for further characteristics.

TABLE 1 | Formulation of RPUF and FR-RPUF composites.

Sample	LY4110 (php)	PM-200 (php)	LC (php)	AK-8805 (php)	A33 (php)	Water (php)	TEA (php)	ADP (php)	EG (php)
RPUF	100	150	0.5	2	1	2	3	0	0
RPUF/ADP30	100	150	0.5	2	1	2	3	30	0
RPUF/ADP24/EG6	100	150	0.5	2	1	2	3	24	6
RPUF/ADP22.5/EG7.5	100	150	0.5	2	1	2	3	22.5	7.5
RPUF/ADP20/EG10	100	150	0.5	2	1	2	3	20	10
RPUF/ADP18/EG12	100	150	0.5	2	1	2	3	18	12
RPUF/ADP15/EG15	100	150	0.5	2	1	2	3	15	15
RPUF/ADP12/EG18	100	150	0.5	2	1	2	3	12	18
RPUF/ADP10/EG20	100	150	0.5	2	1	2	3	10	20
RPUF/ADP7.5/EG22.5	100	150	0.5	2	1	2	3	7.5	22.5
RPUF/ADP6/EG24	100	150	0.5	2	1	2	3	6	24
RPUF/EG30	100	150	0.5	2	1	2	3	0	30

Measurement and Characterization

Scanning electron microscopy (SEM, JSM-6490LV, JEOL Ltd, Japan) was introduced to observe the cell structure of the specimens with accelerating voltage of 20 kV. Before the observation, the sample surface was coated with a thin conductive layer.

Thermal conductivity was tested according to GB/T 10,297-2015 by thermal conductivity meter (TC3000E, Xiaxi Electronic Technology Co., Ltd, China). The sample size was 30 mm × 30 mm×25 mm. Five parallels for each sample were tested and the average value was obtained.

The apparent density of RPUF composites was measured according to ISO 845-2006. The size of the sample was more than 100 cm^3, and five samples were tested to obtain the average value.

Thermogravimetric analysis (TGA) was conducted by Q5000IR (TA Instruments, United States) thermoanalyzer instrument. 5–10 mg sample was loaded and heated from room temperature to 800°C with heating rate of 20°C/min in N_2 condition. The onset decomposition temperature ($T_{-5\%}$) was defined as the temperature at which 5% of the original weight was lost. The midpoint temperature ($T_{-50\%}$) was defined as the temperature at which 50% of the original weight was lost.

Limiting oxygen index (LOI) test was performed at room temperature by JF-3 oxygen index instrument (Jiangning Analysis Instrument Co., Ltd, China) according to ASTM D2863-97. The sample size was 127 mm × 10 mm × 10 mm.

UL-94 vertical burning test was performed by CZF-3 instrument (Jiangning Analysis Instrument Co., Ltd, China) according to ASTM D3801-96. The specimen dimension was 127 mm × 13 mm × 10 mm.

Combustion properties of the sample were characterized by microscale combustion calorimetry (Govmark, United States) according to ASTM D7309-7. 4–6 mg sample was heated from 100 to 650°C with heating rate of 1°C/s in a stream of N_2 flow of 80 ml/min. The volatile anaerobic thermal degradation products in N_2 gas stream were mixed with 20 ml/min stream of pure O_2 gas prior to entering a 900°C combustion furnace. The MCC data obtained were reproducible to about 3%.

Cone calorimetry test of the samples was performed by cone calorimeter (Fire Testing Technology, United Kingdom) according to ISO 5660. The sample with dimension of 100 mm × 100 mm × 4 mm was wrapped with aluminum foil and exposed horizontally to 35 kW/m^2 external heat flux.

Thermogravimetric analysis-Fourier Transform Infrared Spectrometer (TG-FTIR) was conducted by using Q5000IR (TA Instruments, United States) thermoanalyzer instrument which was connected with Nicolet 6700 FTIR spectrophotometer (Thermo Scientific Nicolet, United States). About 5–10 mg of the sample was put in an alumina crucible and heated from 30 to 700°C. The heating rate was 20°C/min in nitrogen atmosphere with flow rate of 70 ml/min.

Char residues of the sample were obtained by calcining the composites in 600 C for 10 min. The morphology of the char residue was investigated by scanning electron microscopy (JSM-6490LV, JEOL Ltd, Japan) with accelerating voltage of 20 kV. The specimens were sputter-coated with a conductive layer.

X-ray photoelectron spectroscopy (XPS) with a VG Escalab Mark II spectrometer (Thermo-VG Scientific Ltd. United States) using Al Ka excitation radiation (hν = 1,253.6 eV) was introduced to investigate the char residues.

Structural Characterization

The RPUF and FR-RPUF composites exhibit different morphologies with various formulations (**Table 1**). The surface microstructure of polyurethane foams can be observed by scanning electron microscope (SEM). As shown in **Figure 1A**, the pure RPUF sample shows the honeycomb obturator bubble structures with relatively smooth surface, and the diameters range from 500 to 800 μm. After the addition of EG, the bubbles RPUF/EG30 are relatively complete, and the bubble size is obviously reduced compared with pure sample (**Figure 1B**). Meanwhile, RPUF/EG30 presents better pore size distribution, which may be due to the nucleation effect of EG. In addition, some open pore structures can be observed in a few bubbles, because of local internal stress and unbalanced foam growth (He et al., 2020). For RPUF/ADP30, the regularity and integrity of bubbles are

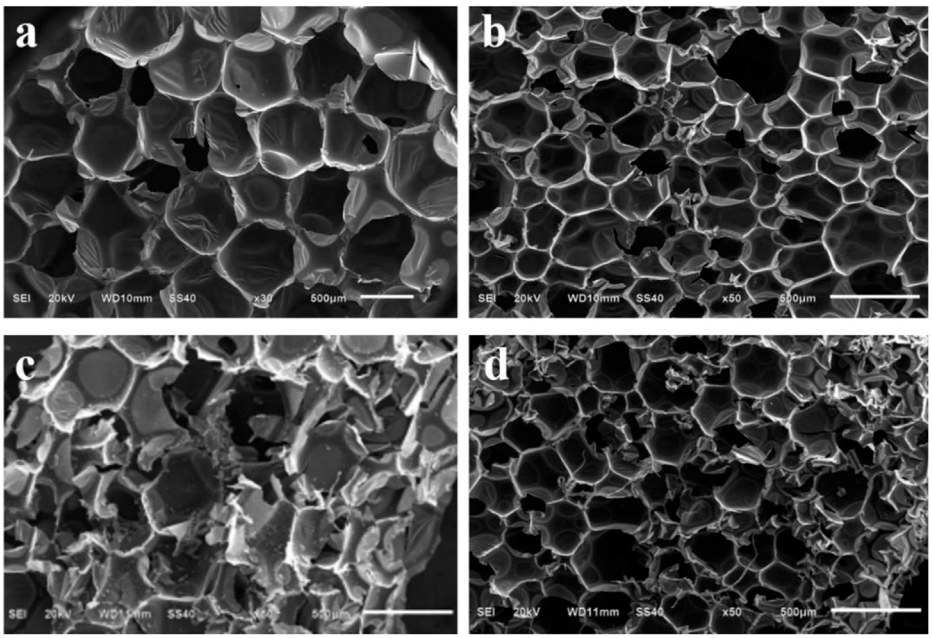

FIGURE 1 | SEM images of RPUF and FR-RPUF composite: **(A)** RPUF; **(B)** RPUF/EG30; **(C)** RPUF/ADP30; **(D)** RPUF/ADP15/EG15.

TABLE 2 | Apparent density and thermal conductivity of RPUF and FR-RPUF composites.

Sample	ρ (kg/m^3)	λ (W/m·k)
RPUF	58.8	0.0392
RPUF/ADP30	58.0	0.0468
RPUF/ADP24/EG6	63.7	0.0419
RPUF/ADP22.5/EG7.5	64.0	0.0438
RPUF/ADP20/EG10	60.2	0.0439
RPUF/ADP18/EG12	58.8	0.0443
RPUF/ADP15/EG15	57.3	0.0446
RPUF/ADP12/EG18	57.1	0.0450
RPUF/ADP10/EG20	57.3	0.0452
RPUF/ADP7.5/EG22.5	52.7	0.0466
RPUF/ADP6/EG24	51.2	0.0474
RPUF/EG30	69.3	0.0467

significantly reduced, and the unevenly dispersed ADP particles are clearly observed on the surface of the bubbles (**Figure 1C**). This result indicates the poor compatibility between ADP and RPUF, and it is not beneficial to the improvement of flame retardant efficiency and mechanical properties of RPUF. When combining ADP and EG together in RPUF, the bubble pore size is further reduced with lower morphology regularity compared with RPUF/EG30. Meanwhile, there appears obvious pore collapse and surface curling phenomenon, due to the joint action of ADP and EG. However, compared to the sample with ADP alone, no obvious exposed ADP particles are observed (**Figure 1D**). The density of RPUF usually has an important influence on the performance of the material. The densities of rigid foam with different components were summarized in **Table 2**. The density of neat RRUF was 58.8 kg/m^3, and the addition of ADP and EG changed the density of foams. When ADP and EG were combined together in RPUF, the density of foam decreases with the increase of EG content. However, when 30 php EG was added, the foam density increased significantly to 69.3 kg/m^3.

Thermal Conductivity

For RPUF, thermal insulation is an important performance index. Thermal insulation performance will be affected by many factors, such as the type of foaming agent, cell size, ratio of open and closed cells, and foam density (Debski et al., 2001). The influence of ADP and EG on thermal conductivity was also listed in **Table 2**. It can be seen that the thermal conductivity of pure RPUF was as low as 0.0392 W/m·K. With the addition of different proportions of ADP and EG in RPUF, the thermal conductivity of all FR-PURF composites increased. It was worth noting that the thermal conductivity increased, as the content of EG in RPUF increased. When the addition of ADP and EG were 6 and 24 php, respectively, the thermal conductivity of RPUF/ADP6/EG24 increased to the maximum 0.0474 W/mk. The increase may result from the shrinkage of the cells caused by EG.

Thermal Stability

RPUF usually exhibits an anaerobic thermal decomposition process during combustion; thus the thermal stability of RPUF was investigated by TGA in nitrogen atmosphere (**Figure 2**). And some important parameters such as the temperatures at a specific weight loss ($T_{-5\%}$ and $T_{-50\%}$), the temperature at maximum mass loss rate (T_{max}), and the residues at 800°C are listed in **Table 3**. As shown in **Figure 2**, the pure RPUF presents the two-stage thermal degradation process. The first stage occurred at around 180–325°C with 34.3% weight loss, caused by the decomposition of hard segments in polyurethane molecular chains, producing polyols,

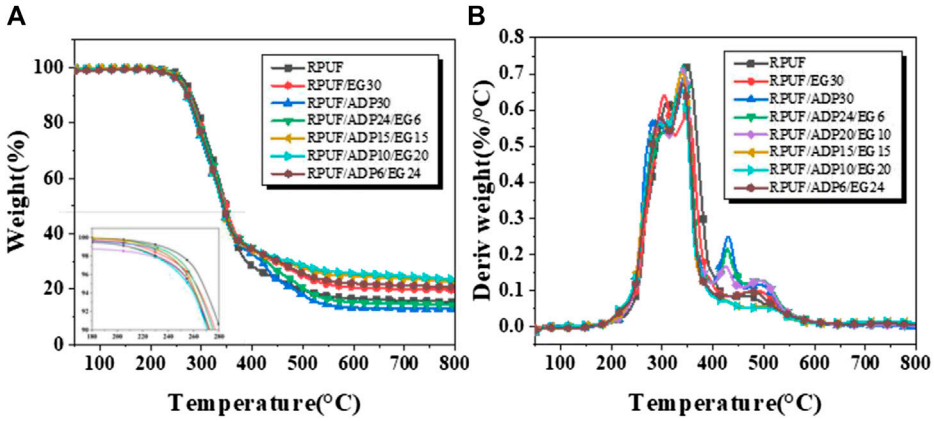

FIGURE 2 | (A) TGA and **(B)** DTG curves of RPUF and FR-RPUF composites under N_2.

TABLE 3 | TGA results of RPUF and FR-RPUF composites under N_2. Flame retardant performance.

Samples	$T_{-5\%}$ (°C)	$T_{-50\%}$ (°C)	T_{max} (°C)	Residue (wt%)
RPUF	267.3	348.4	350.6	15.54
RPUF/EG30	261.7	348.1	304.0	19.72
RPUF/ADP24/EG6	261.2	345.4	340.9	14.44
RPUF/ADP20/EG10	257.4	341.7	340.9	14.27
RPUF/ADP15/EG15	258.6	341.3	338.9	22.71
RPUF/ADP10/EG20	255.4	341.2	338.3	23.58
RPUF/ADP6/EG24	257.0	343.1	340.2	20.78
RPUF/ADP30	258.8	341.0	342.8	12.97

isocyanates carbon dioxide, amines, and so on. Corresponding to a weight loss of 49%, the second stage occurred at temperature between 325 and 590°C and was attributed to the decomposition of soft polyol segments. For FR-RPUF, the $T_{-5\%}$ of all samples were decreased to a certain extent, due to breaking of weak bonds and the earlier degradation of polyurethane molecular, which resulted from acid substance released from the EG and ADP. In particular, the $T_{-5\%}$ decreased with the increasing ADP contents. However, the earlier degradation of flame retardant was beneficial to the improvement of flame retardant performance for FR-RPUF composites. It is worth noting that ADP and EG had different effects on the thermal degradation process of RPUF. With the increase of ADP content, a new peak at 400–550°C gradually appeared on the DTG curve of the RPUF/ADP30, resulting in 20% weight loss approximately, due to the formation of volatile phosphinate compounds (Zhan et al., 2015). Also, the $T_{-50\%}$ for samples containing ADP were slightly decreased. Though EG component exhibits no obvious influence on $T_{-50\%}$, it causes the significant reduction on T_{max}. Additionally, it is notable that the T_{max} of RPUF/EG30 was lower than $T_{-50\%}$ at a great extent, indicating more foam matrix can be retained during combustion. In fact, the char residues of RPUF/EG30 are 19.72%, which is much higher than 15.54% of RPUF and 12.97% of RPUF/ADP30. It has been reported that a low-density worm-like insulation layer would be produced steadily on the surface of matrix, when EG is activated during heating process, which effectively inhibits the transfer of heat

TABLE 4 | LOI and UL-94 test results of RPUF and FR-RPUF composites.

Sample	LOI	UL-94. 10.0 mm bar		
	vol%	t_1/t_2[a](s)	Dripping	Rating
RPUF	18.8	28.2/0	N	NR[b]
RPUF/ADP30	23.0	16.4/0	N	V-1
RPUF/ADP24/EG6	23.2	19.9/0	N	V-1
RPUF/ADP22.5/EG7.5	23.9	18.2/0	N	V-1
RPUF/ADP20/EG10	24.5	17.9/0	N	V-1
RPUF/ADP18/EG12	24.3	18.3/0	N	V-1
RPUF/ADP15/EG15	24.5	18.2/0	N	V-1
RPUF/ADP12/EG18	25.3	16.8/0	N	V-1
RPUF/ADP10/EG20	25.9	14.2/0	N	V-1
RPUF/ADP7.5/EG22.5	25.3	12.2/0	N	V-1
RPUF/ADP6/EG24	25.7	12.1/0	N	V-1
RPUF/EG30	25.2	12.3/0	N	V-1

[a]*t_1 and t_2, average combustion times after the first and the second applications of the flame.*
[b]*NR, no rating.*

and substances (Acuña et al., 2020). Taking all parameters into considerations, RPUF/ADP10/EG20 shows the best thermal stability with the highest residues and the lowest onset decomposition temperature, which would promote the formation of protective layer in a fire.

The flame retardant properties of pure RPUF and FR-RPUF were firstly evaluated by limiting oxygen index (LOI) test, as shown in **Table 4**. The LOI value of pure RPUF is 18.8 vol%. With the addition of 30 php of ADP, the LOI value of RPUF/ADP30 increased to 23.0 vol%. After adding 30 php of EG, the LOI value of RPUF/EG30 can reach 25.2 vol%, higher than the composites modified by ADP alone. When EG and ADP are added at the same time, the LOI values of RPUF are obviously higher than that of RPUF/ADP30. However, the samples show different LOI values with different EG and ADP additions. Among them, the LOI value of RPUF/ADP10/EG20 can reach the maximum 25.9 vol%. It is worth noting that RPUF/ADP12/EG (Akdogan et al., 2020), RPUF/ADP10/EG20, RPUF/ADP7.5/EG22.5, and RPUF/ADP6/EG24 composites have greater LOI values

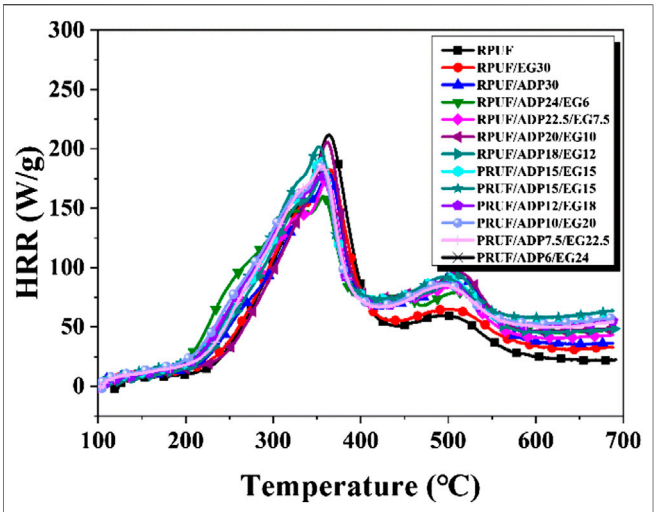

FIGURE 3 | MCC results of RPUF and FR-RPUF composites.

compared with RPUF/ADP30 and RPUF/EG30. These results indicate that there exists a good synergistic flame retardant effect between ADP and EG. Vertical burning test (UL 94) is used to evaluate the flame retardant performance of RPUF and FR-RPUF composites. As shown in **Table 4**, compared with no rating of the pure RPUF, all FR-RPUF exhibited V-1 rating, indicating the improved flame retardancy of the composites.

As a simple screening method, MCC analysis was performed, where only a small amount of samples was needed to investigate the combustion of the RPFU and FR-RPUF composite (Chu et al., 2018). Heat release rate (HRR) curves can be obtained from MCC and were depicted in **Figure 3**. Meanwhile, as an important parameter to evaluate the flame retardancy of materials, peak heat release rate (PHRR) was summarized in **Table 5**. Compared with pure RPUF, all modified FR-RPUF exhibits lower PHRR values. In comparison with the 211.86 W/g of pure RPUF, the PHRR values of RPUF/EG30 and RPUF/ADP30 were reduced to 180.15 and 179.61 W/g, respectively, with the addition of 30 php of EG and ADP. When EG and ADP were combined together in RPUF, the PHRR values of the samples presented a certain difference under different component contents. Among them, RPUF/ADP24/EG6 had the lowest PHRR value of 159.85 W/g, which was 52.01 W/g lower than that of pure RPUF.

The combustion properties of pure RPUF and FR-RPUF were tested through cone calorimeter. HRR and total heat release (THR) curves were depicted in **Figure 4**, and the data were listed in **Table 5**. As shown in **Figure 4A**, pure RPUF reached the peak of maximum heat release rate soon after ignition (298.28 kW/m^2). All FR-RPUF exhibited a different heat release behavior from pure RPUF. Compared with pure RPUF, the PHRR of RPUF/EG30 was reduced to 161.27 kW/m^2, experiencing 45.93% of decrement. The reason why RPUF with addition of EG had such a low PHRR was as follows: When heated, EG expanded and a large amount of worm-like carbon layer was formed, which served as a physical barrier in the condensed phase and gas phase of the combustion zone. Moreover, the large amount of incombustible gas formed by the expansion would dilute the concentration of the fuel. However, RPUF modified with EG had longer flaming combustion time, due to the delayed release of combustible gases in the presence of EG. The THR of RPUF/EG30 was 23.08 MJ/m^2, decreased by 18.65% compared with the pure RPUF. The reduction in THR was not as great as that in PHRR. That was because EG modified RPUF possessed a higher density than pure RPUF; thus more fuel would be contained in the combustion process. Two peaks can be seen in the HRR curves of some samples. This may be ascribed to the expansion of the sample during the combustion process, which shortened the distance between the sample surface and the heating coil. Thus, higher thermal radiation can be received by samples, and the combustion will release more heat.

Gaseous Phase Analysis

The volatile products of RPUF and FR-RPUF composites during the pyrolysis process were investigated by TG-IR. The Gram-Schmidt (GS) curves and the absorbance intensity of the typical gas products were shown in **Figure 5A**. The absorbance intensity of RPUF composites was significantly reduced compared with pure RPUF, with the addition of EG and ADP. Moreover, RPUF/ADP15/EG15 showed lower absorbance intensity than RPUF/EG and RPUF/ADP, indicating the synergistic smoke suppression effect between the EG and ADP. The absorption intensities of released CO_2 compounds and hydrocarbons were presented in **Figure 5E**, and the intensity of RPUF was lower than that of RPUF/EG30. This may be due to the structural characteristics of expandable graphite itself, which made it easy to release volatile hydrocarbons during combustion. However, due to the expandability of expanded graphite and its high temperature resistance, expandable graphite expanded rapidly at high temperatures. At the same time, the produced expanded graphite materials covered the surface of the substrate, isolating heat radiation and oxygen. The acid radicals inside the interlayer can be released during expansion, which also promoted the carbonization of the substrate. When combined with ADP in RPUF, the thermal decomposition products of ADP had a strong dehydration effect, and the covered polymer surface was carbonized to form a carbon film. Thus, a good flame

TABLE 5 | PHRR and THR from MCC and cone.

Sample	PHRR (W/g, MCC)	PHRR (kW/m^2, cone)	THR (MJ/m^2)
RPUF	211.86	298.28	28.37
RPUF/ADP30	179.61	322.48	21.31
RPUF/ADP24/EG6	159.85	296.06	34.30
RPUF/ADP22.5/EG7.5	172.80	—	—
RPUF/ADP20/EG10	205.50	372.50	33.64
RPUF/ADP18/EG12	180.16	—	—
RPUF/ADP15/EG15	191.88	323.57	32.55
RPUF/ADP12/EG18	201.71	—	—
RPUF/ADP10/EG20	177.87	286.30	35.10
RPUF/ADP7.5/EG22.5	185.35	—	—
RPUF/ADP6/EG24	185.41	310.79	37.84
RPUF/EG30	180.15	161.27	23.08

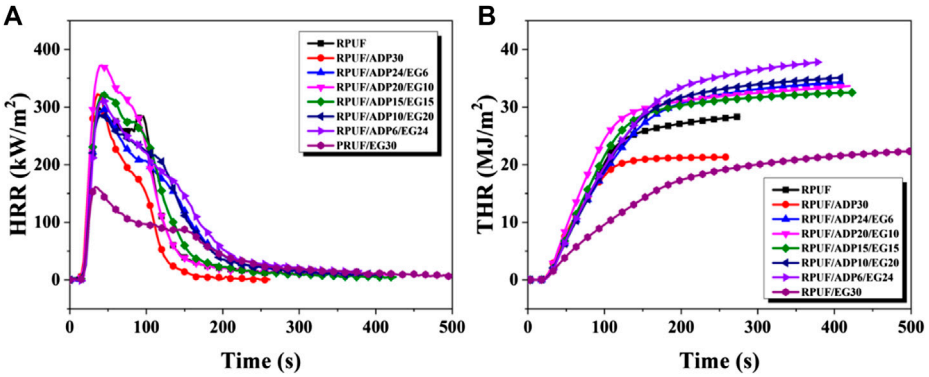

FIGURE 4 | HRR **(A)** and THR **(B)** curves vs time of RPUF and FR-RPUF composites.

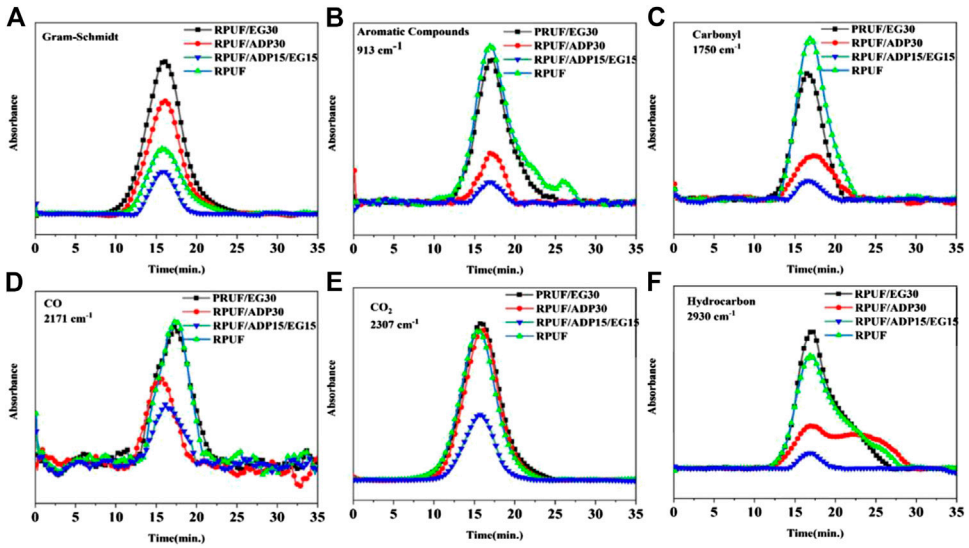

FIGURE 5 | Absorbance of gaseous products of RPUF and FR-RUUF composites versus time: **(A)** Gram-schmidt; **(B)** aromatic compounds; **(C)** carbonyl; **(D)** CO; **(E)** CO_2; **(F)** hydrocarbon.

retardant effect can be achieved through this synergistic flame retardant method. Furthermore, the decrease in the strength of the aromatic compound may imply a reduction in the yield of aromatic volatiles, which lead to suppression of smoke particles that were formed by these condensed aromatic fragments. Moreover, poisonous gas products such as CO and carbonyl can threaten the safety of human life seriously (Chu et al., 2018; Shi et al., 2019; Liu et al., 2020; Shi et al., 2020; Chu et al., 2021). Therefore, it is important to reduce the release of these toxic substances. The corresponding absorption intensities of CO and carbonyl were given in **Figures 5C,D**, respectively. With the addition of EG and ADP, a significant decrease in absorbance can be achieved and RPU/ADP15/EG15 had the lowest intensity. This indicates that the combination of EG and ADP can effectively inhibit the burning toxicity of the polymer. In addition, the polymer added with ADP would also produce an expanded carbon layer during the combustion process to achieve the effects of heat and oxygen insulation and further prevented the spread of surface flames, playing a key role in flame retardancy (Qiu et al., 2019).

Condensed Phase Analysis

SEM was used to further characterize the external and internal char residues of four different polyurethane foams, which can further explain their different performance in flame retardancy (Xu et al., 2020). As shown in **Figure 6**, there were many carbon micron spheres on the surface of residues of pure RPUF, without a continuous and dense char layer. The internal carbon layer had obvious rupture, which had a weak inhibition effect on the release of fuel from the matrix and the transfer of heat to the matrix. Finally, the pure RPUF showed poor fire safety performance. In contrast, RPUF/ADP30 presented a much smaller number of carbon micron spheres on the surface of residual. A relatively continuous char layer can be formed on the surface, and the char layer inside was also more compact. Compared with the pure

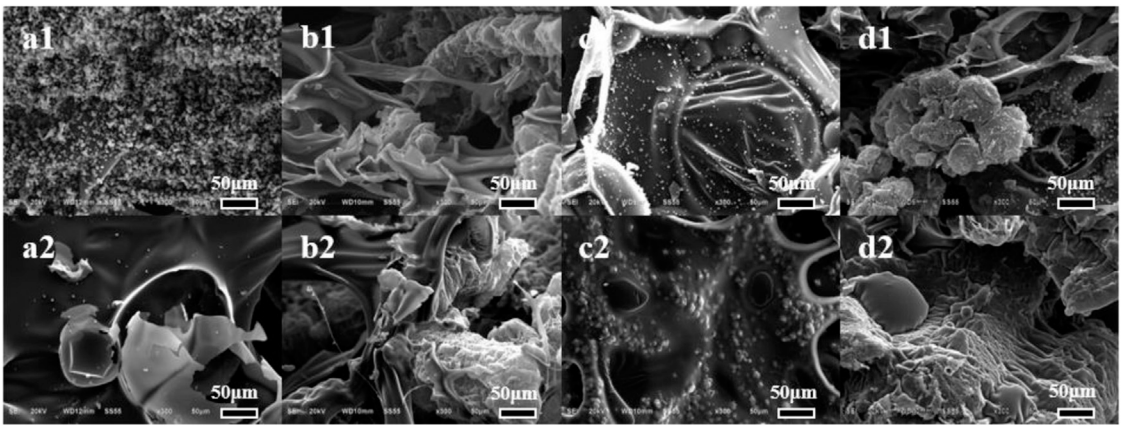

FIGURE 6 | SEM images of the external and internal char residues of RPUF and FR-RPUF composites: **(A)** RPUF; **(B)** RPUF/EG30; **(C)** RPUF/ADP30; **(D)** RPUF/ADP15/EG15.

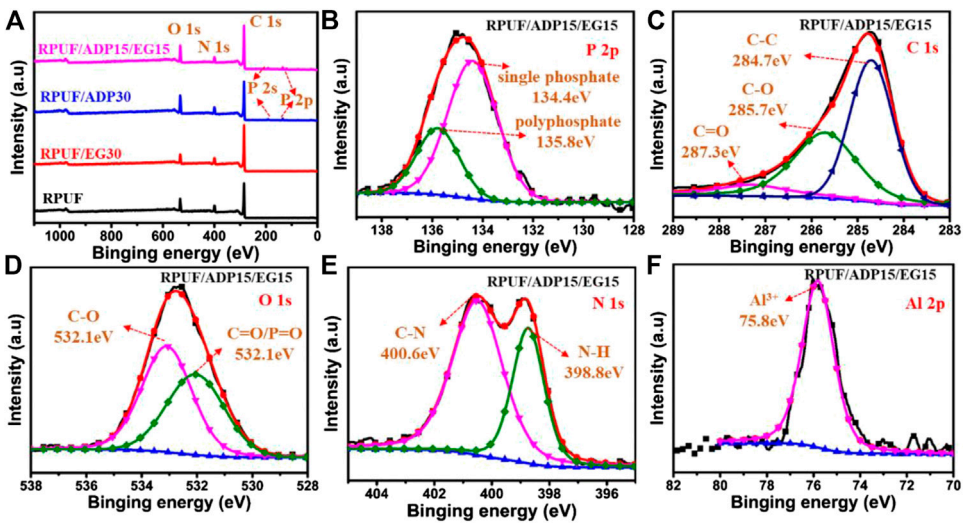

FIGURE 7 | (A) XPS survey spectrum of the residual char for RPUF and its nanocomposites after cone tests; high-resolution, **(B)** P 2p, **(C)** C 1s, **(D)** O 1s, **(E)** N 1s, and **(F)** Al 2p XPS spectra of RPUF/ADP15/EG15.

RPUF, the flame retardant performance of RPUF/ADP30 was significantly improved. However, some obvious holes were observed on the surface of char layers, which limited the suppression effect of mass and heat transfer. In the case of ADP and EG combined, there were also carbon micron spheres on the surface of the external char layer. The specific worm-like char layer formed by expandable graphite had obvious rupture, which was not conducive to the improvement of flame retardant performance, while the internal char layer presented dense and continuous morphology.

For the RPUF with only EG added, the internal and external morphology were similar. On outside, there appeared continuous and relatively loose worm-like carbon layer, and the formed char framework was continuously dense, without any carbon micron ball. Meanwhile, the worm-like char layer and char layer framework inside were more dense, which had an advantage in improving the flame retardant performance.

The more diversified information about the surface composition and chemical state of the residual chars can be offered by the XPS analysis. As shown in **Figure 7A**, the XPS survey spectra of RPUF and RPUF/EG30 were composed of C, N, and O elements, but there were additional P elements in the residual char of RPUF/ADP30 and RPUF/ADP15/EG15 nanocomposites. Moreover, the O content in the surface char layer of RPUF/ADP30 and RPUF/ADP15/EG15 was 15.9 and 13.1%, respectively, higher than that of RPUF and RPUF/EG30 (12.1 and 8.4%), respectively. This result is due to the decomposition of ADP to produce POx during combustion process, which can promote carbon formation (Zhou et al., 2020). **Figures 7B–F** showed the P 2p, C 1s, O 1s, N 1s, and Al 2p spectra of the external char of RPUF/ADP15/EG15. As shown in the P 2p

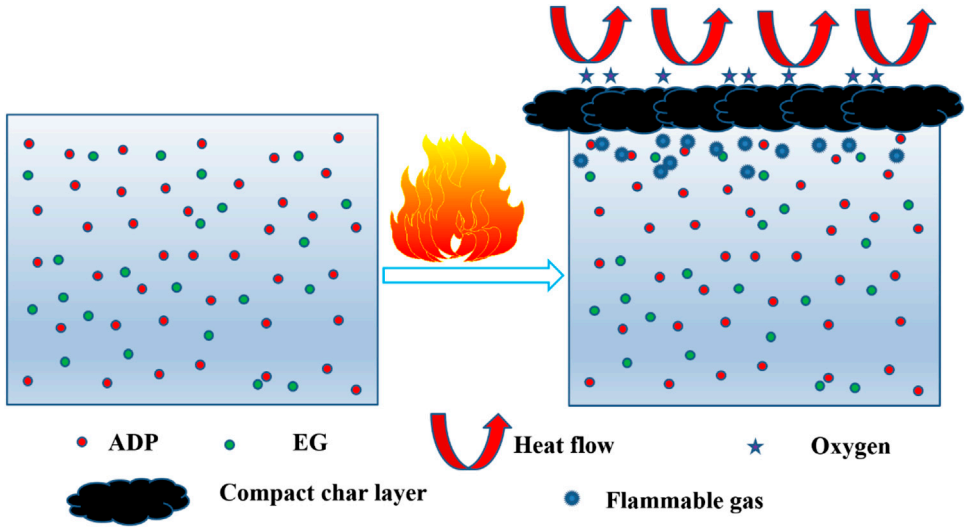

FIGURE 8 | Schematical illustration of flame retardant mechanism for RPUF/ADP/EG composites.

spectrum, two peaks appear in the 134.4 and 135.8 eV, which was attributed to single phosphate and pyrophosphate, respectively, revealing the formation of cross-linked phosphorus oxide compounds (Zhou et al., 2020). As shown in C 1s spectrum, the C 1s peaks can be deconvoluted into three peaks at 284.7, 285.7, and 287.3 eV corresponding to C-C, C-O, and C=O bonds, respectively. Correspondingly, C-O and C=O can also be found in O 1s spectrum, and the peak corresponding to C=O also corresponds to P=O in phosphate groups (Qiu et al., 2020). Two peaks at 398.8 and 400.6 eV assigned to N-H and C-N bondings were found in the N 1s spectrum (Qiu et al., 2019), owing to the carbonitride after the decomposition of RPUF. A peak at 75.8 eV is found in the Al 2p spectrum, representing phosphate and/or aluminum pyrophosphate (Tang et al., 2013).

Mechanism Consideration

Based on the above investigation, possible fire retarded mechanism of RPUF/ADP/EG composites was proposed and the corresponded schematical illustration was presented in **Figure 8**. As being ignited, the fire usually started on the surface of the composites. EG particles could expand and form worm-like structure with some holes by the released SO_2 or NO_2 (Wang et al., 2011). ADP particles decomposed into oligomers of phosphinates, diethylphosphinic acid, and aluminum phosphate (Orhan et al., 2012; Kaya and Hacaloglu, 2014). Oligomers of phosphinates further decomposed into P and PO, which could quench H· and HO· in gas phase. Diethylphosphinic acid could further promote polyurethane chain into char and reduce the production of combustible gas. The char combined with aluminum phosphate to form carbon film and cover on the surface of worm-like structure, significantly enhancing compactness of the char residue. The compact char residue could significantly inhibit heat and substance transfer and thus effectively suppress burning of underlying materials and obviously enhance fire retarding of RPUF/ADP/EG composites. Thus, ADP/EG systems mostly play their role by gas-solid flame retardant mechanism.

CONCLUSION

This work investigated the effect of EG and ADP on the structure, thermal conductivity, thermal stability, and flame retardant performance of RPUF and FR-RPUF. When the addition of ADP and EG was 6 and 24 php, respectively, the thermal conductivity of RPUF/ADP6/EG24 increased to the maximum 0.0474 W/m·k. The increase may be caused by the shrinkage of the cells caused by EG. For FR-RPUF, the thermal stability decreased with the increasing ADP contents, and the char residues increased as EG contents increased. Meanwhile, the results in flame retardant performance indicated the addition of ADP and EG can improve the flame retardancy of RPUF, and there existed a good synergistic flame retardant effect between ADP and EG. The flame retardant mechanism was investigated from gaseous and condensed phase, respectively.

DATA AVAILABILITY STATEMENT

The original contributions presented in the study are included in the article/Supplementary Material; further inquiries can be directed to the corresponding author.

AUTHOR CONTRIBUTIONS

YH: Formal analysis, Investigation, Visualization, Writing-original draft. ZZ: Formal analysis, Investigation, Writing & reviewing. SL: Conceptualization, Resources, Supervision. DY: Methodology, Project administration, Writing-reviewing & editing. SZ: Investigation, Writing-original draft. YH: Investigation, Writing-original draft.

REFERENCES

Acuña, P., Lin, X., Calvo, M. S., Shao, Z., Pérez, N., Villafañe, F., et al. (2020). Synergistic effect of expandable graphite and phenylphosphonic-aniline salt on flame retardancy of rigid polyurethane foam. *Polym. Degrad. Stabil.*, 179, 109274. doi:10.1016/j.polymdegradstab.2020.109274

Akdogan, E., Erdem, M., Ureyen, M. E., and Kaya, M. (2020). Synergistic effects of expandable graphite and ammonium pentaborate octahydrate on the flame-retardant, thermal insulation, and mechanical properties of rigid polyurethane foam. *Polym. Compos.*, 41 (5), 1749–1762. doi:10.1002/pc.25494

Barkoula, N. M., Alcock, B., Cabrera, N. O., and Peijs, T. (2008). Flame-retardancy properties of intumescent ammonium poly(phosphate) and mineral filler magnesium hydroxide in combination with graphene. *Polym. Polym. Compos.* 16 (2), 101–113. doi:10.1002/pc

Bhoyate, S., Ionescu, M., Kahol, P. K., and Gupta, R. K. (2019). Castor-oil derived nonhalogenated reactive flame-retardant-based polyurethane foams with significant reduced heat release rate. *J. Appl. Polym. Sci.* 136 (13), 1–7. doi:10.1002/app.47276

Chen, Y., Luo, Y., Guo, X., Chen, L., and Jia, D. (2020). The synergistic effect of ionic liquid-modified expandable graphite and intumescent flame-retardant on flame-retardant rigid polyurethane foams. *Materials* 13 (14), 3095. doi:10.3390/ma13143095

Chen, Y., Luo, Y., Guo, X., Chen, L., Xu, T., and Jia, D. (2019). Structure and flame-retardant actions of rigid polyurethane foams with expandable graphite. *Polymers* 11 (4), 686. doi:10.3390/polym11040686

Cheng, J., Niu, S., Ma, D., Zhou, Y., Zhang, F., Qu, W., et al. (2020). Effects of ammonium polyphosphate microencapsulated on flame retardant and mechanical properties of the rigid polyurethane foam. *J. Appl. Polym. Sci.* 137 (48), 2–9. doi:10.1002/app.49591

Chu, F., Xu, Z., Zhou, Y., Zhang, S., Mu, X., Wang, J., et al. (2021). Hierarchical core–shell TiO2@LDH@Ni(OH)2 architecture with regularly-oriented nanocatalyst shells: towards improving the mechanical performance, flame retardancy and toxic smoke suppression of unsaturated polyester resin. *Chem. Eng. J.* 405, 126650. doi:10.1016/j.cej.2020.126650

Chu, F., Yu, X., Hou, Y., Mu, X., Song, L., and Hu, W. (2018). A facile strategy to simultaneously improve the mechanical and fire safety properties of ramie fabric-reinforced unsaturated polyester resin composites. *Compos. Appl. Sci. Manuf.* 115, 264–273. doi:10.1016/j.compositesa.2018.10.006

Chu, F., Zhang, D., Hou, Y., Qiu, S., Wang, J., Hu, W., et al. (2018). Construction of hierarchical natural fabric surface structure based on two-dimensional boron nitride nanosheets and its application for preparing biobased toughened unsaturated polyester resin composites. *ACS Appl. Mater. Interfaces* 10 (Issue 46), 40168–40179. doi:10.1021/acsami.8b15355

Debski, K., Magiera, J., and Pielichowski, J. (2001). The effect of the structure of rigid polyurethane foams blown with a hydrocarbon blowing agent on foam's apparent thermal conductivity. *Polimery/Polymers* 46 (9), 631–637. doi:10.14314/polimery.2001.631

Han, S., Zhu, X., Chen, F., Chen, S., and Liu, H. (2020). Flame-retardant system for rigid polyurethane foams based on diethyl bis(2-hydroxyethyl) aminomethylphosphonate and *in-situ* exfoliated clay. *Polym. Degrad. Stabil.* 177, 109178. doi:10.1016/j.polymdegradstab.2020.109178

He, W., Kang, P., Fang, Z., Hao, J., Wu, H., Zhu, Y., et al. (2020). Flow reactor synthesis of bio-based polyol from soybean oil for the production of rigid polyurethane foam. *Ind. Eng. Chem. Res.* 59 (39), 17513–17519. doi:10.1021/acs.iecr.0c01175

Hejna, A., Kosmela, P., Kirpluks, M., Cabulis, U., Klein, M., Haponiuk, J., et al. (2018). Structure, mechanical, thermal and fire behavior assessments of environmentally friendly crude glycerol-based rigid polyisocyanurate foams. *J. Polym. Environ.* 26 (5), 1854–1868. doi:10.1007/s10924-017-1086-2

Kaya, H., and Hacaloglu, J. (2014). Thermal degradation of polylactide/aluminium diethylphosphinate. *J. Anal. Appl. Pyrol.* 110 (1), 155–162. doi:10.1016/j.jaap.2014.08.015

Li, P., Xiao, Z., Chang, C., Zhao, S., and Xu, G. (2020). Efficient synthesis of biobased glycerol levulinate ketal and its application for rigid polyurethane foam production. *Ind. Eng. Chem. Res.* 59 (39), 17520–17528. doi:10.1021/acs.iecr.9b06038

Liu, C., Wu, W., Shi, Y., Yang, F., Liu, M., Chen, Z., et al. (2020). Creating MXene/reduced graphene oxide hybrid towards highly fire safe thermoplastic polyurethane nanocomposites. *Compos. B Eng.*, 203 (October), 108486. doi:10.1016/j.compositesb.2020.108486

Liu, L., and Wang, Z. (2018). High performance nano-zinc amino-tris-(methylenephosphonate) in rigid polyurethane foam with improved mechanical strength, thermal stability and flame retardancy. *Polym. Degrad. Stabil.* 154, 62–72. doi:10.1016/j.polymdegradstab.2018.05.023

Orhan, T., Isitman, N. A., Hacaloglu, J., and Kaynak, C. (2012). Thermal degradation of organophosphorus flame-retardant poly(methyl methacrylate) nanocomposites containing nanoclay and carbon nanotubes. *Polym. Degrad. Stabil.* 97 (3), 273–280. doi:10.1016/j.polymdegradstab.2011.12.020

Pan, Y., Song, L., Wang, W., and Zhao, H. (2020). Polydimethylsiloxane wrapped aluminum diethylphosphinate for enhancing the flame retardancy of polyamide 6. *J. Appl. Polym. Sci.*, 137 (35), 1–8. doi:10.1002/app.49027

Qiu, S., Zhou, Y., Ren, X., Zou, B., Guo, W., Song, L., et al. (2020). Construction of hierarchical functionalized black phosphorus with polydopamine: a novel strategy for enhancing flame retardancy and mechanical properties of polyvinyl alcohol. *Chem. Eng. J.*, 402, 126212. doi:10.1016/j.cej.2020.126212

Qiu, S., Zhou, Y., Zhou, X., Zhang, T., Wang, C., Yuen, R. K. K., et al. (2019). Air-Stable polyphosphazene-functionalized few-layer black phosphorene for flame retardancy of epoxy resins. *Small*, 15 (10), e1805175. doi:10.1002/smll.201805175

Shi, Y., Liu, C., Duan, Z., Yu, B., Liu, M., and Song, P. (2020). Interface engineering of MXene towards super-tough and strong polymer nanocomposites with high ductility and excellent fire safety. *Chem. Eng. J.* 399 (June), 125829. doi:10.1016/j.cej.2020.125829

Shi, Y., Liu, C., Liu, L., Fu, L., Yu, B., Lv, Y., et al. (2019). Strengthening, toughing and thermally stable ultra-thin MXene nanosheets/polypropylene nanocomposites via nanoconfinement. *Chem. Eng. J.* 378, 122267. doi:10.1016/j.cej.2019.122267

Tang, G., Liu, X., Zhou, L., Zhang, P., Deng, D., and Jiang, H. (2020). Steel slag waste combined with melamine pyrophosphate as a flame retardant for rigid polyurethane foams. *Adv. Powder Technol.* 31 (1), 279–286. doi:10.1016/j.apt.2019.10.020

Tang, G., Wang, X., Xing, W., Zhang, P., Wang, B., Hong, N., et al. (2012). Thermal degradation and flame retardance of biobased polylactide composites based on aluminum hypophosphite. *Ind. Eng. Chem. Res.* 51 (37), 12009–12016. doi:10.1021/ie3008133

Tang, G., Zhang, R., Wang, X., Wang, B., Song, L., Hu, Y., et al. (2013). Enhancement of flame retardant performance of bio-based polylactic acid composites with the incorporation of aluminum hypophosphite and expanded graphite. *J. Macromol. Sci., Pure Appl. Chem.* 50 (2), 255–269. doi:10.1080/10601325.2013.742835

Tang, G., Zhou, L., Zhang, P., Han, Z., Chen, D., Liu, X., et al. (2020). Effect of aluminum diethylphosphinate on flame retardant and thermal properties of rigid polyurethane foam composites. *J. Therm. Anal. Calorim.*, 140 (2), 625–636. doi:10.1007/s10973-019-08897-z

Wang, B., Hu, S., Zhao, K., Lu, H., Song, L., and Hu, Y. (2011). Preparation of polyurethane microencapsulated expandable graphite, and its application in ethylene vinyl acetate copolymer containing silica-gel microencapsulated ammonium polyphosphate. *Ind. Eng. Chem. Res.*, 50 (20), 11476–11484. doi:10.1021/ie200886e

Wang, C., Wu, Y., Li, Y., Shao, Q., Yan, X., Han, C., et al. (2018). Flame-retardant rigid polyurethane foam with a phosphorus-nitrogen single intumescent flame retardant. *Polym. Adv. Technol.* 29 (1), 668–676. doi:10.1002/pat.4105

Wang, S. X., Zhao, H. B., Rao, W. H., Huang, S. C., Wang, T., Liao, W., et al. (2018). Inherently flame-retardant rigid polyurethane foams with excellent thermal insulation and mechanical properties. *Polymer*, 153, 616–625. doi:10.1016/j.polymer.2018.08.068

Wang, S., Yang, X., Li, Z., Xu, X., Liu, H., Wang, D., et al. (2020). Novel eco-friendly maleopimaric acid based polysiloxane flame retardant and application in rigid polyurethane foam. *Compos. Sci. Technol.* 198, 108272. doi:10.1016/j.compscitech.2020.108272

Xu, Z., Duan, L., Hou, Y., Chu, F., Jiang, S., Hu, W., et al. (2020). The influence of carbon-encapsulated transition metal oxide microparticles on reducing toxic gases release and smoke suppression of rigid polyurethane foam composites. *Composites Part A: applied science and manufacturing* 131, 105815. doi:10.1016/j.compositesa.2020.105815

Zhan, Z., Xu, M., and Li, B. (2015). Synergistic effects of sepiolite on the flame retardant properties and thermal degradation behaviors of polyamide 66/aluminum diethylphosphinate composites. *Polym. Degrad. Stabil.* 117, 66–74. doi:10.1016/j.polymdegradstab.2015.03.018

Zhou, Q., Gong, K., Zhou, K., Zhao, S., and Shi, C. (2019). Synergistic effect between phosphorus tailings and aluminum hypophosphite in flame-retardant thermoplastic polyurethane composites. *Polym. Adv. Technol.*, 30 (9), 2480–2487. doi:10.1002/pat.4695

Zhou, Y., Chu, F., Qiu, S., Guo, W., Zhang, S., Xu, Z., et al. (2020). Construction of graphite oxide modified black phosphorus through covalent linkage: an efficient strategy for smoke toxicity and fire hazard suppression of epoxy resin. *J. Hazard Mater.* 399 (May), 123015. doi:10.1016/j.jhazmat.2020.123015

Conflict of Interest: YH, SL, DY, SZ, and YH were employed by company China Construction Fifth Engineering Division Co., Ltd.

The remaining authors declare that the research was conducted in the absence of any commercial or financial relationships that could be construed as a potential conflict of interest.

frontiers in Materials

ORIGINAL RESEARCH
published: 19 March 2021
doi: 10.3389/fmats.2021.661906

Study on Flame Retardancy and Mechanism of Talc Composite Foams

Xiujuan Li[1,2]*, *Ruisong Guo*[1]* and *Xiaodong Qian*[2]*

[1]Key Laboratory of Advanced Ceramics and Machining Technology of Ministry of Education, School of Materials Science and Engineering, Tianjin University, Tianjin, China, [2]School of Criminal Investigation, China People's Police University, Langfang, China

Under high temperature, aqueous film forming foam extinguishing agent has poor flame retardancy and low fire efficiency. In order to solve this problem, talc was introduced into foam to form composite foam. The fire resistance and fire extinguishing properties of the composite foam were studied. The results showed that talc composite foam had good flame retardant resistance. when the concentration of talc reached 40 g/100 ml, the 50% liquid separation time of the composite foam was 21.1 min. The fuel burning in the anti burning tank did not ignite the gasoline in the oil pan, and burned out at 51.5 min. It was related to the structure of composite foam and the properties of talc. Due to the introduction of talc, the viscosity of the composite foam increased. The network structure of composite foam was important to the improved stability of foam. Talc powder formed a dense layer covering the oil surface, which effectively isolated the oil from the air.

Keywords: flame retardancy, talc, composite foams, stability, mechanism

OPEN ACCESS

Edited by:
Anthony Chun Yin Yuen, University of New South Wales, Australia

Reviewed by:
Hu Long, University of New South Wales, Australia
Richard Kwok Kit Yuen, City University of Hong Kong, Hong Kong

***Correspondence:**
Xiujuan Li
leely78@163.com
Ruisong Guo
rsguo@tju.edu.cn
Xiaodong Qian
wjxyqxd@hotmail.com

Specialty section:
This article was submitted to Polymeric and Composite Materials, a section of the journal Frontiers in Materials

Received: *31 January 2021*
Accepted: *16 February 2021*
Published: *19 March 2021*

Citation:
Li X, Guo R and Qian X (2021) Study on Flame Retardancy and Mechanism of Talc Composite Foams. Front. Mater. 8:661906. doi: 10.3389/fmats.2021.661906

INTRODUCTION

Talc is used mainly in medicine, cosmetics, ceramics, paper making, coatings, wires and cables, and various chemical industries (Liu et al., 2020; Nair and Sairam, 2021). The main component of talc is hydrous magnesium silicate, the molecular formula is Mg_3 $[Si_4O_{10}]$ $(OH)_2$, and the density is 2.7 ~ 2.80 g/cm^3. Talc belongs to monoclinic system, and the crystal is in the shape of pseudo hexagonal or rhombic flake. Talc is a layered silicate mineral with water content of 2:1. Each crystal layer is composed of two layers of Si-O tetrahedron sandwiched with a layer of Mg-O (O-H) octahedron. In its lattice structure, the Si-O tetrahedron is connected into layers to form a continuous hexagonal network layer with active oxygen facing one side, and then the active oxygen of each hexagonal network layer is facing each other through a layer of "magnesium hydroxide" layer. Aqueous film forming foam is considered to be the best oil fire extinguishing agent. But the foam formed by aqueous film forming foam is not stable. The sealing time to oil surface and the reburning time are relatively short. The performance in isolating hot liquid and reburning resistance is poor (Wang, 2014; Zhao, 2014). The researches show that foam with particles has significantly improved stability (Alargova et al., 2004; Horozov, 2008; Mohamedi et al., 2012; Shi et al., 2019). Talc was considered to be added into aqueous film forming foam. The flame retardancy and mechanism of talc composite foams should be studied.

EXPERIMENT

Material Preparation

Talc particles had an average diameter of 15 μm. It was produced by Shanghai Chuangyu Chemical Co., Ltd. The aqueous film forming foam was produced by Hebei Langfang Rongshun Co., Ltd.

Testing Methodology

Fire resistance and fire extinguishing performance are important properties of fire extinguishing agent. In order to evaluate the performance of composite foam with talc, flame retardant experiments and fire extinguishing test were carried out. The viscosity and drainage time of the composite foam were measured, so as to study the effect of talc on the flame retardancy and fire extinguishing of the foam.

Measurement of Flame Retardancy

The talc of 0, 10, 20, 30, 40, 50 and 60 g were added into the 100 ml aqueous film forming foam respectively and the composite foam was prepared by Waring- Blender method.

3,000 ml water was poured into the bottom of an oil pan. After the liquid level was stationary, 300 ml gasoline and 2000 ml composite foam were poured onto the oil surface. A steel anti burning pot was put in the middle of the oil pan and filled up with the gasoline (about 100 ml). The liquid level and the oil pan's liquid level were kept on the same level surface. The composite foam should be kept in the oil pan and not enter the anti burning pot. The timing started from igniting the oil in the anti burning tank and stopped when the oil pan was fully on fire. This period was recorded as the anti burning time which was expressed by t_c. When talc was added into the foam to form composite foam, there might be a self extinguishment of the gasoline in the anti burning tank, while the oil pan surface had never been burned. In this case, the time of self extinguishment of the gasoline in the anti burning tank was recorded as t_c.

Measurement of Fire Extinguishing Performance

In order to study the fire extinguishing performance of the composite foam, the experiment was carried out in the indoor fire experimental platform of the building fire extinguishing facility laboratory, the experimental platform size was 3.0 m × 2.8 m × 2.8 m. In the middle of the experimental platform, place 0.4 m × 0.4 m empty oil pan, add 2000 ml water into the oil pan, add 300 ml gasoline, fill 3,000 ml composite foam (c = 30 g/100 ml) to the fire extinguishing device, spray out composite foam by means of nitrogen pressure, ignite gasoline with an igniter, and wait 45 s for pre-burning. Start the foam spraying device at 2 m far away, spray the composite foam until the flame goes out, and record the fire extinguishing time.

Measurement of Foam Viscosity

Considering that the performance of composite foam was related to the viscosity of composite foam, the viscosity was measured by using a Stormer viscosimeter. The experimental methods were as follows: composite foam with talc was poured into the measuring cup. When the foam height was about 10 mm from the measuring cup, it stopped. A measuring cup with talc was placed on the container seat and the lifting handle was pressed down. The stirring blade was immersed in the foam and the marking line of the impeller shaft was aligned with the liquid level. At this point, the impeller immediately rotated, the viscosity value on the display was recorded after 10 s. After the measurement finished, the lifting handle was lifted up to the height.

Determination of Liquid Separation Time

At room temperature, 100 ml of 6% AFFF solution with distilled water was prepared. talc and the mixed solution were blended and poured into the Waring- Blender stirring cup. The composite foam was obtained by stirring at 5 min at a speed of 3,000 r/min. The generated foam was poured into the 1,000 ml measuring cylinder placed in a constant temperature water bath pot at 25°C. Time started from the pouring. When the bottom of the equivalent cylinder was 15, 25 and 50 ml, time stopped. The time was expressed respectively by t_{15}, t_{25} and $t_{50\%}$.

RESULTS AND DISCUSSION

Flame Retardancy of Talc Composite Foams

Fire Resistance

Fire resistance was an important performance of composite foam (Shi et al., 2020). The talc were added into the 100 ml aqueous film forming foam and blended. The mixture was poured into Waring-Blender cup. In the Blender mixing cup, composite foam was obtained at a speed of 3,000 r/min for 5 min. The fire resistance test of the composite foam containing talc was carried out.

In the experiment, the fire resistance test of composite foam containing talcum powder was carried out. The burning of gasoline in the burning tank caused the foam temperature rising around the anti burning tank. Under the action of thermal shock, the most recent foam near the burning tank was rapidly ruptured and could not completely cover the oil surface. The gap in the foam and the fire of the oil pan expanded. Suddenly, the flame ignited the oil of the oil pan edge. Finally, with the complete rupture of the foam, the oil pan was fully ignited, as shown in **Figure 1**. However, because the viscosity of the composite foam containing talcum powder was low, the foam would quickly replenish and completely cover the gasoline in the oil pan and not easy to ignite.

Table 1 showed the experimental results of firing resistance of composite foam with different concentration of talc. From **Table 1**, it can be seen that the aqueous film forming foam had relatively low burning resistance, and loses its resistance to combustion at about 15.9 min, resulting in the full ignition of the oil pan. The talc enhanced significantly the fire resistance of foam. With the increase of concentration of talc, the fire resistance performance of composite foam increased gradually. When the concentration of talc was 10 g/100 ml, the burning resistance time was about 20.3 min, which was extended by about 4.4 min. When the concentration of talc was 30 g/100 ml, the ignition time was

FIGURE 1 | Burn resistant experiment **(A)** gasoline ignited in fire resisting pot; **(B)** gasoline ignited in oil pan; **(C)** oil pan full of fire.

TABLE 1 | Fire resistance performance test results of composite foam with different concentration talc particles.

Concentration (g/100 ml)	**0.00**	**10.00**	**20.00**	**30.00**	**40.00**	**50.00**	**60.00**
Fire resisting pot	Ignition	Ignition	Ignition	Ignition	Self-extinguishing	Self-extinguishing	Self-extinguishing
Resistance time (min)	15.9	20.3	23.6	25.5	51.5	52.3	51.2

increased by about 9.6 min, reaching 25.5 min. And when the concentration of talc reaches 40 g/100 ml, the oil burning in the anti burning tank did not ignite the gasoline in the oil pan and burned out at 51.5 min.

During the experiment, it was found that the complementarity of talc composite foams was very good because the viscosity of the composite foam containing talcum powder was low. When the foam around the tank was damaged, it could be replenished in time. Thus the anti burning property of the foam was enhanced. During the experiment, it was found that the composite foam with talc formed a strong compact layer on the oil surface, which was conducive to the complete coverage of the oil surface.

Fire Extinguishing Performance

After adding talc, the stability and fire resistance of composite foam were significantly improved. The fire extinguishing experiment was carried out with composite foam containing talc, as shown in **Figure 2**.

The whole process of flame combustion and extinction can be seen from **Figure 2**. **Figure 2A** was the photo when gasoline ignites. After 45 s of pre-combustion, the oil in the oil pan was fully burned, as shown in **Figure 2B**. At this time, the foam was sprayed and time was recorded as 0 s. The fire was basically controlled after injection for 20 s, as shown in **Figure 2C**. The oil fire was completely extinguished after 28 s. It can be seen that the addition of talc was beneficial to the improvement of fire extinguishing performance of composite foam. The foam formed with talc particles form a strong surface layer covering the surface of the fuel and effectively prevents the fuel vapor from air.

Flame-Retardant Mechanism of Talc Composite Foam

Composite Foam Viscosity

Figure 3 showed the viscosity of talc composite foam. The viscosity of the foam without adding talc was 0.076 Pa s. The viscosity of the composite foam with talc of 20 g/100 ml was 0.088 Pa s, while the viscosity of the composite foam with talc of 60 g/100 ml was 0.189 Pa s.

The effect of viscosity on the stability of composite foam containing talc was mainly because that the increasing viscosity was helpful to slow the drainage and thinning of liquid membrane (Koehler et al., 2000; Carn et al., 2009; Long et al., 2016). Excessive viscous resistance hindered the free flow of liquid (Preval et al., 2014). Meanwhile, the channel of liquid precipitation was complex because the size of talc was very small. The prolongation of precipitation path made the time of liquid evolution of composite foam longer. **Figure 4** showed the effect of the viscosity of composite foam on the time of liquid phase separation of talc composite foam. It can be seen from **Figure 4** that the greater the viscosity of the system was, the longer the time of the liquid phase of the composite foam was, and the higher the stability of foam. The viscosity of the foam without adding talc was 0.076 Pa s. At this time, the 15% liquid separating time and the 25% liquid separating time of the foam were 6.4 and 7.9 min respectively. The viscosity of the foam increased after adding talc. When the viscosity was 0.088 Pa s, the 15% liquid separating time and 25% liquid separating time of the foam increase rapidly, which is 8.4 and 11.8 min respectively. The viscosity of the foam increased with the increasing concentration of talc, and the time of liquid separation was lengthened.

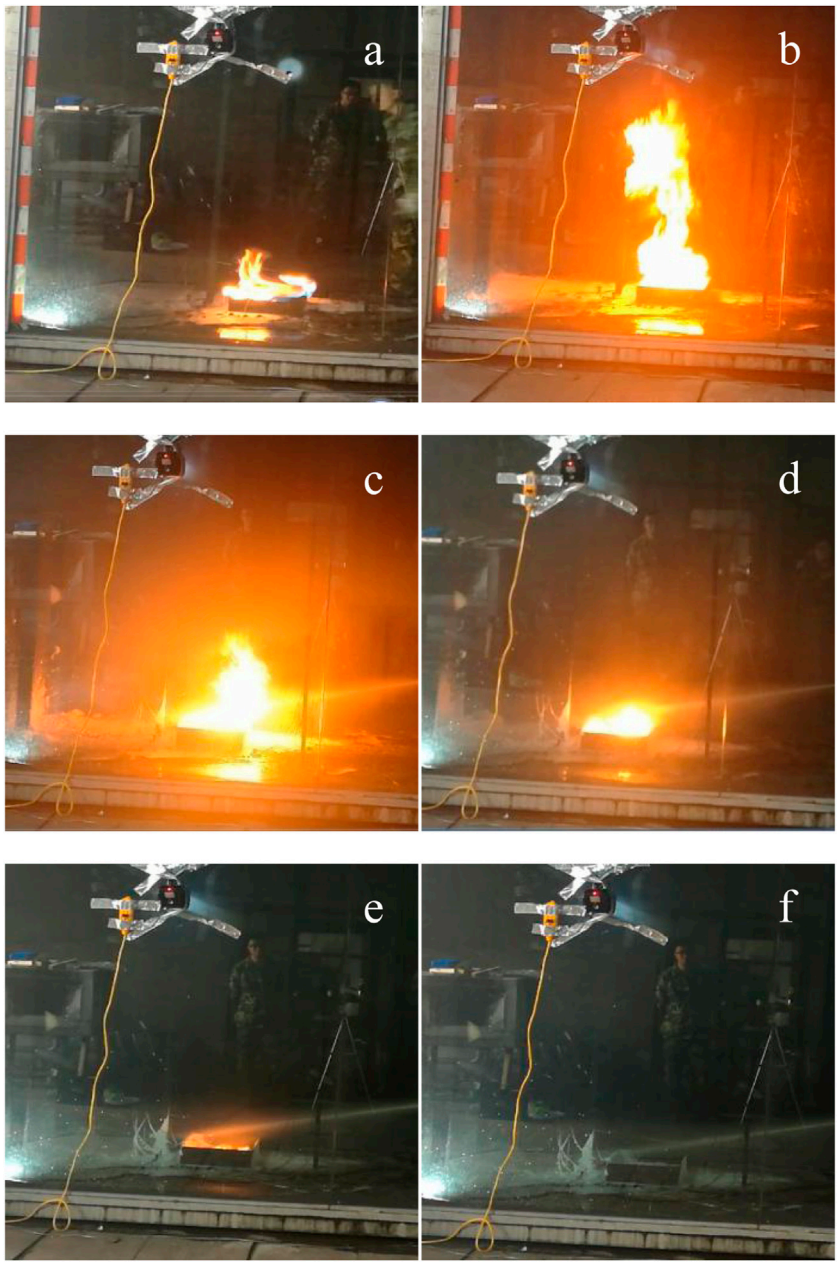

FIGURE 2 | Fire-fighting test with composite foam **(A)** ignite; **(B)** t = 0 s; **(C)** t = 20 s; **(D)** t = 24 s; **(E)** t = 26 s; **(F)** t = 28 s.

When the viscosity of the composite foam reached 0.189 Pa s, the 15% liquid separation time and 25% liquid separation time of the foam reach 13.2 and 18.2 min. The time of the 50% liquid separation time of the composite foam containing talc was greater than that free of talc. The time of the liquid decomposition of the foam without adding talc was 9.4 min. When the addition of talc increased with the viscosity of the composite foam, the dissolution time increased rapidly. When the viscosity was 0.088 Pa s, the 50% liquid precipitation time of the foam increased to 15.4 min. And when the viscosity of the composite foam reached 0.189 Pa s, the 50% liquid separation time of foam increased to 31.3 min.

The effect of viscosity on the stability of the composite foam containing talc was mainly due to the increase of viscosity, which can retard the drainage and thinning of the liquid membrane. The excessive viscous resistance hindered the free flow of the liquid. Meanwhile, the talc size was smaller, the amount of talc powder was more, the liquid outlet channel was more complex and the precipitation path were long, which would lead to the slowing down of the liquid separation process.

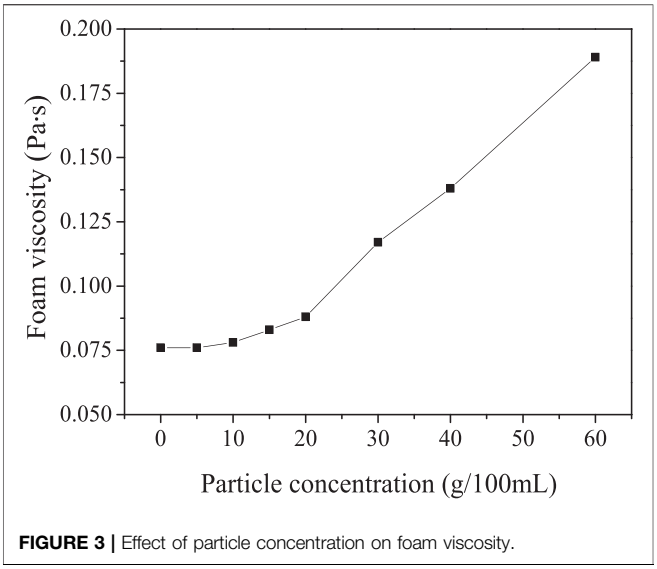

FIGURE 3 | Effect of particle concentration on foam viscosity.

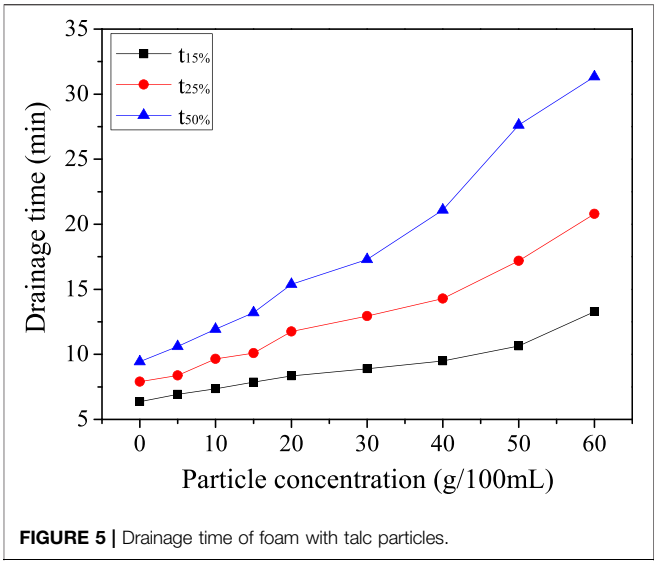

FIGURE 5 | Drainage time of foam with talc particles.

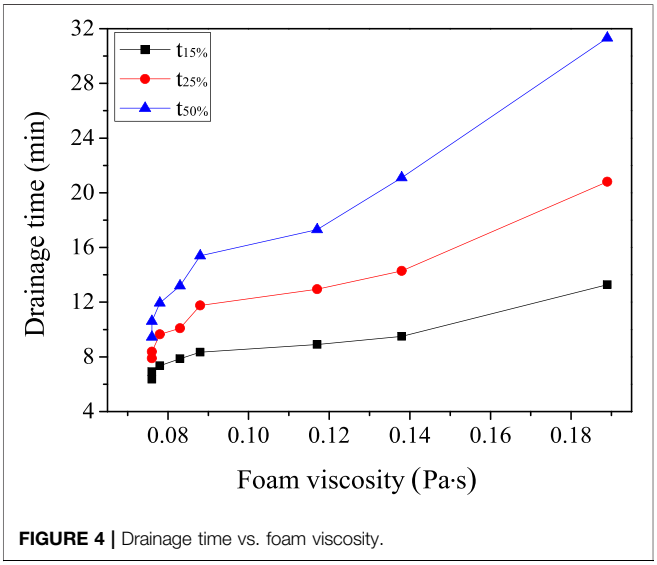

FIGURE 4 | Drainage time vs. foam viscosity.

Liquid Separation Process of Talc Composite Foam

The influence of talc concentration on the whole liquid separation process of the composite foam was studied. The results were shown in **Figure 5**.

As can be seen from **Figure 5**, for the foam solution without talcum powder, the rate of liquid dissolution was very fast. 15% of the liquid precipitated in 6.4 min and 25% of the liquid precipitated in 7.9 min. 50% of the liquid gave off in 9.4 min and finally almost liquid completely precipitated. The foam became very fragile and easily damaged. When the talcum powder was added, the time of liquid separation was prolonged significantly. With the increasing of talc concentration, the rate of liquid dissolution was slower and slower. When talcum powder concentration was 30 g/100 ml, liquid precipitated 15 and 25% in 8.9 and 13 min respectively. But 50% of the liquid precipitated in 17.3 min, which was longer than that of the foam without talcum powder. When the talcum powder concentration was 40 g/100 ml, the time of t_{15}, t_{25} and $t_{50\%}$ was 9.5, 14.3 and 21.1 min respectively. The liquid precipitation rate had become very slow, the composite foam was very stable.

As can be seen from **Figure 5**, the addition of flaky talcum powder had an obvious effect on the rate of liquid separation in the later stage of foaming. Free water released at the beginning of the foaming stage and the rate of liquid dissolution was faster at that time. When the gravitational precipitation was completed, the Plateau discharge took the lead. The time of the dissolution increased with the increasing of talc concentration. The results showed that the 50% liquid separation time of foam without talc was less than 10.0 min. When 30.00 g/100 ml talc powder was added, the 50% liquid separation time was 17.3 min. When the concentration of talc was 40.00 g/100 ml, the 50% liquid separation time was 21.1 min. When the talc content was 60.00 g/100 ml, the 50% liquid separation time reached 31.3 min.

When the viscosity of the foam system was small, the effect on the liquid precipitation was small, so the process of liquid precipitation was faster. When the concentration of talc was high, the viscosity of the foam system was high, the foam structure was complex, and the liquid precipitation channel was prolonged (Stevenson, 2006; Subramaniam et al., 2006). The precipitation time of the first 50% water was prolonged under the action of gravity, but it was not obvious, while the capillary water precipitates under the action of Laplasse. Therefore, if we need to control the time of the liquid phase of the composite foam, we should adjust it from the factors that affect the liquid phase in the later stage.

Talc Composite Foam Structure

The effect of foam structure on foam stability was also very obvious (Stocco et al., 2011; Fameau and Salonen, 2014). The complex network structure included the network structure of the entire foam system and the network structure of interwoven in the liquid film (Aveyard et al., 1994; Al-Qararah et al., 2012; Pang et al., 2018).

In the process of talc composite foam, the bubbles always were spherical structure. The complete surface of the spherical bubbles

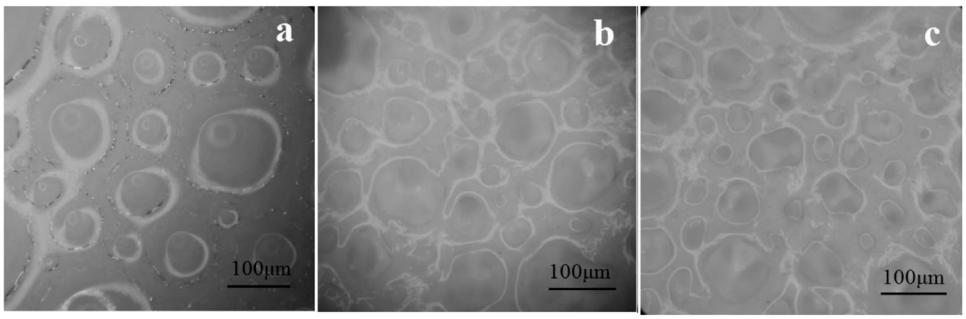

FIGURE 6 | Optical microscopic images of talcum powder in foam **(A)** 5.00 g/100 ml; **(B)** 20.00 g/100 ml; **(C)** 40.00 g/100 ml).

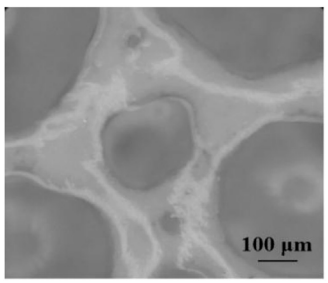

FIGURE 7 | Optical microscopic image of talcum powder in film.

and the aggregation of a large number of spherical bubbles caused the rate of liquid dissolution to slow down. The talc particles gathered at the intersection of the liquid membrane and the liquid membrane, and effectively inhibited the coarsening of the bubbles. Even though most of the liquid had been precipitated, the bubbles still maintained a regular spherical structure. It was surrounded by a shell and was not easy to deform.

The micro-structure of composite foam containing talc powder with different concentrations was observed by an optical microscope. **Figure 6** was a distribution optical microscopic picture of composite foam with different concentrations of talcum powder. The micro-structure of composite foam when talcum powder concentration was 5 g/100 ml was similar to the micro-structure of foam without talcum powder. The liquid foam still occupied the main body of the whole system. The liquid precipitated rapidly under the action of gravity. The speed of coarsening and coalescence of bubbles was very fast and the deformation of bubbles was serious. From **Figure 6**, talcum powder can be seen to gather in the liquid film between the bubbles when the concentration of talcum powder was 20.00 g/100 ml. However, due to less talcum powder in the liquid film, the liquid film was easily affected when the bubbles deform, resulting in more serious deformation of the bubbles.

When the concentration of talc was 40.00 g/100 ml, a large amount of talc powder accumulated in the liquid film, which made the liquid film very thick. The bubble size decreased and the number of bubbles increased. The aggregation of talc powder in the liquid film between bubbles formed a hard shell to protect bubbles, as shown in **Figure 7**. The hindrance between these hard shells obstructed the coalescence of bubbles (Barik and Roy, 2009; Politova et al., 2018). During the whole observation process, the shape of these bubbles remained unchanged and they were not easy to break. The hard shell inhibited the gas diffusion between bubbles and improved the stability of the composite foams.

CONCLUSION

Talc composite foams had good fire resistance. When the concentration of talc was 40.00 g/100 ml, the oil in the burning tank was extinguished without burning the oil in the oil pan. It was closely related to the structure of the composite foams. The accumulation of talc powder in the liquid film between bubbles was very obvious. The liquid film was very thick because of a large amount of talc powder in the liquid film. The bubble size decreased and the number of bubbles increased. The accumulation of talc powder in the liquid film between bubbles formed a hard shell to protect bubbles, and the separation layer formed on the fuel surface was more compact. The talc composite foams could prevent the fuel in the fire-resistant tank from igniting the oil pan when the concentration of talc powder reached 40.00 g/100 ml.

DATA AVAILABILITY STATEMENT

The original contributions presented in the study are included in the article/Supplementary Material, further inquiries can be directed to the corresponding author.

AUTHOR CONTRIBUTIONS

All authors listed have made a substantial, direct, and intellectual contribution to the work and approved it for publication.

FUNDING

National Natural Science Foundation of China (No. 21704111); Cultivation Project of National Natural Science Foundation of China (No. ZKJJPY201714).

REFERENCES

Al-Qararah, A. M., Hjelt, T., Kinnunen, K., Beletski, N., and Ketoja, J. (2012). Exceptional pore size distribution in foam-formed fiber networks. *Nordic Pulp Paper Res. J.* 27, 226–230. doi:10.3183/npprj-2012-27-02-p226-230

Alargova, R. G., Warhadpande, D. S., Paunov, V. N., and Velev, O. D. (2004). Foam superstabilization by polymer microrods. *Langmuir* 20 (24), 10371–10374. doi:10.1021/la048647a

Aveyard, R., Binks, B. P., Fletcher, P. D. I., Peck, T. G., and Rutherford, C. E. (1994). Aspects of aqueous foam stability in the presence of hydrocarbon oils and solid particles, *Adv. Colloid Interf. Sci.* 48,93–120. doi:10.1016/0001-8686(94)80005-7

Barik, T. K., and Roy, A. (2009). Statistical distribution of bubble size in wet foam. *Chem. Eng. Sci.* 64, 2039–2043. doi:10.1016/j.ces.2009.01.039

Carn, F., Colin, A., Pitois, O., Vignes-Adler, M., and Backov, R. (2009). Foam drainage in the presence of nanoparticle—surfactant mixtures. *Langmuir* 25, 7847–7856. doi:10.1021/la900414q

Fameau, A. L., and Salonen, A. (2014). Effect of particles and aggregated structures on the foam stability and aging. *C.R. Physique* 15, 748–760. doi:10.1016/j.crhy.2014.09.009

Horozov, T. S. (2008). Foams and foam films stabilised by solid particles. *Curr. Opin. Colloid Interf. Sci* 13, 134–140. doi:10.1016/j.cocis.2007.11.009

Koehler, S. A., Hilgenfeldt, S., and Stone, H. A. (2000). A generalized view of foam drainage: experiment and theory. *Langmuir* 16, 6327–6341. doi:10.1021/la9913147

Liu, C., Wu, W., Shi, Y., Yang, F., Liu, M., Chen, Z., et al. (2020). Creating MXene/reduced graphene oxide hybrid towards highly fire safe thermoplastic polyurethane nanocomposites. *Composites B* 203, 108486. doi:10.1016/j.compositesb.2020.108486

Long, X., Sha, R., Meng, Q., and Zhang, G. (2016). Mechanism study on the severe foaming of rhamnolipid in fermentation. *J. Surfact Deterg* 19, 833–840. doi:10.1007/s11743-016-1829-4

Mohamedi, G., Azmin, M., Pastoriza-Santos, I., Huang, V., Pérez-Juste, J., Liz-Marzán, L. M., et al. (2012). Effects of gold nanoparticles on the stability of microbubbles. *Langmuir* 28, 13808–13815. doi:10.1021/la302674g

Nair, N. A., and Sairam, V. (2021). Research initiatives on the influence of calcium silicate in cement-based construction material-A review. *J. Clean. Prod.* 283, 124665. doi:10.1016/j.jclepro.2020.124665

Pang, X. Y., Singh, J., and Jimenez, W. C. (2018). Characterizing gas bubble size distribution of laboratory foamed cement using X-ray micro-CT. *Constr Build Mater.* 167, 243–252. doi:10.1016/j.conbuildmat.2018.02.030

Politova, N., Tcholakova, S., Valkova, Z., Golemanov, K., and Denkov, N. D. (2018). Self-regulation of foam volume and bubble size during foaming via shear Mixing. *Colloids Surf. A: Physicochem. Eng. Asp.* 539, 18–28. doi:10.1016/j.colsurfa.2017.12.006

Preval, E. S. D., Fabrice, D., and Gilles, M. (2014). Influence of surface properties and bulk viscosity on bubble size prediction during foaming operation. *Colloids Surf. A: Physicochem. Eng. Asp.* 442, 88–97.

Shi, Y. Q., Liu, C., Duan, Z. P., Yu, B., Liu, M., and Song, P. (2020). Interface engineering of MXene towards super-tough and strong polymer nanocomposites with high ductility and excellent fire safety. *Chem. Eng. J.* 399, 125829. doi:10.1016/j.cej.2020.125829

Shi, Y. Q., Liu, C., Liu, L., Fu, L., Yu, B., Lv, Y., et al. (2019). Strengthening, toughing and thermally stable ultra-thin MXene nanosheets/polypropylene nanocomposites via nanoconfinement. *Chem. Eng. J.* 378, 122267. doi:10.1016/j.cej.2019.122267

Stevenson, P. (2006). Dimensional analysis of foam drainage. *Chem. Eng. Sci.* 61, 4503–4510. doi:10.1016/j.ces.2006.02.026

Stocco, A., Garcia-Moreno, F., Manke, I., Banhart, J., and Langevin, D. (2011). Particle-stabilised foams: structure and aging. *Soft Matter* 7, 631–637. doi:10.1039/c0sm00166j

Subramaniam, A. B., Mejean, C., Abkarian, M., and Stone, H. A. (2006). Microstructure, morphology, and lifetime of armored bubbles exposed to surfactants. *Langmuir* 22, 5986–5990. doi:10.1021/la060388x

Wang, B. Q. (2014). Study on the cause of oil tank fire and fire prevention countermeasure. *Adv. Mater. Res.* 864–867, 866–870. doi:10.4028/www.scientific.net/amr.864-867.866

Zhao, B. (2014). Radiation thermal transfer of the LPG tank under the pool fire. *Eng* 8, 33–40. doi:10.2174/1872212107666131213224912

Conflict of Interest: The authors declare that the research was conducted in the absence of any commercial or financial relationships that could be construed as a potential conflict of interest.

frontiers in Materials

ORIGINAL RESEARCH
published: 22 March 2021
doi: 10.3389/fmats.2021.646509

Preparation and Absorption Carbon Monoxide Properties of a Novel Flame Retardants Based Fire-Fighting Foam

Xiujuan Li[1,2]*, *Ruisong Guo*[1]* and *Xiaodong Qian*[2]*

[1]Key Laboratory of Advanced Ceramics and Machining Technology of Ministry of Education, School of Materials Science and Engineering, Tianjin University, Tianjin, China, [2]School of Criminal Investigation, China People's Police University, Langfang, China

The toxicity of CO threatens the life of people in the fire site. In this study, flame retardants of nano magnesium hydroxide particles and water-soluble flame retardant 8124 are used to be mixed into the aqueous film forming fire extinguishing agent (AFFF). Smoke-suppressed fire extinguishing agent was prepared in Waring-Blender mixing cup and then stirred at 3,000 r/min for 5 min. The new extinguishing agent shows a good performance of absorption of CO and reducing the flue gas temperature. The concentration of CO was decreased below 131 ppm and flue gas temperature was basically kept below 40°C, which was 367 ppm and 83.1°C less than that in free-fire. Using new extinguishing agent can effectively reduce the harm to the trapped personnel and firemen in the fire site. It was of great significance. The harm of CO concentration below 131 ppm and flue gas temperature below 40°C was low. The time to reach the maximum CO concentration and the maximum flue gas temperature was delayed, which ensures that people have more time to escape. Even if there was not enough time to escape, people will not be seriously threatened.

Keywords: flame retardant, CO concentration, fire risk, magnesium hydroxide, flue gas

OPEN ACCESS

Edited by:
Yongqian Shi,
Fuzhou University, China

Reviewed by:
Xin-xiao Lu,
China University of Mining and Technology, China
Siqi Huo,
Wuhan Institute of Technology, China
Gongqing Chen,
Wuhan University of Technology, China
Weiyi Xing,
University of Science and Technology of China, China

***Correspondence:**
Xiujuan Li
leely78@163.com
Ruisong Guo
rsguo@tju.edu.cn
Xiaodong Qian
wjxyqxd@hotmail.com

Specialty section:
This article was submitted to Polymeric and Composite Materials, a section of the journal Frontiers in Materials

Received: *27 December 2020*
Accepted: *08 February 2021*
Published: *22 March 2021*

Citation:
Li X, Guo R and Qian X (2021) Preparation and Absorption Carbon Monoxide Properties of a Novel Flame Retardants Based Fire-Fighting Foam. Front. Mater. 8:646509. doi: 10.3389/fmats.2021.646509

INTRODUCTION

The fire typical gas carbon monoxide (CO), which can cause loss of human life, is unavoidable during combustion of fuels. It is the most lethal component of the toxic smoke (Zhao, 2012; Hampson et al., 2019). Toxic gas has brought great difficulties to personnel evacuation and fire fighting (Liu et al., 2020). Some researches indicated that myocardial infarction was associated with exposure to ambient carbon monoxide (Lee et al., 2020). Altered regional homogeneity in delayed encephalopathy, which is manifested as local brain dysfunctions, will be found after carbon monoxide poisoning (Wu et al., 2020). Reducing CO concentration and temperature of flue gas in fire site is the key to save the life of people (Zarca et al., 2015; Qiu et al., 2019; Shi et al., 2020). Therefore, it is important to develop new fire extinguishing agents for improving the CO emission inhibition performance.

Smoke suppression flame retardants have been widely used in wire and cable, indoor building decoration materials and engineering plastics (Sain et al., 2004; Tang et al., 2013; Shan et al., 2020). Therefore, smoke suppressive flame retardants are considered to be added into foam extinguishing agent. Researchers believe that solid particles can improve the stability and fire efficiency of fire foam (Xie et al., 2011; Jiang et al., 2016). Superfine magnesium hydroxide flame retardant has the advantages of low price, low toxicity, good smoke elimination and less dripping (Kuang et al., 2008; Lu et al., 2018). It shows excellent performance in smoke suppression and flame retardant, which is the result of physical and chemical actions. The superfine magnesium hydroxide powder has a great

FIGURE 1 | Free-burning experiment.

improvement in fire extinguishing efficiency compared with ordinary ammonium phosphate powder because of its large specific surface area, high activity, fast decomposition speed and strong ability to capture free radicals when heated (Wang et al., 2009). A large amount of water vapor released during the decomposition process can not only reduce the actual temperature of the flame, but also dilute the concentration of oxygen and combustible gas near the flame.

EXPERIMENTAL

Materials

The aqueous film forming fire extinguishing agent (AFFF) used in the experiment was produced by Hebei Langfang Rongshun Fire-fighting Pharmaceutical Co., Ltd. Both nano magnesium hydroxide particles and water-soluble flame retardant 8124 are produced by Shandong Weifang Wanfeng New Material Science and Technology Co., Ltd. Nano magnesium hydroxide particles can be used as flame retardant or powder fire extinguishing agent. The water-soluble flame retardant 8124 is white water-soluble powder, which is easy to dissolve in water and dosen't contain Nitrogen element that is harmful to the environment. It is an environmentally friendly flame retardant with properties of non decomposition, no smell, flame retardant and smoke suppression because it does not contain halogen, heavy metal and other prohibited components.

Specimen Processing

We prepared 100 ml solution containing 6% AFFF and 94% distilled water at room temperature. 10, 20, and 30 g nano magnesium hydroxide solid particles or a water-soluble flame retardant 8124 were added to the solution in order to study the effect of nano magnesium hydroxide solid particles and water-soluble flame retardant 8124 on the performance of fire extinguishing foam. The mixture was poured into Waring-Blender mixing cup and then stirred at 3,000 r/min for 5 min.

Test Methods

A small oil pan with a diameter of 10 cm was placed at the bottom of the cylindrical container with the diameter of 30 cm. 20 ml of gasoline was poured into the oil pan with a measuring cylinder. Xima carbon monoxide meter [(0~1,000) ppm, ±10%, AS8700A, Shanghai Baoxin Instrument Co., Ltd.] which was fixed with an iron stand was 50 cm above the top of the cylindrical container. The detection port of the portable CO concentration meter was facing down and the instrument switch was opened for preparation. The CO concentration and flue gas temperature during the experiment were recorded by a camera fixed in front of the CO meter. Ignited the gasoline in the oil pan with the igniter, covered the circular filter screen with a diameter of 40 cm, and started timing with the stopwatch.

RESULTS AND DISCUSSION

CO Concentration in Free-Burning Test and by AFFF Foam

In order to compare the effect of AFFF foam with different flame retardants, a blank experiment of free-burning was carried out, as shown in **Figure 1**. A lot of CO was produced during the experiment. The CO concentration and flue gas temperature were obtained. The results are as shown in **Figure 2**. It was shown that CO concentration and flue gas temperature increases significantly in free-burning. Flue gas temperature begins to increase after about burning for 8 s and reaches 123.1°C at 41 s, which was the maximum temperature. The release of CO starts at 14s and the concentration of CO reaches the largest at 48 s. There was a lot of CO released in the whole process. The highest CO concentration was 498 ppm. It was believed that it was harmful if CO concentration was over 24 ppm. Therefore, it was dangerous for people to exposure to high temperature and high CO concentration.

After igniting the gasoline in the oil pan, AFFF foam was covered on the circular filter screen. The smoke passed through AFFF foam. CO was probably absorbed during the process. **Figure 3** was the absorption of CO by AFFF foam and

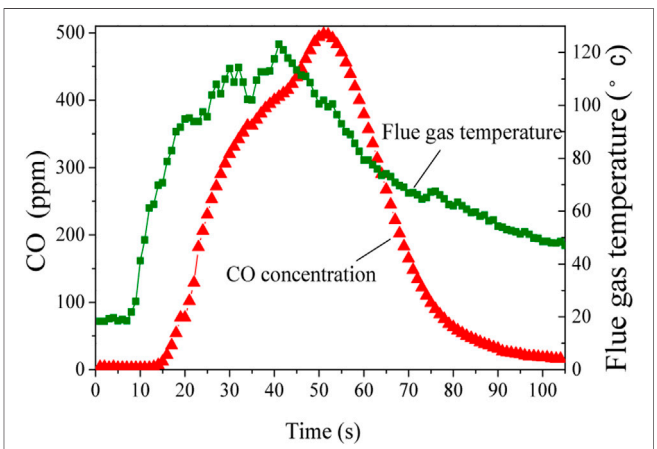

FIGURE 2 | CO concentration and flue gas temperature of free-burning.

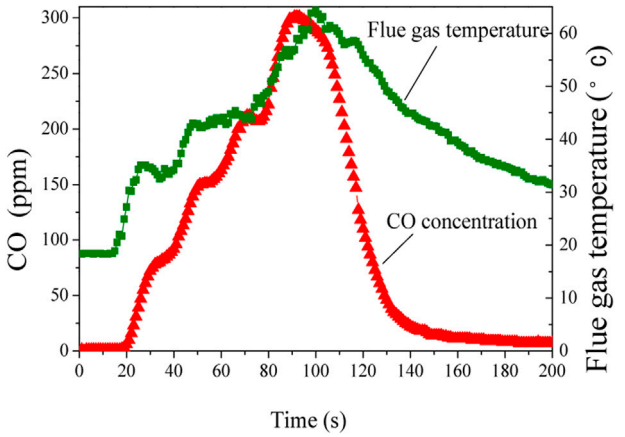

FIGURE 3 | CO concentration and flue gas temperature by using AFFF foam.

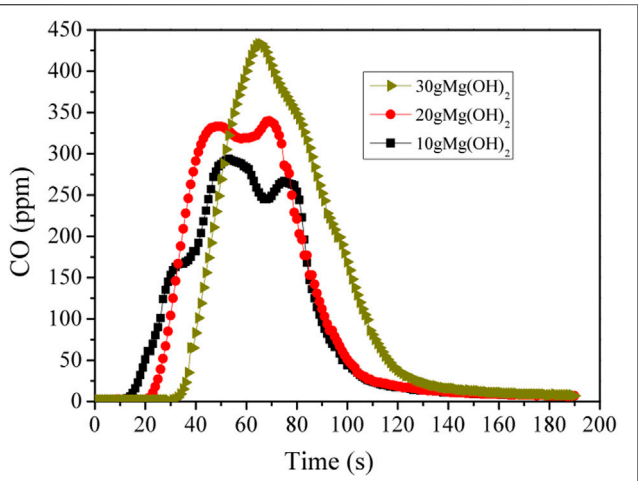

FIGURE 5 | CO concentration by using foam with $Mg(OH)_2$.

FIGURE 4 | AFFF foam in CO concentration determination experiment.

temperature curve. It can be seen from **Figure 3** that the CO concentration and the flue gas temperature decrease. The maximum CO concentration which was reduced to 301 ppm at 91 s was 197 ppm less than that of 498 ppm in **Figure 2**. And then the CO concentration decreases rapidly. The highest temperature of flue gas drops by 10°C from 123.1 to 64.3°C. It was clear that foam was helpful for reducing flue gas temperature and absorbing CO released. AFFF foam can lead the temperature decreased because that AFFF foam contains a certain amount of water. When the flue gas spreads through the foam, the moisture in the foam can effectively reduce the temperature of the flue gas. After 20 s, the fuel burned intensely and the CO released increased sharply. But the stability of AFFF foam was reduced after heating. Bubbles burst and AFFF foam gradually lost the ability of filtering smoke, as shown in **Figure 4**. With the rupture of AFFF foam, the CO concentration rapidly increased. The increased flame temperature accelerated the rupture of AFFF foam until the foam completely disappeared.

CO Absorbed by Foam With $Mg(OH)_2$

Magnesium hydroxide, with good smoke suppression performance, is widely used in flame retardant materials which can release very little toxic smoke in the process of polymer combustion (Ma et al., 2020). The outer combustion product area has the function of diluting and absorbing smoke, so the smoke suppression effect of $Mg(OH)_2$ is very obvious. Superfine magnesium hydroxide powder, which can be used as dry powder extinguishing agent, is easy to be suspended in the hot air around the flame when it is sprayed into the flame (Sener and Demirhan, 2008; Shi et al., 2019). That a large number of free radicals ·OH and H· in the flame are absorbed and transformed sharply reduces the number of free radicals and causes the chain reaction of combustion to break.

Nano magnesium hydroxide with the weight of 10, 20, and 30 g respectively were added to 100 ml AFFF foam extinguishing agent. The CO absorption experiment was also carried out and the concentration of CO was measured. **Figure 5** shows the CO concentration by using foam extinguishing agent containing different weight nano magnesium hydroxide.

As shown in **Figure 5**, the peak value of CO concentration decreases when nano magnesium hydroxide powders of 10 g/100 ml are added into AFFF foam extinguishing agent. The maximum concentration of CO was about 294 ppm, which happens at 43 s. Compared with the foam without adding magnesium hydroxide, the peak value decreased. It indicates that nano magnesium hydroxide plays a role on filtering and absorbing CO. The stability of foam with magnesium hydroxide increases and the bubbles dose not break easily (Li et al., 2004; Qin et al., 2005; Vijayaraghavan et al., 2006; Lü et al., 2016). The time required for the smoke to pass through the foam was prolonged. The thermal stability of $Mg(OH)_2$ was good.

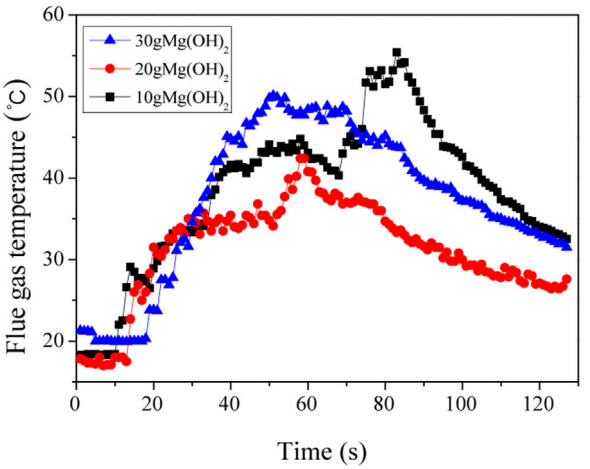

FIGURE 6 | The result of flue gas temperature by using foam with $Mg(OH)_2$.

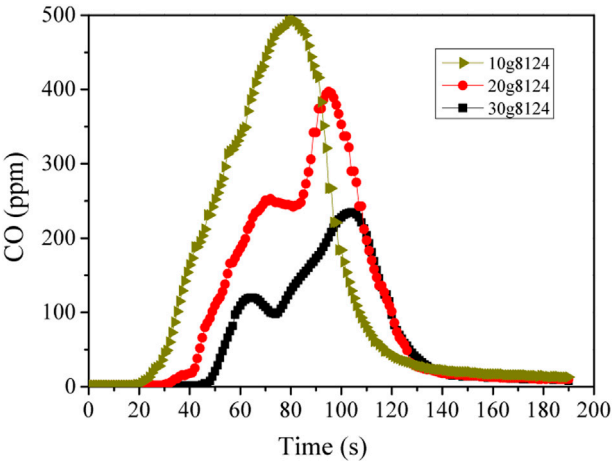

FIGURE 7 | CO concentration by using foam with 8124.

Nano magnesium hydroxide particles of 10 g/100 ml added in the foam are beneficial to reduce the CO release during fuel combustion. However, it was found that when the concentration of nano magnesium hydroxide increases, the role of reducing CO concentration will decrease. The foam with magnesium hydroxide particles of 20 g/100 ml was used for the determination of CO release. The peak value of CO concentration was 333 ppm at 48 s and 340 ppm at 69 s. When the concentration of magnesium hydroxide particles was 30 g/100 ml, the CO concentration reaches a peak value of 433 ppm at 65 s. The CO concentration was higher when adding 30 g $Mg(OH)_2$ particles than that of 10 g $Mg(OH)_2$ particles. It indicates that the foam with too much magnesium hydroxide particles has poor absorption performance on CO released. This may be related to the structure of the foam. When a small number of particles was added, the stability of the foam increases. The bubbles broken will be replenished by liquid surrounding them. But if the concentration of particles in the foam was large, the foam viscosity increases (Li, 2018). The fluidity of the foam was poor. Bubbles burst will be caused by high temperature during the heating process. The foam around can not move to repair the cracked bubbles and the films fails to absorb CO because bubbles burst fast.

Although the effect of foam with $Mg(OH)_2$ on absorption of CO released was not obvious, flue gas temperature decreases significantly. **Figure 6** depicts the measurement result of flue gas temperature. For an easier comparison, the results obtained show that there was a remarkable decline of flue gas temperature. It drops below 55°C. And it dose not exceed 45°C if $Mg(OH)_2$ concentration was 20 g/100 ml. Obviously, this temperature does little harm to people.

Absorption of CO by Foam With Flame Retardant 8124

Figure 7 was the CO concentration change curve by using foam with water-soluble flame retardant 8124.

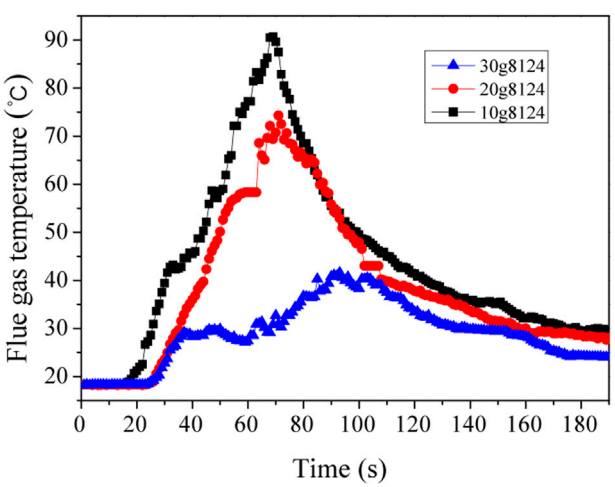

FIGURE 8 | The result of flue gas temperature by using foam with 8124.

The increase of flue gas temperature and the release of CO are delayed by using foam with 8124. And the concentration of water-soluble flame retardant 8124 has a remarkable influence on CO concentration as shown in **Figure 7**. The CO concentration increases sharply if the concentration of flame retardant 8124 was 10 g/100 ml and the peak value reaches to 495 ppm at 55 s. The maximum CO concentration reaches 495 ppm, which was similar to that in free-burning. But it decreases with the increase of the concentration of flame retardant 8124. The maximum CO concentration was 397 ppm of 20 g/100 ml and 235 ppm of 30 g/ 100 ml.

Water-soluble flame retardant 8124 of 30 g/100 ml was obvious contributed to reducing flue gas temperature, as shown in **Figure 8**. After 93 s it reaches the maximum temperature of 41.6°C which was safe for people. It's almost below 38°C during burning.

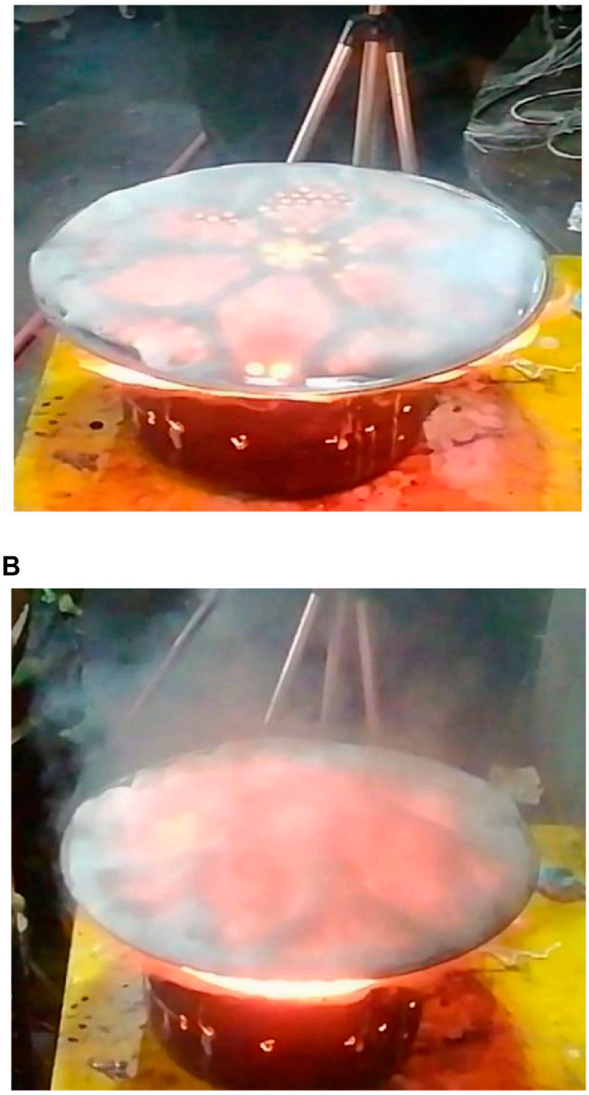

FIGURE 9 | Foam with 8124 **(A)** at 0 s; **(B)** at 24 s.

This phenomenon may be related to the stability of the liquid film when heated. Images are shown in **Figure 9**. When a certain amount of flame retardant 8124 was added, the burning-resistance ability of the liquid film under the high temperature action was improved. After local heating, the liquid film would form a bulge and was not easy to crack, as shown in **Figure 9B**. Flames and smoke will spread out from the outside of the filter screen, which shows that the liquid film has strong resistance to high temperature and good coverage effect to flame. It was only under the action of high temperature for a long time that the liquid film breaks down.

Carbon Monoxide Absorption Ability of Compound Foam

In order to study the performance of compound foam, several groups of composite experiments had bee done. The result was shown in **Figure 10**. The interaction of $Mg(OH)_2$ and 8124 is helpful to the inhibition and absorption of CO. It can be seen that the efficiency of compound foam was good when the concentration of $Mg(OH)_2$ and 8124 was high.

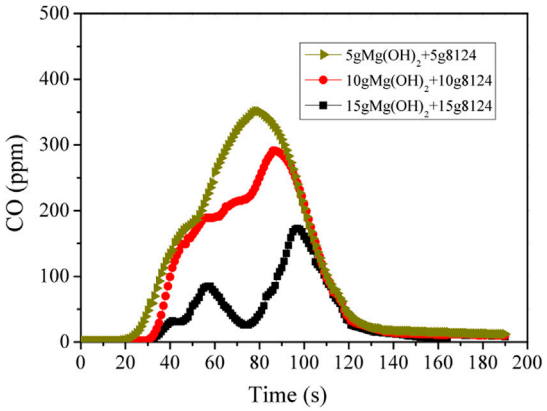

FIGURE 10 | CO concentration of compound foam with $Mg(OH)_2$ and 8124.

According to the above experimental results, appropriate amount of nano magnesium hydroxide or water-soluble flame retardants 8124 was beneficial to fire-fighting foam agents. When adding 20 g/100 ml magnesium hydroxide, a good extinguishing foam with good cooling effect was obtained. Foam with water-soluble flame retardants 8124 of 30 g/100 ml has good performance of absorption of CO and cooling effect. Therefore, the combination of nano magnesium hydroxide of 20 g/100 ml and water-soluble flame retardant 8124 of 30 g/100 ml are considered to be added into extinguishing agent foam. **Figure 11** shows CO concentration and flue gas temperature.

It can be seen from **Figure 11** that CO concentration only reaches 131 ppm at 91 s, which was the maximum. And it only lasts for 20 s when the concentration of CO exceeds 100 ppm. It was believed that when the concentration of CO in the

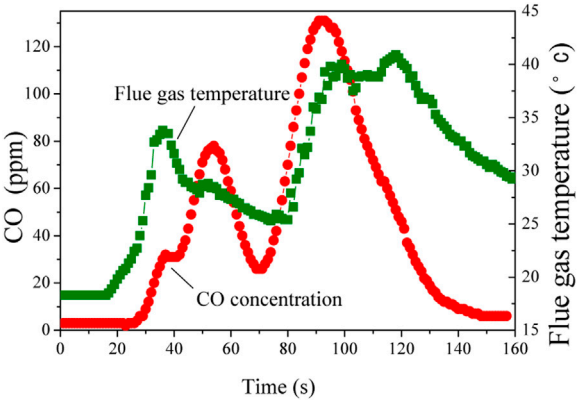

FIGURE 11 | CO concentration and flue gas temperature by using compound foam with nano magnesium hydroxide of 20 g/100 ml and water-soluble flame retardant 8124 of 30 g/100 ml.

FIGURE 12 | Composite foam extinguishing agent in CO concentration determination experiment.

environment exceeds 100 ppm (100×10^{-6}), the human body will have dizziness, fatigue and other discomfort. Therefore, it is safe for people that CO concentration is below 100 ppm (Dogan et al., 2019). During the whole process, it was only 9 s when the temperature exceeds 40°C. And the highest temperature was 40.9°C, then it rapidly decreases. After the oil pan fires, the foam covers on the filter net. Only a very small number of filter holes are burnt through, as shown in **Figure 12**.

The performance of compound foam formed by adding two kinds of flame retardants was the best. $Mg(OH)_2$ in the foam has good smoke suppression performance. Most of free radicals OH and H in the flame were absorbed and the chain reaction of combustion was broken. The adding of water-soluble flame retardant 8124 to AFFF foam can improve effectively the viscoelasticity of the foam. Therefore the compound foam was helpful in absorbing CO and reducing the flue gas temperature. The foam has strong toughness and the effect on inhibiting CO release was very good.

CONCLUSION

In view of the problem that CO release is likely to cause death in the case of fire, this study proposes to add flame retardant nano magnesium hydroxide and water-soluble flame retardant 8124 to AFFF water film foam extinguishing agent. The concentration of CO and flue gas temperature are significantly decreased. Composite foam extinguishing agent (6% AFFF + 20 g/100 ml $Mg(OH)_2$ + 30 g/100 ml 8124) exhibits excellent performance of inhibiting CO and reducing flue gas temperature. It can effectively reduce the harm of toxic smoke CO to the personnel at the site of fire, extinguish the fire efficiently, reduce the temperature of the fire site, and has a good application prospect.

DATA AVAILABILITY STATEMENT

The raw data supporting the conclusions of this article will be made available by the authors, without undue reservation.

AUTHOR CONTRIBUTIONS

RG designed experiments; LX carried out experiments; LX and QX analyzed experimental results. Attributed equally to the manuscript.

FUNDING

National Natural Science Foundation of China (No. 21704111); Cultivation Project of National Natural Science Foundation of China (No. ZKJJPY201714).

REFERENCES

Doğan, F. S., Güneysel, Ö., Gökdağ, E., Merve Güneş, M. D., and Selin Gamze Sümen, M. D. (2019). Demographic characteristics and delayed neurological sequelae risk factors in carbon monoxide poisoning. *Am. J. Emerg. Med.* 38 (12), 2552–2556. doi:10.1016/j.ajem.2019.12.037

Hampson, N. B., Hauschildt, K. L., Deru, K., and Weaver, L. K. (2019). Carbon monoxide poisonings in hotels and motels: the problem silently continues. *Prev. Med. Rep.* 16, 100975–100977. doi:10.1016/j.pmedr.2019.100975

Jiang, X. S., Zhai, Y., Feng, J., and Lu, K. (2016). Influence factors of the formation and stability of fire-fighting three–phase foam. *J. Logist. Eng. Univ.* 32 (02), 41–46. doi:10.3969/j.issn.1672-7843.2016.02.008

Kuang, K., Huang, X., and Liao, G. (2008). A comparison between superfine magnesium hydroxide powders and commercial dry powders on fire suppression effectiveness. *Process Saf. Environ. Prot.* 86 (3), 182–188. doi:10.1016/j.psep.2007.11.002

Lee, K. K., Spath, N., Miller, M. R., Mills, N. L., and Shah, A. S. V. (2020). Short-term exposure to carbon monoxide and myocardial infarction: a systematic review and meta-analysis. *Environ. Int.* 143, 105901–105910. doi:10.1016/j.envint.2020.105901

Li, X. J. (2018). Study on particle concentration effect on three-phase foam property. *J. Armed Police Aceade.* 10, 18–23. doi:10.3969/j.issn.1008-2077.2018.10.005

Li, Z. Q., Xiang, L., and Wei, F. (2004). Fire Resistant&Smoke vanishing mechanismand production method of flame retardant type magnesium hydroxide. *Haihuyan Yu Huagong* 33 (2), 1–7. doi:10.1016/j.proeng.2013.02.150

Liu, C., Wu, W., Shi, Y. Q., Yang, F., Liu, M., Chen, Z., et al. (2020). Creating MXene/reduced graphene oxide hybrid towards highly fire safe thermoplastic polyurethane nanocomposites. *Compos. Part B* 203, 108486. doi:10.1016/j.compositesb.2020.108486

Lü, K. Z., Jiang, X. S., and Zhai, Y. (2016). The experimental study on thermal stability and oil fire extinguishing performance of three–phase foam extinguishing agent. *J. Logist. Eng. Univ.* 32 (06), 56–60. doi:10.3969/j.issn.1672-7843.2016.06.009

Lu, Y. H., Wu, C. F., and Xu, S. A. (2018). Mechanical, thermal and flame retardant properties of magnesium hydroxide filled poly(vinyl chloride) composites: the

effect of filler shape. *Compos. Part A* 113, 1–11. doi:10.1016/j.compositesa.2018.07.012

Ma, J. L., Wang, X., Li, J., Chen, R., and Wei, J. (2020). Facile preparation of flame retardant cotton fabric via adhesion of $Mg(OH)_2$ by the assistance of ionic liquid. *Polymers* 12 (2), 259–268. doi:10.3390/polym12020259

Qin, B. T., Wang, D. M., Chen, J. H., and Liang, X.-Y. (2005). Experimental investigation of high-performance three-phase foam for mine fire control. *J. China Univ.Min. Technol.* 34, 14–18. doi:10.3321/j.issn:0253-9993.2005.02.005

Qiu, X. B., Wei, Y. B., Li, N., Guo, A., Zhang, E., Li, C., et al. (2019). Development of an early warning fire detection system based on a laser spectroscopic carbon monoxide sensor using a 32-bit system-on-chip. *Infrared Phys. Technol.* 96, 44–51. doi:10.1016/j.infrared.2018.11.013

Sain, M., Park, S. H., Suhara, F., and Law, S. (2004). Flame retardant and mechanical properties of natural fibre-PP composites containing magnesium hydroxide. *Polym. Degrad. Stab.* 83 (2), 363–367. doi:10.1016/s0141-3910(03)00280-5

Sener, A. A., and Demirhan, E. (2008). The investigation of using magnesium hydroxide as a flame retardant in the cable insulation material by cross-linked polyethylene. *Mater. Des.* 29 (7), 1376–1379. doi:10.1016/j.matdes.2007.05.008

Shan, X. Y., Han, J., and Song, Y. (2020). Flame retardancy of epoxy resin/β-cyclodextrin @resorcinol bisdiphenyl phosphate inclusion composites. *J. Wuhan Univ. Technol. Mater. Sci. Ed.* 35, 455–463. 10.1007/s11595-020-2278-5.

Shi, Y. Q., Liu, C., Duan, Z. P., Yu, B., Liu, M., and Song, P. (2020). Interface engineering of MXene towards super-tough and strong polymer nanocomposites with high ductility and excellent fire safety. *Chem. Eng. J.* 399, 125829. doi:10.1016/j.cej.2020.125829

Shi, Y. Q., Liu, C., Liu, L., Fu, L., Yu, B., Lv, Y., et al. (2019). Strengthening, toughing and thermally stable ultra-thin MXene nanosheets/polypropylene nanocomposites via nanoconfinement. *Chem. Eng. J.* 378, 122267. doi:10.1016/j.cej.2019.122267

Tang, H., Zhou, X.-b., and Liu, X.-l. (2013). Effect of magnesium hydroxide on the flame retardant properties of unsaturated polyester resin. *Procedia Eng.* 52, 336–341. doi:10.1016/j.proeng.2013.02.150

Vijayaraghavan, K., Nikolov, A., and Wasan, D. (2006). Foam formation and mitigation in a three-phase gas-liquid-particulate system. *Adv. Colloid Interf. Sci.* 123–126, 49–61. doi:10.1016/j.cis.2006.07.006

Wang, L., Xu, P., and Luo, Y. (2009). The study on fire extinguishing performance of ultra-thin magnesium hydroxide powder. *Fire Sci. Technol.* 28 (6), 425–428. doi:10.1016/j.proeng-2017.12.035

Wu, K. F., Liu, M., Zhao, G. S., He, L., and Tan, Y. (2020). Altered regional homogeneity in delayed encephalopathy after carbon monoxide poisoning: a resting-state fMRI study. *Neurosci. Lett.* 729, 135002–135007. doi:10.1016/j.neulet.2020.135002

Xie, Z. H., Li, X. C., and Liu, M. M. (2011). Application of three-phase foam technology for spontaneous combustion prevention in longdong coal mine. *Procedia Eng.* 26, 63–69. 10.1016/j.proeng.2011.11.2140.

Zarca, G., Ortiz, I., and Urtiaga, A. (2015). Recovery of carbon monoxide from flue gases by reactive absorption in ionic liquid imidazolium chlorocuprate(I): mass transfer coefficients. *Chin. J. Chem. Eng.* 23 (5), 769–774. doi:10.1016/j.cjche.2014.06.040

Zhao, X. Y. (2012). Application and development status of foam extinguishing agent. *J. Hebei Acad. Sci.* 29 (03), 65–68. doi:10.3969/j.issn.1001-9383.2012.03.016

Conflict of Interest: The authors declare that the research was conducted in the absence of any commercial or financial relationships that could be construed as a potential conflict of interest.

Advantages of publishing in Frontiers

OPEN ACCESS
Articles are free to read for greatest visibility and readership

FAST PUBLICATION
Around 90 days from submission to decision

HIGH QUALITY PEER-REVIEW
Rigorous, collaborative, and constructive peer-review

TRANSPARENT PEER-REVIEW
Editors and reviewers acknowledged by name on published articles

Frontiers
Avenue du Tribunal-Fédéral 34
1005 Lausanne | Switzerland

Visit us: www.frontiersin.org
Contact us: .frontiersin.org/about/contact

REPRODUCIBILITY OF RESEARCH
Support open data and methods to enhance research reproducibility

DIGITAL PUBLISHING
Articles designed for optimal readership across devices

FOLLOW US
@frontiersin

IMPACT METRICS
Advanced article metrics track visibility across digital media

EXTENSIVE PROMOTION
Marketing and promotion of impactful research

LOOP RESEARCH NETWORK
Our network increases your article's readership